Spectroscopic investigations of high pressure multiphase systems

Von der Fakultät für Mathematik, Informatik und Naturwissenschaften der RWTH Aachen University zur Erlangung des akademischen Grades einer Doktorin der Naturwissenschaften genehmigte Dissertation

vorgelegt von

Diplom-Chemikerin
Sonja Hardy
aus Aachen

Berichter: Universitätsprofessor Dr. rer. nat. Marcel A. Liauw
Universitätsprofessor Dr. rer. nat. Walter Leitner

Tag der mündlichen Prüfung: 06. Dezember 2013

Diese Dissertation ist auf den Internetseiten der Hochschulbibliothek online verfügbar.

Ich möchte die Gelegenheit nutzen, einigen Menschen zu danken, die mich während meiner Promotion sehr unterstützt haben:

meinem Doktorvater, Herrn Prof. Liauw
meinen Prüfern, Herrn Prof. Leitner, Herrn Prof. Stahl und Herrn Prof. Weinhold
den Mitarbeitern des Instituts, besonders Ralf Thelen, Günther Wirtz, Stefan Aey, Hannelore Eschmann und Julia Wurlitzer
den Mitarbeitern des Arbeitskreises, besonders Hanna Praefke, Steffen Heddrich und Sonja Winterle
den Kollegen des AK Leitner, besonders Irene de Wispelaere und Julia Hahne
Lukas Küpper, Clemens Minnich, Dirk Prinz, Lasse Greiner, Jörn Viell, Christian Löhr und Thorsten Epping
Claudia Houben, Robin Heedfeld, Sören Lehmkuhl und Manuel Noack
meinen Freunden und meiner Familie, besonders Daniel und meinen Eltern

Teile dieser Arbeit wurden bereits veröffentlicht:

Artikel:

Comprehensive monitoring of a biphasic switchable solvent synthesis, S. Hardy, I. M. de Wispelaere, W. Leitner, M. A. Liauw, *Analyst* **2013**, *138*, 819-824.

Mixing behaviour investigation of a switchable solvent synthesis using ATR-IR spectroscopy, S. Hardy, M. A. Liauw, *Chemical Engineering Journal* **2013**, *233*, 292-296.

Contents

1. Introduction **1**

2. Hydrogenation of glucose: from single sample to in situ analytics **15**
2.1. Context 15
2.2. Introduction 16
2.3. Outline 17
2.4. Comparison of spectra 19
2.5. Quantification model 21
2.6. Comparison with reference analytics 25
2.7. Parameter influences 31
2.8. Summary 36
2.9. Conclusions 37

3. Hydrogenation of glucose: combination of mIR and Raman in the liquid phase **39**
3.1. Context 39
3.2. Introduction 40
3.3. Outline 42
3.4. Comparison of spectra 43
3.5. Quantification model 45
3.6. Comparison of IR and Raman results 47
3.7. Hydrogen detection 50
3.8. Summary 52
3.9. Conclusions 53

4. Switchable solvent synthesis: two-phase analysis towards a total mass balance 57
4.1. Context . . . 57
4.2. Introduction . . . 58
4.3. Outline . . . 60
4.4. Comparison of spectra and quantification . . . 61
4.5. Model system: absorption of CO_2 in hexanol . . . 64
4.6. IL synthesis and total mass balance . . . 65
4.7. Assessment of limiting factors . . . 67
4.8. Analysis of reaction parameters . . . 70
4.9. Summary . . . 77
4.10. Conclusions . . . 79

5. Switchable solvent synthesis: two sensors in one for space-dependent analysis 81
5.1. Context . . . 81
5.2. Introduction . . . 82
5.3. Outline . . . 84
5.4. Evaluation of conductivity values . . . 85
5.5. Analysis of conductivity parameters . . . 86
5.6. Comparison with IR spectroscopy . . . 90
5.7. Impedance spectroscopy . . . 93
5.8. Summary . . . 95
5.9. Conclusions . . . 96

6. Summary and Conclusion 99

7. Theory 105
7.1. Introduction . . . 105
7.2. Analytical methods . . . 106
7.2.1. Mid-infrared . . . 106
7.2.2. Raman . . . 109
7.2.3. Conductivity measurement . . . 110

References **119**

A. Experimental procedures **121**
A.1. Chemicals 121
A.2. Reaction procedures 122
A.2.1. Hydrogenation 122
A.2.2. Switchable solvent synthesis 123
A.3. Reactor set-up 123
A.3.1. Hydrogenation 1 123
A.3.2. Hydrogenation 2 125
A.3.3. Switchable solvent synthesis 127
A.3.4. Conductivity measurements 127

B. Calibrational data **133**

C. Additional figures **147**

List of Figures

1.1. Spectroscopic probe configurations 5
1.2. High pressure view-cell 6
1.3. Spectroscopic probe with IRE and electrode surface . . . 10
1.4. Hydrogenation reaction of glucose to sorbitol 11
1.5. Synthesis of switchable IL from DBU and hexanol 11

2.1. Hydrogenation of glucose and further dehydration steps . 17
2.2. IR spectrum of glucose in water as a solvent 20
2.3. IR spectrum of sorbitol in water as a solvent 21
2.4. IR spectrum of glucose with and without catalyst 22
2.5. Results of validation 25
2.6. Results of validation 2 26
2.7. Comparison of HPLC and IR results 28
2.8. HPLC and IR profiles of the hydrogenation 30
2.9. HPLC and IR profiles of the hydrogenation 2 32
2.10. Temperature variation of hydrogenation 33
2.11. Pressure variation of the hydrogenation 34

3.1. Raman spectra of glucose and sorbitol 44
3.2. Raman spectrum of glucose with and without catalyst . . 45
3.3. IHM data of glucose 47
3.4. Raman profiles of glucose and sorbitol 49
3.5. Comparison of IR and Raman profiles 50
3.6. Raman spectra before and after hydrogen addition 51

4.1. IR spectrum of hexanol 61

4.2. IR spectra of DBU/hexanol and IL 62
4.3. Results of IHM validation 63
4.4. Concentration of CO_2 during dissolution 65
4.5. Concentration profiles of IL, DBU/hexanol and CO_2 . . . 66
4.6. Concentration profiles of IL and DBU/hexanol 71
4.7. Concentration profiles of IL and DBU/hexanol 2 72
4.8. Concentration profiles of IL and DBU/hexanol (no reaction) 73
4.9. Parameter map 75

5.1. Electrode distance variation 87
5.2. Stirring speed variation 88
5.3. Temperature dependence of IL conductivity 89
5.4. Reproducibility of conductivity measurements 91
5.5. Comparison of conductivity measurements 92
5.6. Impedance spectra 94

7.1. Schematic of ATR measurement principle 108
7.2. Schematic of Raman measurement principle 110

A.1. Photograph of 10 mL finger autoclave 124
A.2. Photograph of 30 mL window autoclave 129
A.3. Photograph of 30 mL window autoclave 2 130
A.4. Photograph of 75 mL autoclave 130
A.5. Schematic of conductivity measurement circuit 131

C.1. IR spectra of glucose 147
C.2. IR spectra of sorbitol 148
C.3. Initial slopes of temperature variation 148
C.4. Initial slopes of pressure variation 149
C.5. Raman spectra of glucose/sorbitol mixtures 149
C.6. IR spectra with and without current applied 150

List of Tables

B.1. Results of glucose IR quantification 133
B.2. Results of glucose Raman quantification 138
B.3. Results of DBU/hexanol IR quantification 138
B.4. Results of IL IR quantification 142
B.5. Results of CO_2 IR quantification 145

C.1. Sample compositions of Raman calibration 150

Abbreviations

ATR	attenuated total reflectance
DBU	1,8-diazabicyclo[5.4.0]undec-7-ene
hexanol	1-hexanol
GC	gas chromatography
glucose	D-(+)-glucose
HPLC	high performance liquid chromatography
IHM	indirect hard model
IL	ionic liquid
IR	infrared
IRE	internal reflection element
isosorbide	D-isosorbide
mIR	mid-infrared
RMS	root mean square
sorbitol	D-sorbitol

Symbols

Ar	argon
c	centi 10^{-2}
F	farad
g	gram
Hz	Hertz
k	kilo 10^{3}
L	litre
m	milli 10^{-3}
Ma	Marangoni number
mol	mole
μ	micro 10^{-6}
p	pressure
Pa s	Pascal-second
R^2	coefficient of determination
Ra	Rayleigh number
Re	Reynolds number
S	Siemens
T	temperature

1. Introduction

Multiphase reactions offer a high versatility. This is not only illustrated by the wide range of applications in heterogeneous catalysis[1,2], but also by a large number of liquid-liquid reactions, gas-liquid reactions and reactive extractions[3–8]. In academic research, many of these concepts are increasingly applied for the sustainable production of fuels from biomass[9,10]. Gas-liquid reactions such as hydrogenations are carried out in order to reduce the oxygen content of biomass derived platform chemicals and reactive extractions enable the processing of unstable intermediates and products. Whilst multiphase reactions are unavoidable in many cases where substrates and products show different solubilities, they can be very desirable in many cases, too.

In homogeneous reactions, separation tasks often present a problem to the realisation of a large scale process, whether a catalyst has to be separated from the products for recycling[11], products have to be separated from side-products or products have to be separated from a substrate mixture[12]. Depending on the properties of the substances involved in the separation and the process requirements further downstream of the separation, different separation techniques have been developed[13]. They can be roughly divided into processes that only carry out separations and processes where this task is combined with a second unit operation, e.g. for reactive distillations. Separations are mostly carried out via distillation or extraction, but distillations have a high energy demand and are therefore not very desirable and extractions use a high volume of solvent, which has to be separated from the product afterwards, leading not only to a high solvent demand, but requiring the installation of an additional

process step.

In heterogeneous reactions on the other hand, a separation of at least one of the reactants occurs naturally, rendering an additional separation step for this reactant unnecessary. Prominent examples are of course all heterogeneously catalysed reactions, where the solid catalyst can be easily removed by filtration [14,15], liquid-liquid reactions, where one reactant forms a second liquid phase and can be removed by gravity separation [16], and gas-liquid reactions [17], where the gaseous reactant can be separated by simple depressurisation.

The presence of an additional phase automatically adds a further parameter and so offers more room for variations, thus making multiphase reactions more versatile. By changing the volume ratio of the phases, the ratio of the reactants can be adjusted to give the best results for the reaction, but at the same time, this change can also cause a different mixing behaviour of the phases. This can be an important reaction parameter, for example in emulsion polymerisation [18], where the phase ratio influences the properties of the polymer that is produced. In the case of gas phase reactions, the change of phase ratios causes a change in pressure, another important reaction parameter. If the pressure is raised by adding an inert gas, this normally means that even though the gas is inert, it still has a certain solubility in the liquid phase which is directly proportional to the pressure and thus the concentrations in the liquid phase are altered due to the dissolution of the inert gas. If a reactive gas is used to raise the pressure, it too will be dissolved in the liquid, in this case leading to a higher reactant concentration in the mixture and thus to a faster reaction. Depending on the desired effect, the choice of gas can be made.

Still, multiphase reactions always pose the problem of phase contacting. If the reactants are in a different phase than the catalyst or one of the reactants is in a different phase than the other reactant, they have to

be contacted in order for a reaction to take place[19]. This is only possible if one of the reactants crosses the phase boundary or if the reaction takes place at the phase boundary itself. In each case, a large phase boundary area and a high substrate concentration at the phase boundary will lead to a faster reaction. A larger phase boundary area increases the number of places where either a reaction can take place or a phase transition is possible. A higher substrate concentration at the phase boundary will lead to a faster reaction depending on the concentration dependence of the kinetics or will increase the mass transfer rate according to Fick's first law, which states that the higher the concentration gradient over the phase boundary, the higher the mass transfer rate. Both can be influenced by mixing, which can produce a larger phase boundary area by creating an uneven phase boundary area or bubble entrainments and which creates an inner phase circulation, transporting substrate from the bulk of the phase to the phase boundary, where it can react, again lowering the substrate concentration at the phase boundary[20]. All of this shows that in multiphase reactions, the phase contacting, which is dependent on the mixing, and the reaction itself are strongly interdependent, each influencing the concentrations of the reactive phase. Since the concentration is usually the main observable and used to monitor the reaction, a distinction between reaction and mass transport induced concentration changes becomes more difficult and extensive analytics at the same time more important. Only an exact knowledge of the concentration changes in both phases helps to distinguish the effects so as to obtain the pure reaction kinetics and the mass transport rates.

For the monitoring of high pressure multiphase reactions, implementation of suitable analytics becomes even more difficult, since they have to work under elevated pressure. One possibility is high pressure sampling[21], after which the extracted samples can be analysed at normal pressure by standard analytic techniques. Alternatively, analysis can be carried out *in situ*, requiring the analytical technique to be pressure resistant. For all invasive analytics, the main problem apart from the tech-

nical challenge is the disturbance that the sampling causes to the phase equilibrium. Even if the pressure can be kept constant during sampling, the removal of a volume fragment from one phase causes a change in the phase ratio. If samples of all phases are taken proportionally at exactly the same time, the high loss in total volume causes a change in the mixing behaviour and in the relative phase boundary area. Taking all these challenges into account, non-invasive analytical concepts are often applied where high pressure multiphase reactions are to be monitored. Spectroscopy is the most common choice in this context [22–29], although techniques such as rheology, refraction measurements or electrical measurements are also possible in some cases. Spectroscopy is the most versatile alternative, though, since it can be applied to a wide range of substances and process set-ups. The combination of several spectroscopies can help to further broaden the scope of detectable substances [30]. Spectroscopic measurement can be configured either as probe measurements or by conducting light through an appropriate window arrangement. Windows are more restricted as to the applicable pressure range and they require more mounting space in the reactor. Probes can reach a lower diameter than windows and for most applications, only one probe is required, while for window based transmission spectroscopy, two windows have to be installed. There are two different probe configurations (fig. 1.1), depending on the measurement that is to be carried out, either as a slit, allowing transmission measurements through the slit and collecting the transmitted beam with the same probe, or a crystal, where the light reaches the medium through the crystal and is collected again by the same crystal, e.g. for attenuated total reflectance (ATR) measurements.

While many examples in literature use spectroscopy for reaction monitoring of high pressure gas-liquid reactions and even integrate several combined spectroscopies into a high pressure set-up such as an autoclave as a further step towards monitoring under reaction conditions [31,32], many of the devices accommodate several spectroscopic probes for analy-

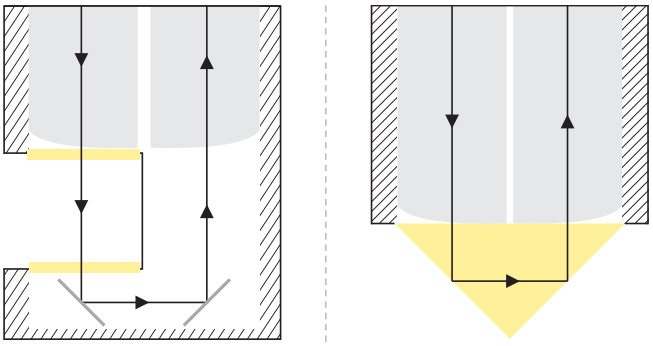

Figure 1.1.: Probe configurations for transmission (left) and ATR (right) spectroscopy

sis of the liquid phase only. The only information that is available about the second phase, which is the gas phase, is the recorded pressure. The exact composition of the gas phase remains unknown. A proposed solution to this problem is to carry out the reaction twice under the same conditions, once in a set-up that allows measurements of the liquid phase and once in a spectroscopic cell that measures the gas phase[33]. This approach mainly depends on the reproducibility of both the reaction and the conditions applied. It is not easy to guarantee this reproducibility when the handling of parameters like temperature, pressure, flow profile and phase volume is influencing the reaction. The quasi-simultaneous measurement of both phases in one reactor suggested by *Baiker et al.*[34] seems more promising (fig. 1.2). The autoclave can be equipped with an ATR element at the bottom to monitor the liquid phase and two transmission windows to analyse the gas phase. The ATR element also allows the measurement of a heterogeneous catalyst fixed to its surface for operando studies. In addition, the phase behaviour of the reaction mixture can be checked via an inspection window.

A drawback is that only mid-infrared (mIR) spectroscopy can be applied in this set-up. A combination of several spectroscopies is not im-

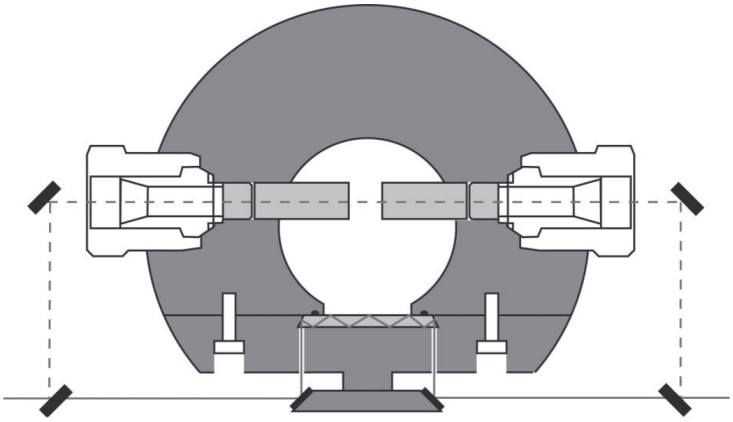

Figure 1.2.: Cross section of the high pressure view-cell as suggested by Baiker et al.[34]

plemented. Furthermore, the transmission mode installed in the upper part of the reactor is just suitable for gases and clear liquids with a low concentration.

Ideally, a set-up for high pressure gas-liquid reactions would comprise a combination of several spectroscopic methods for the gas phase as well as the liquid phase. Especially for high concentrations and turbid phases, ATR measurements are advantageous and have the additional benefit of being process compatible, so that results can easily be adapted in the development of new processes based on a process analytical control system and could help to propagate the use of process analytical technology and to shorten the production development time[35].

Still, at present such measurement set-ups are not the standard approach towards analytics in high pressure multiphase reactions and the main part of these reactions are analysed with a standard technique such as gas chromatography (GC), high performance liquid chromatography

(HPLC) or chromatography after they have been aborted and depressurised. This approach may not only give a wrong idea about the composition under reaction conditions because it is not carried out *in situ*, but is also restricted to one single composition measurement of the state of the reaction at the point of abortion, with no information on the course of the reaction up to this point. For these reasons, it cannot be an adequate method neither for the determination of kinetic behaviour, nor for the monitoring of the reactive and transport processes over time.

Evolving from this starting point, this work will show how analytical measurements in high pressure multiphase reaction systems can be improved and how the manifold analytical possibilities can be adapted and combined to match the specific characteristics and requirements of different reactions.

In trying to find out how this can be achieved, a change from single sample analytics towards *in situ* measurements with a frequency below 1 min^{-1} will first have to take place (chapter 2). This new approach gives the opportunity to trace the course of the reaction and analyse how the temperature, pressure and catalyst choice influence the reaction time and the concentration profile of the reaction. It is implemented by the simplest possible set-up, where a single mIR probe is introduced into the standard 10 mL autoclave already established as the reaction vessel. Thus, the changes to the existing set-up are minimal and the results should be comparable, while the information density is raised considerably. Since the mentioned system only contains a probe for one spectroscopic measurement range, in this case mIR, composition measurements are restricted to a narrow wavelength region and only one substrate and the product are detectable. The second gaseous substrate cannot be detected by the probe and any assumptions on its concentration have to be based on pressure measurements of the gas phase and on the detected product.

That is why in a second step, the set-up is altered so that it matches the original measurement less, but with the advantage of allowing room for combined mIR and Raman spectroscopy (chapter 3). With the additional spectroscopic method, an improved detection of the product in the liquid phase and, most importantly, a detection of the gaseous substrate dissolved in the liquid phase are aimed at. Information on the concentration of dissolved gas in the liquid phase can help to draw conclusions about the limiting factors of the reaction. If the concentration is very low, then this implies that the transport from the gas phase into the liquid is limiting the reaction rate and is not able to supply the substrate as fast as it is consumed by the reaction. While these experiments give a better idea of the transport processes involved in the reaction, they do not give a complete picture, because the gas phase is not monitored properly. While pressure information is available, it does not define the composition of the gas phase, an aspect that is increasingly important at elevated temperatures where the liquid component or the solvent will partially evaporate to add to the total detected pressure. Accordingly, a change in pressure might either be ascribed to a change in temperature or to a consumption of the gaseous substrate.

Based on these considerations, the third step is the construction of a set-up that combines several spectroscopic methods at two different positions, so that the liquid and the gas phase can both be analysed by at least two spectroscopies simultaneously (chapter 4). By these means, the composition of the gas phase and the composition of the liquid phase can be monitored and all substances involved in the reaction can be detected and quantified. The result is the first example of how quantitative concentration data can be obtained for each component in both gas and liquid phase and how these can be used to establish a total mass balance. The depletion and propagation sequences of the reaction can be traced and attributed to reaction and transport processes. The evaluation of the measurements also shows that for fast reactions and slow stirring, the concentrations in the bulk will very likely be heterogeneous, with mixing

behaviour dominating the concentration distribution. This means that even if different measuring techniques are integrated into the same reactor, they might detect different compositions due to the space-dependent concentration fluctuation of the bulk. If measuring in this regime, it is therefore important to keep in mind that concentration measurements of different methods may vary due to their different detection position inside the reactor. In order to be able to compare measurements by different methods, one has to make sure that they are detected at exactly the same point, measuring the same volume element.

The latter aspect is addressed in the last part, where the concept of two sensors in one is realised and evaluated (chapter 5). This concept is based on the idea that the smallest possible difference in measuring position can be achieved if the measurements are carried out with the same sensor. An infrared (IR) probe was therefore tailored in such a way that it can also accommodate electrical measurements without damage to the probe, serving as an electrode as well as an immersion probe. Thanks to this arrangement, the electrical measurements take place at the front probe surface positioned around the internal reflection element (IRE) of the spectroscopic probe (fig. 1.3).

The distance is thus minimised to approximately 1 mm, which is far below the distance that can be realised with a two-sensor approach. Of course, a second electrode has to be added to the set-up for any electrical experiments, which can be either a simple standard electrode or a second probe. Results show that this arrangement works and that the spectroscopic measurements are not impeded by the current that circulates.

Of course, not all of the described options are always applicable or necessary, so the challenge still remains to find and choose the most appropriate and simplest measuring technique for each reaction, but without relinquishing important information that can help to explain the system's behaviour. Accordingly, this work can only present some examples of versatile and exemplary set-ups to help and raise the awareness of the

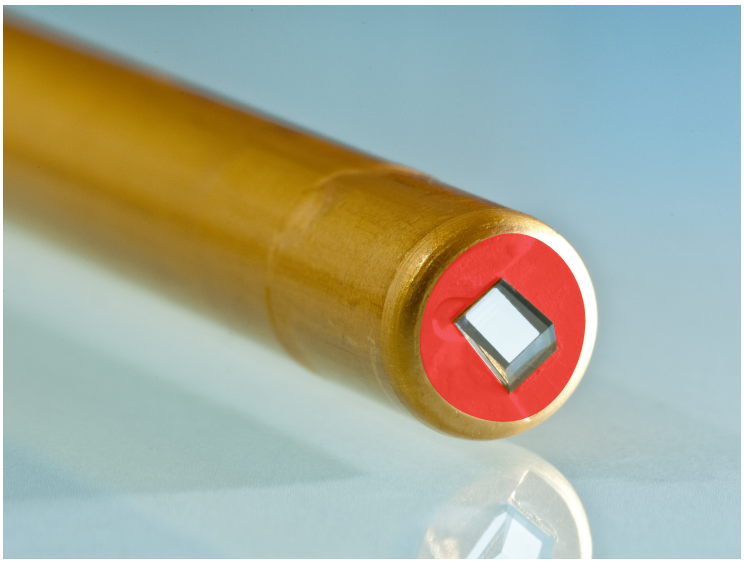

Figure 1.3.: Spectroscopic probe with IRE and electrode surface

many possibilities available for the analysis of high pressure multiphase systems. The chosen applications are two reactive systems with very different demands on analytics.

The catalytic hydrogenation reaction of D-(+)-glucose (glucose) to D-sorbitol (sorbitol) (fig. 1.4) in water as a solvent is a good example of the challenges that arise from the change from fossil to renewable energy sources such as wood and foliage. The use of new feedstock such as carbohydrates and sugars requires a detection method with a very high structural resolution, since the substrates and resulting products show similar structural features and functional groups. These cause a similar strength of absorption in a similar spectral region, making a distinction of the substances difficult.

But the trend towards more sustainable processes does not stop there;

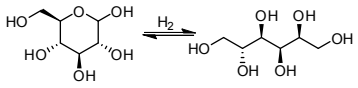

Figure 1.4.: Hydrogenation reaction of glucose to sorbitol

it also results in the increased use of water as a solvent, for obvious reasons. While water may be readily available, non-toxic and easily disposable, it is also a more challenging solvent when it comes to analytics. NIR, which is already a standard tool for online and *in situ* process analytics in industry, is very sensitive to water because of the strong absorption in this spectroscopic region. That means that if water is present in the system, the detection of any other substance becomes very difficult. The specific features of the reaction system also include the presence of a suspended catalyst, which renders transmission spectroscopy impossible. These two aspects strongly influence the choice of spectroscopic tool appropriate for detection. ATR-mIR spectroscopy is not as sensitive to water as NIR and shows a high structural resolution, important for the detection of similar functional groups. The ATR technique can be applied in turbid media because the penetration depth is so small that the particles are not detected and no scattering can occur. So it suits the system with a suspended particulate catalyst. The quantification method is adapted to this case by choosing a multivariate method, so that even small spectral changes and highly overlapping signals can be quantified.

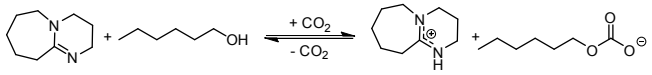

Figure 1.5.: Synthesis of switchable IL from DBU and hexanol

The switchable solvent synthesis is an example of how the design of new solvents can offer new possibilities for a "greener" process design. Their

ability to readily switch between different solvent properties can eliminate the need for a solvent separation by distillation. Currently, switchable solvents and membrane processes are the most promising candidates for a more energy efficient coupling of reaction and separation. Switchable solvents have therefore received growing attention in the past decade, both in academia and industry. The presented case of the reaction of an amine and an alcohol with CO_2 to an ionic liquid (IL) (fig. 1.5) has the advantage of using an IR active gas as a reactant. This facilitates the analysis of the gaseous reactant and reduces the number of spectroscopic methods that are required, because no additional technique is necessary for the detection of the gas. Also, the IR signals of all components are very strong and not strongly overlapping, so that an indirect hard model (IHM) method rather than a multivariate method can be applied for quantification. This method is better suited to adjust to the expected temperature increase due to the high exothermicity of the reaction, which influences the spectra. Another advantage of the system is that the high difference in ionic strength between the substrate mixture and the product can be used for conductivity measurements in order to test the electrical measurement arrangement. A challenge is the strong viscosity increase during the reaction, to which the set-up has to be adapted, and the speed of the reaction, both resulting in mixing problems which have to be addressed and which, as already mentioned, lead to inhomogeneities in the bulk concentration, making the comparison of different measurements difficult.

As the many differences between these two example reactions and the employed analytical systems demonstrate, the individual demands of reactions have to be taken into account when looking for suitable analytics in high pressure multiphase systems. Still, specific characteristics of the reactive system can often be found and turned into advantages to benefit an improved analysis of the reaction. Ideally, the results of these analyses can then be employed for a more sound understanding of the processes involved in the reaction and for an enhancement of the production set-up.

2. Hydrogenation of glucose: from single sample to in situ analytics

2.1. Context

The hydrogenation of glucose is a good example of the state of standard analysis that is currently employed for high pressure two phase reactions in research. Literature[36] shows that for the evaluation of a successful reaction run, the reaction is cooled down after a standard reaction time, in this case 15 hours, carefully depressurised and then centrifuged, filtered and diluted as a preparation for analysis. Afterwards, offline GC and HPLC measurements are carried out to obtain the conversion and selectivity of the reaction. While this procedure will give a good first impression of scopes and general trends, it says little about the reaction rate, the apparent reaction order or any non-continuous behaviour that may occur in the system due to the heating period, a possible run-in period, preceding catalyst activation or a deactivation with time. To gain such information, a higher time resolution of the analytics and a measurement at reaction conditions is necessary. Whereas a higher time resolution yields a concentration profile, *in situ* analysis gives access to all pressure and temperature dependent effects. Such aspects are especially important when dealing with high pressure multiphase reactions, since they are often directly related to transport limitations and the relationship between transport and reaction. Their understanding renders

the improvement of factors such as phase ratio, mixing and pressure possible. Therefore, in this chapter a conversion from analysis based on one sample to an automated *in situ* analysis will be performed. For the analysis of sugar transformations, this will be the first case of a spectroscopic analysis and since the implementation is kept quite simple, this will hopefully encourage a more widespread application in the field.

2.2. Introduction

As part of the production of fuels from biomass, the most molecule and energy efficient route is the dissociation, separation and conversion of wood or foliage into platform molecules and subsequent processing into fuel molecules[9,10]. Biomass components have a high oxygen content, which leads to negative burning properties in the engine if untreated. A reduction of the oxygen content is therefore inevitable and can be achieved by a hydrogenation followed by a dehydration. The hydrogenation can be catalysed by a variety of metal-based catalysts[37–41]. In this case, IL stabilised ruthenium nanoparticles on a silica support are chosen. These cannot only catalyse the hydrogenation from glucose to sorbitol, but can also promote a further dehydration to sorbitan and D-isosorbide, depending on the chosen reaction medium[36] (fig. 2.1). The reaction is carried out in water to avoid the dehydration and hence narrowing down the product spectrum. This is an appropriate simplification adopted for the first trials of a new analytical method. Glucose as a substrate and sorbitol as the product show very similar structural and functional elements, therefore a distinction is difficult. Mid-IR offers the advantage of a high structural resolution of the spectra, but signals of the two substances still show strong overlaps. Consequently, a multivariate quantification method has to be developed, which can help to distinguish even small differences in the spectra of the two substances and also small concentration changes during the reaction.

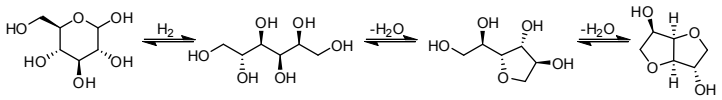

Figure 2.1.: Hydrogenation of glucose and further dehydration steps to sorbitan and isosorbide

A further challenge for the quantification of this reaction system is the reaction temperature. The hydrogenation is by default carried out at 60 °C, which can significantly influence the spectra that are obtained due to the vibrations that are excited by the heat absorption. All calibration samples were equilibrated and measured at 60 °C to give the most accurate base for the model building, but the heating period at the beginning of the reaction and temperature alterations during pressurisation may not be represented correctly.

The first aim is therefore to develop and evaluate a quantification method that can describe the concentration profile of the hydrogenation reaction from glucose to sorbitol with a high time resolution in order to create a tool for reaction monitoring that can be used to investigate the influence of parameters such as pressure and temperature on the reaction course.

2.3. Outline

A detailed comparison of the spectra of glucose and sorbitol will be carried out to see how they can best be analysed. This will take place in the presence of water as a solvent, because water itself also generates strong IR absorption signals and therefore should be taken into account early on. During the comparison, the focus will lie on the regions with the strongest differences in signals for glucose and sorbitol, but these regions will also be evaluated with respect to the rise in signal strength

with a concentration increase. Both aspects have to be considered, because a signal that can be distinctly attributed to one substance, but does not show a strong concentration dependence, will not be suited for quantitative evaluations. In addition, the influence of the presence of the catalyst on the spectra will be checked to ensure that it does not falsify the measurements. Even though the catalyst has no characteristic absorption signals, interactions between the catalyst and the substrate or the product can still cause a significant shift of the signals. Due to its high sensitivity even to small alterations, this would compromise the quantification method.

Following these considerations, the second step will be the building of a quantification model. This will not only be based on the mentioned qualitative survey, but will also be supported by a cross-validation and will own its reliability to the high number of calibration samples incorporated. The use of many calibration samples ostensibly lowers the quality of the model by increasing the specified error R^2, but an average over many measurements is in truth of course more reliable, even if the scattering induces a higher error value. For the same set and number of calibration samples, the error value remains a creditable indication of the quality of different quantification models. It will therefore also be consulted during the model building process.

After this internal validation, the established quantification model will be used to analyse the real hydrogenation reaction. This is especially important because even though many calibration samples were used and care was taken during temperature equilibration, none of these were recorded under actual process conditions. For further evaluation of the reaction analysis, external reference measurements with HPLC are therefore conducted. Together with the known initial concentration, these allow a comparison of the starting and end concentrations of the reaction with the results of the IR analysis. Assuming reproducibility of the reaction, the experiments can be stopped at different reaction times and anal-

ysed with HPLC to render a higher number of comparison point along the concentration profile of the reaction. The use of reference analytics also makes a comparison with standard single sample measurements possible, so that the knowledge gained in earlier works can be transferred and exploited.

Building on the successful implementation of the spectroscopic method, a parameter study of the influence of pressure and temperature on the reaction course is carried out. This shows how the new method facilitates the reaction monitoring and provides new information that can then be used for optimisation. It will also point out the restrictions that still arise from this kind of set-up and the kind of questions that cannot be answered despite the improved analysis.

2.4. Comparison of spectra

A spectrum of glucose in water with a concentration of $2.5 \cdot 10^{-3}$ mol/g shows the characteristic signals (fig. 2.2). Between 2600 and 3000 cm^{-1}, the broad signals of ν(OH) and ν(CH) form a shoulder to the ν(OH)-signal of water. The regions of 1180-1500 cm^{-1} and 950-1180 cm^{-1} are dominated by broad multiple overlapping signals. This is the classical fingerprint region, where an exact assignment of the individual signals is difficult, but which is mainly made up of the deformation vibrations δ(CH), $\delta(CH_2)$ and δ(OH) and the valence vibration ν(CO) of the ether group. A further two signals at 880-940 cm^{-1} and 752-782 cm^{-1}, which can be attributed to the $\delta(CH_2)$ rocking, again form shoulders to a water peak.

For sorbitol with a concentration of $2.4 \cdot 10^{-3}$ mol/g in water (fig. 2.3), broad ν(OH) and ν(CH) signals similar to those of glucose are detected between 2600 and 3000 cm^{-1}, but the maximum in this case is made up of two main overlapping peaks, contributing to a doublet. At 1160-1500 cm^{-1} and 970-1160 cm^{-1}, in a similar region to that of glucose, multiple overlap-

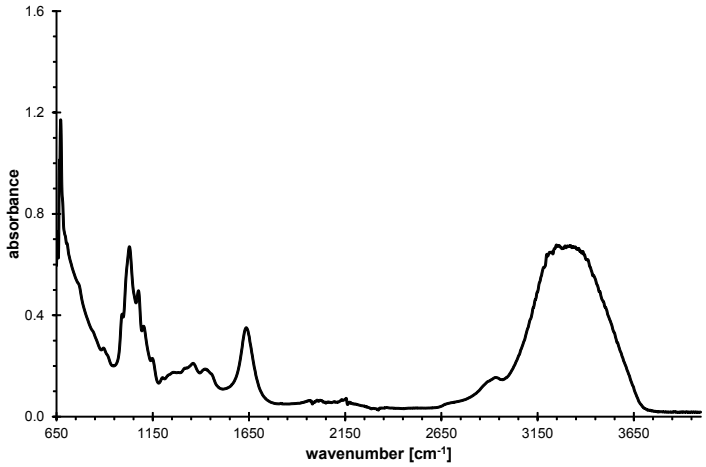

Figure 2.2.: IR spectrum of glucose in water as a solvent

ping signals of a slightly different general shape can again be correlated to the deformation vibrations δ(CH), δ(CH_2) and δ(OH).

A comparison of the spectra of glucose and sorbitol reveals ten positions of detectable differences. They are located at 771, 883, 915, 990, 1105, 1149, 1211, 1359, 1406 and 2945 cm^{-1} and although the deviations are small, they could possibly be used for the model building. At 771 cm^{-1}, the noise is quite high, which manifests itself in the spectrum of pure water as well as in the substance spectra, so this region is not considered further. A more detailed look at the dependence of the signal intensity on the concentration can reveal whether the signals change enough to be suitable for calibration (figs. C.1 and C.2). Luckily, this is the case for the signals of both substances, where in both cases a strong growth of all signals with an increase in concentration arises. So, nine of the ten mentioned positions are suitable for the calibration.

The next point for consideration is whether the presence of the ruthe-

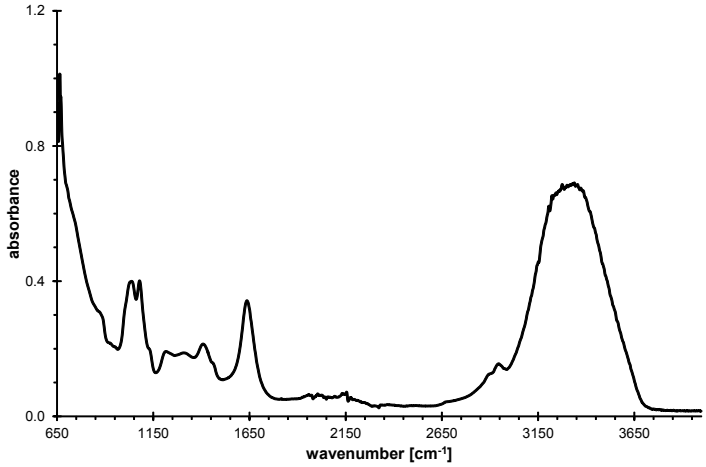

Figure 2.3.: IR spectrum of sorbitol in water as a solvent

nium catalyst interferes with any part of the spectrum. This was tested by comparison of the spectra of one sample with and one without catalyst (fig. 2.4). The results show that although the catalyst should not be detectable by the ATR probe at all, a slight influence in the region of 1200 cm^{-1} can be recognised. Since the influence is not very strong, this region was not excluded from use in the calibration model.

2.5. Quantification model*

From the qualitative analysis of the positions with the highest difference between glucose and sorbitol and the strongest influence of the concentration, the eight identified positions were transferred into the model by choosing calibration regions that enclose these positions. The chosen re-

*Calibration measurements of glucose and sorbitol were carried out by Manuel Noack as part of his research studies.

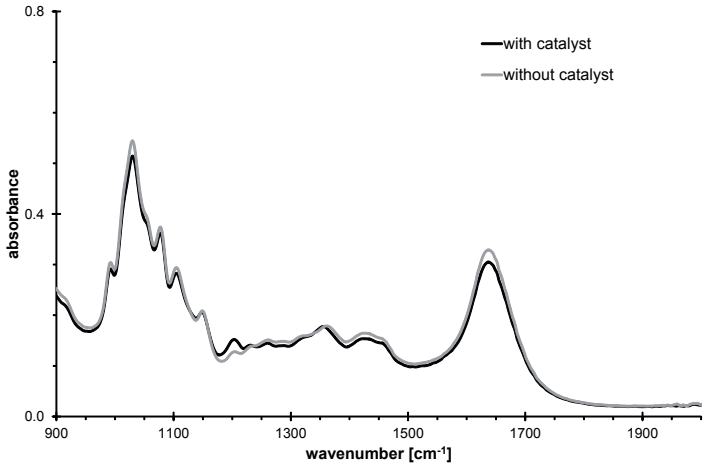

Figure 2.4.: IR spectrum of glucose in water with and without ruthenium catalyst

gions were 832-900 cm^{-1}, 962-998 cm^{-1}, 998-1061 cm^{-1}, 1064-1092 cm^{-1}, 1095-1134 cm^{-1}, 1139-1176 cm^{-1}, 1177-1255 cm^{-1}, 1293-1381 cm-1, 1380-1508 cm^{-1} and
2594-2984 cm^{-1}. These comprise a further two added regions between 999 and 1092 cm^{-1} which do not show such a strong difference, but may none the less be suitable. Calibration regions will not necessarily be included in the final quantification model, but they are the regions that will be considered during the evaluation process. Each of the regions is tested for its influence on the model and then either included or discarded. This also means that the final model can be made up of several or up to all of these regions. The advantage is that such a model with several calibration regions will be better able to describe a complex system with many overlapping signals than a univariate model that is only based on one region and is therefore strongly dependent on the quality of this one region.

For this approach, a quantification method that can incorporate several

regions and that can test all the regions automatically for their suitability is needed. One application is the multivariate Quant2 method implemented in the Opus software (Bruker Optics GmbH, Germany). Within this application, additional options can be chosen, including data pretreatment. For this quantification, the subtraction of a constant offset, the subtraction of a linear slope, vector standardisation, first derivation, second derivation and of course the possibility of no data pretreatment were chosen from the pool of possible data pretreatment strategies. All of these pretreatments offer the advantage of reducing the negative influence of parameters such as the temperature on the spectra. An increase in temperature during the measurement can cause a shift of the baseline of the spectra. If this shift is not corrected by a pretreatment method, it will likely be interpreted as an increase in concentration, because the signal intensity rises. To avoid this, the easiest method is to subtract a constant value off the whole spectrum to compensate the baseline shift. For other influences, the appropriate pretreatment method may be different, which is why several can be chosen to be tested.

For building the quantification model, a basis of 140 calibration spectra with a concentration range of $6.3 \cdot 10^{-5}$ to $2.5 \cdot 10^{-3}$ mol/g for glucose and $1.0 \cdot 10^{-4}$ to $2.4 \cdot 10^{-3}$ mol/g for sorbitol was used. This is a large calibration set, but as a rule of thumb, the number of calibration samples should always be adapted to the number of components in the system and the complexity of the spectrum. Since in this case, there are two components, the calibration set should include more than 100 samples. As already mentioned, a high number of calibration samples always increases the error R^2 when compared to a smaller set of samples because the random scattering that occurs induces a higher error value. Since for the different regions and data pretreatment methods that are tested for this quantification, the calibration set has always the same size, this effect does not have to be taken into account. On the contrary, averaging over more samples should reduce the make the model more reliable by reducing the influence of outliers. To get the most accurate samples possible,

the calibration mixtures were heated to 60 °C and a period of 30 minutes was taken for thermal equilibration. This procedure ensures that the calibration samples are measured under the same conditions that occur during the reaction later on (appendix A.2.1). To reduce the noise of the calibration spectra, a high number of scans per spectrum, in this case 100, is chosen. The quality of the spectra is also enhanced by a high resolution of 4 cm^{-1}. The spectra are recorded from 650 to 4000 cm^{-1} with a scanner velocity of 40 kHz, exactly as for the hydrogenation experiments.

With these settings, the validation of the different quantification options was run. The results appear in order of their cross-validation error, which already gives a good first indication of the quality of the models. Other aspects should be considered, though. The models with the smallest R^2 were therefore further analysed. An important aspect is the number of ranks. This measure indicates how complex the model is and how many factors have to be incorporated into the model to match the calibration data. If this number is very small, it is very likely that some important influences cannot be described by the model, but if it is too large, the model uses factors that do not represent any real influence, an aspect that is well known in model building. Another aspect is the concentration dependence of the deviations between the model prediction and the measurement. If the deviations are caused by random scattering and the model represents all the influences of the system sufficiently, the deviations should not show a trend with concentration, but should be approximately the same size for high and low concentrations.

After careful consideration of these validation aspects, a model including the calibration regions 2594-2984 cm^{-1}, 1177-1255 cm^{-1}, 998-1134 cm^{-1} and 831-900 cm^{-1} and vector standardisation as a data pretreatment was chosen. This model shows a very good correlation between the predicted concentration values and the measurements (fig. 2.5 and table B.1), which also shows in the R^2 of 99.86 %. It includes 8 ranks and shows no concentration dependence of the deviations (fig. 2.6).

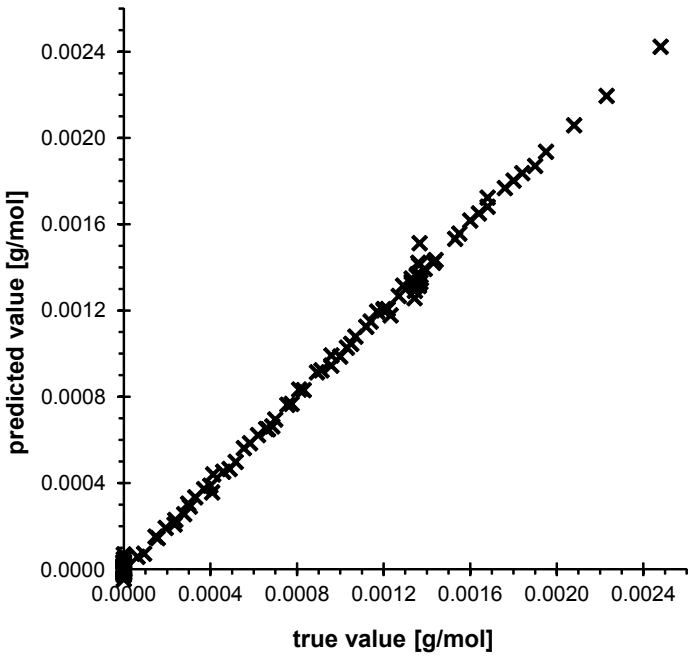

Figure 2.5.: Results of validation, comparison of calibration data (true value) and prediction of the model

2.6. Comparison with reference analytics

The measurement settings of the IR for the experimental monitoring are different from the calibration settings. While the spacial resolution and the scanner velocity were kept the same, the number of scans per spectrum was reduced significantly. This will of course result in a lower signal-to-noise ratio, lowering the quality of the acquired spectra, but the time resolution is increased, which is important for two reasons. Firstly, reaction monitoring with a higher time resolution represents the behaviour of the reaction better and shows the trend even of fast reactions. Secondly, averaging over more data points only gives better results if the composition of the mixture stays constant. In that case, the statis-

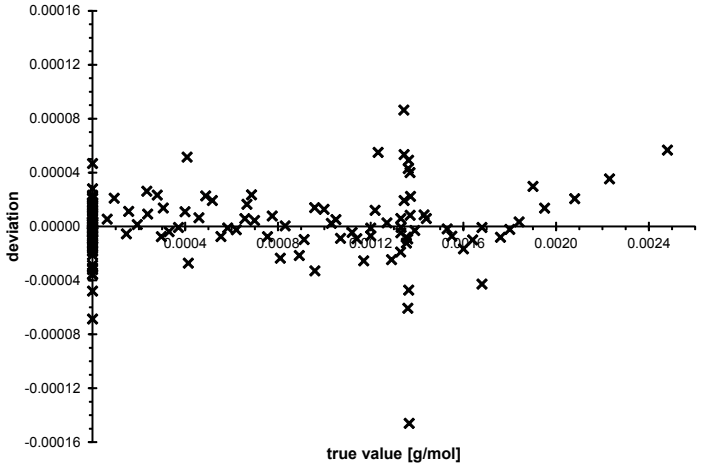

Figure 2.6.: Results of validation, deviation as a function of the concentration

tic error is minimised and the quality of the spectra is enhanced. If the spectra are taken during a reaction, the composition is not constant and the average is taken over different spectra representing different concentration, in which case more scans over a longer time and thus over a wider concentration range will not necessarily lead to a better quality of the spectra, even though the statistical noise is reduced. Consequently, an average over 32 scans, which is equivalent to a measurement time of 0.56 minutes, was chosen. All subsequent hydrogenation experiments were carried out with these settings. After data collection, the spectra were analysed with the described quantification model, which renders concentration profiles of the reaction over time.

To evaluate whether these data correspond to the true absolute values, the simplest method for external evaluation is a comparison of the obtained starting concentrations ($conc_{pred}$) with the amounts that were initially weighed out for the reaction ($conc_{real}$). If the quantification

model works, then

$$\frac{conc_{pred}(initial)}{conc_{real}(initial)} = 1 \tag{2.1}$$

.

Any difference between the predicted and real value results in a deviation from one. This approach makes the comparison of the results for different reactions with different initial concentrations easier, so that an average error of the prediction of the initial value can be calculated. If a similar approach is used for all predicted values over time, then the obtained profiles are no longer concentration profiles, but profiles of the fraction of substrate left, which is in this case linearly dependent on the conversion, because there is no side reaction.

$$\frac{conc_{pred}(t)}{conc_{real}(initial)} = fraction_{glucose} = 1 - conversion \tag{2.2}$$

This approach is especially helpful when working with small substrate amounts. Even if different substrate amounts are weighed in, the results of all experiments stay comparable.

If all the initial values are compared, an average error of 5 % can be calculated. The predicted values from the IR analysis are on average underestimations, but the agreement with the true values is very good and the quantification model seems applicable under reaction conditions.

For a little more detailed external evaluation, the final concentration of each reaction run was compared with a value from HPLC reference analysis. To obtain the HPLC data, the reaction was cooled down and depressurised after a certain reaction time and a sample was taken from the reactor. This was centrifuged, filtered and diluted and then analysed on a precalibrated Nucleogel 810 Ca column. The reactions were stopped after different time intervals, so the final substrate ratios are not the same and cannot be compared with each other, but they can be compared to

the results of the spectroscopy. The comparison of some of the values predicted from IR measurements with the HPLC results shows a smaller deviation than for the initial values (fig. 2.7). On average, the error adds up to 3 %, confirming this first impression.

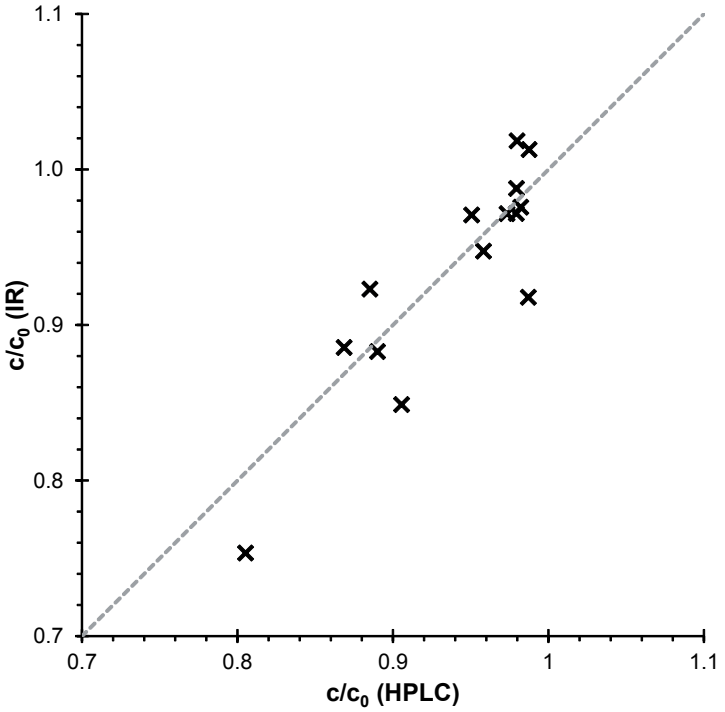

Figure 2.7.: Comparison of HPLC and IR results after different reaction times

In most cases, the IR values lie below the HPLC values, predicting a lower glucose concentration and a higher conversion, but since this is not always the case, the error is not necessarily systematic. In this case, the deviation can either be due to an error in the IR quantification or due to an error in the HPLC measurements. For the initial concentrations,

the weighed amounts can be assumed as true, since they only contain the random weighing error, which is quite small (0.01 %). The HPLC data on the other hand are obtained from a second measuring technique, which can itself have a measuring error and in addition, the samples are pretreated before the measurements, so errors can occur during filtering or dilution. The IR data are just as prone to measuring errors and a systematic error could occur due to temperature effects. If the temperature during the reaction is not exactly 60 °C, but slightly differs, the conditions do not match the calibration conditions, so the predicted values could be overestimated or underestimated. Any or even all of these reasons could lead to deviations, but the good agreement of the final values, especially compared to that of the initial values, makes the quantitative analysis still satisfactory.

To be able to compare a whole reaction profile with an external reference, it is necessary to carry out several reactions and to stop them at different reaction times to obtain samples for the HPLC measurements. If this is carried out and all the data are assembled, an HPLC reaction profile is received. This is a very time consuming method, but will result in reliable reference samples. Even with an amount of 20 individual reactions conducted, the time resolution is at best 0.03 min^{-1}. To make the best use of the samples, the resolution was differed, with more samples being taken in the beginning of the reaction when the reaction rate is higher and less samples taken afterwards, when the reaction rate has already slowed down. Even if carried out accurately and after an exact amount of time, the cooling and depressurising procedure to stop the reaction results in a very vague reaction time. In order to minimise the error, the reaction was slowed down so that a difference in timing results only in a small difference of conversion. That is why the reaction was carried out at 60 °C, 60 bar pressure and a low catalyst loading. Even after 48 hours, none of the reaction mixtures show conversions above 20 %, showing that these conditions really slow down the reaction. The low conversion is not a drawback, since the experiments do not aim at

optimising the reaction conditions, which has already been undertaken in literature, showing that full conversion can readily be achieved after 15 hours. Under these chosen reaction conditions, reproducibility remains the most important factor in order for all the HPLC measurements to make up one true reaction profile. IR and HPLC experiments with the same reaction time were conducted to check if the results are similar. The HPLC results agree very well with a deviation of only 2 % and the IR profiles confirm that the course of the reaction is reproducible as well. On this basis, all HPLC results and an IR profile can be plotted in one diagram for comparison (fig. 2.8).

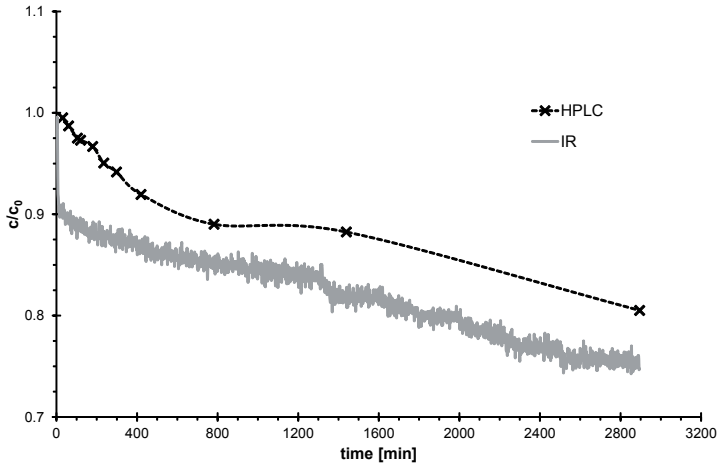

Figure 2.8.: HPLC and IR profiles of the hydrogenation at 60 °C and 60 bar

The graphical comparison shows that the trend of the IR and HPLC measurements is the same. The curve shape that can be deduced from the single point HPLC measurements matches that of the IR profile. The most pronounced difference of the two curves appears right at the beginning of the reaction, where the IR values drop very sharply by about 10 % within 10 minutes whereas the HPLC measurements show a slower de-

crease within about 500 minutes. Afterwards, the deviation between the IR and HPLC values varies less, since the profile shapes are very similar. This is very important because profile shape is a main tool for the kinetic analysis. The drop in the IR measurements may be due to stronger temperature variations subsequent to the pressure appliance. The absolute values can of course also be compared. They show a deviation that is in the range of 8 % and can have the same reasons as already mentioned for the final values. While the error is small and the comparison of the absolute values shows that a quantification based on IR measurements is possible, it should still be kept in mind for further data treatment and is surely larger than for many other analytical methods.

A second set of data points shows a completely different trend (fig. 2.9). In this case, no conversion was detected, neither by HPLC nor by IR. This is very likely due to a deactivation of the catalyst and since both analytical methods agree, these measurements were treated separately. Even in this case, the results match very well and the deviation is small. If carried out online, IR measurements would have the advantage of saving time by showing a deactivation very early on, so that the experiment can be stopped early.

2.7. Parameter influences*

For the measurement of the temperature dependence, two experiments with the same pressure, catalyst amount and substrate amount were carried out, one at 60 and one at 100 °C. This strong difference in temperature should make any effects very apparent. A comparison of the trends should be possible, even if the absolute values are not reliable at 100 °C. The predicted values for the starting points show that even though at the

*Measurements of pressure and temperature dependence were carried out by Claudia Houben as part of her research studies.

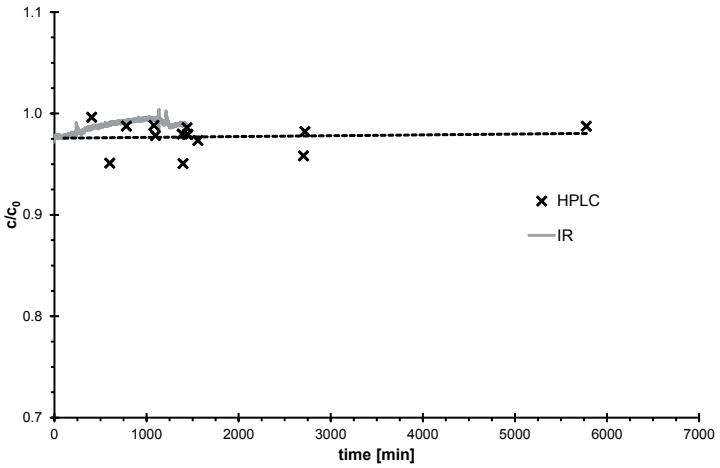

Figure 2.9.: HPLC and IR profiles of hydrogenation (catalyst deactivation)

higher temperatures the deviance from the true initial concentration is higher, it is still only about 8 %, notwithstanding that the quantification model is not calibrated for higher temperatures.

The profiles of the two reactions clearly have very different trends (fig. 2.10). As was to be expected, the slope at 60 °C is less steep and appears almost linear, while at 100 °C, a fast start of the reaction and a subsequent slowing down of the reaction rate after about 400 minutes is apparent. The concentration after 780 minutes is exactly halved for the run at the higher temperature. A comparison of the initial slopes (fig. C.3) as a measure for the reaction rate reveals that the reaction at 100 °C is indeed more than four times as fast with a value of 0.0026 as compared to 0.0006 at 60 °C. Even though this trend matches the expectations, it is less pronounced than kinetic theory would suggest. This might be owed to the deficiencies of the quantification model at higher temperatures. At these conditions, the reaction should reach full conver-

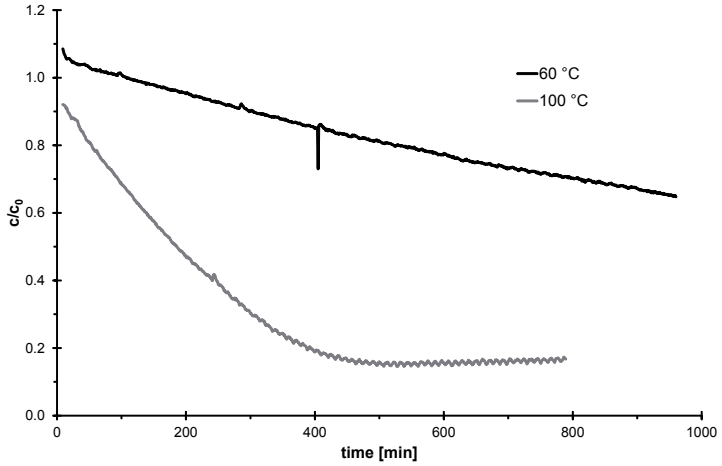

Figure 2.10.: Temperature variation of hydrogenation at 50 bar

sion, but the values after 400 minutes approach 0.16 rather than zero. These values might be overestimated by the model and therefore be too high, resulting in a vertical compression of the profile and hence in an apparently lower reaction rate. The literature values for conversions at similar conditions after 15 hours state a value of 100 %, so no glucose should be left. Clearly, predictions are difficult outside the calibrated temperature and absolute values are not reliable, but the experiments can still give an idea of the trends and of course for more exact measurements, the calibration could be expanded to incorporate different temperatures.

Pressure variations all carried out at the same temperature are more likely to give reliable data, should be comparable and the pressure does not have such a strong influence on the spectra as the temperature. A set of three experiments at different pressures of 50, 70 and 90 bar, all at 100 °C with the same catalyst and substrate amount, were conducted to get an impression of the pressure influence on the reaction. The starting

values differ from the true value by 12 %, which is similar to the temperature experiment. The deviations show no trend with the pressure, so the quantification model seems to be appropriate for different pressures.

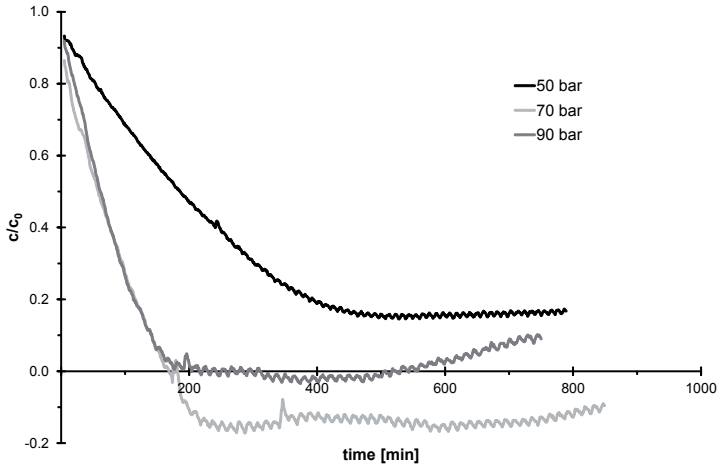

Figure 2.11.: Pressure variation of the hydrogenation at 100 °C

The profiles for all three experiments (fig. 2.11) end at very different conversions, with 16 % glucose left at 50 bar, a value fluctuating around 0 % for 90 bar and a negative glucose content at 70 bar. Theoretically, full conversion with a final glucose content of 0 would be expected, but the high deviations and the negative prediction at 70 bar show that while the general trend is again realistic, the absolute values provided by the quantification method are not dependable. Still, the deviations cannot be associated with the pressure influence, since the values for 70 bar clearly lie below those for 90 bar. So the conversion is not limited by the amount of hydrogen present in the reaction. Since even at the lowest pressure, more than 1.8 equivalents of hydrogen are applied, this was to be expected.

The reaction profiles have a similar shape, but the final value is reached at different reaction times. For 50 bar, it takes about 500 minutes, at 70 bar, the final value is reached after 250 minutes and for 90 bar, even though this is more difficult to define, the time needed is in the range of 200 minutes. So an increase of the hydrogen pressure results in a higher reaction rate and a lower reaction time. This can also be demonstrated by looking at the initial slopes (fig. C.4), which are 0.0026 at 50 bar, 0.0059 at 70 bar and 0.0069 at 90 bar. So between 50 and 90 bar, the slope is more than twice as steep, representing a much faster reaction, too.

There are two possible explanations for an increase of the reaction rate with an increase in pressure. This can have either kinetic or transport reasons. When looking at the kinetics of the reaction, the hydrogen is a substrate and the reaction should become faster if the hydrogen concentration increases. Hydrogen has a very low solubility in water. Values differ between molar fractions of 0.00076 at 50 °C and 60 bar and 0.00151 at 50 °C and 120 bar[42], so at higher pressures, the hydrogen concentration in the reactive phase is indeed augmented. This could lead to an increased reaction speed, but since the effect is only minor, it is not necessarily the reason in this case. Transport could be similarly affected by an increased hydrogen pressure. If the reaction is transport limited, the increased hydrogen supply causes a higher concentration gradient between the gas and liquid phase, which results in a higher phase transfer rate. In this case, the concentration of hydrogen in the liquid phase would be assumed to lie below the solubility limit, because the dissolved hydrogen is consumed faster than fresh hydrogen is transported from the gas phase into the liquid. Since the concentration of hydrogen in the liquid phase is unknown, the acceleration of the reaction cannot be clearly attributed to either effect.

2.8. Summary

The most important result concerning the hydrogenation of glucose is that an IR quantification model could be developed that gives access to information on the fraction of glucose in the liquid phase and accordingly on the conversion.

The model was validated both externally and internally to help to evaluate its dependability. The internal evaluation was based on a cross validation of all calibration samples containing glucose, sorbitol and water at 60 °C. The high R^2 value of 99.87 % confirms that the prediction of the calibration samples is very accurate. The external evaluation was carried out under reaction conditions with HPLC measurements as reference analytics. A comparison of all HPLC results at different reaction times supplemented by the gravimetric starting values with the IR results at the same conditions shows a deviation between 5 and 10 %. This means that the predicted IR values are only reliable as absolute values within quite a large error margin, but they depict the reaction profile very well. In contrast to the HPLC values, they offer the possibility of very high time resolution data acquisition and a much easier handling with less time consumption and no error source due to work-up procedures.

Temperature and pressure variations also showed that although IR measurements are often very sensitive to temperature changes, the prediction is still very good and the deviations of the starting values are in the same range as for the calibrated temperature. The pressure does not influence the quality of the prediction, either. Both demonstrate the robustness of the model, which is especially important for process applications. Overall, this model is the first example of spectroscopic online measurement of a hydrogenation of carbohydrates. Its high time resolution, dependable reaction profiles and good robustness towards temperature and pressure changes encourage hope for a transfer of this method to

similar carbohydrate based reaction systems. For the production of fuels from biomass, this allows a more detailed look at the reaction course and can open up new process windows at conditions which were not analytically accessible before. Apart from the achievement that such structurally and functionally very similar substances can now be distinguished and quantified spectroscopically, the online availability of the concentration data during the reaction renders the adjustment of process parameters during the reaction according to its course and an early abortion in case of catalyst deactivation possible. Both can save time and resources during production and so help to advance the aim of a more sustainable and energy efficient production of fuels.

2.9. Conclusions

For the analysis and monitoring of high pressure two phase reactions, the step from single sample analysis towards *in situ* analytics that was exemplarily carried out for the hydrogenation of glucose is of basic importance. This change in analytical method paves the way for a more detailed look at the reaction kinetics under reaction conditions, but also for online analysis and control of industrial processes.

Especially a look at the pressure dependence of the reaction illustrates the achievements and remaining weaknesses of the analytical method that was employed. Single sample analysis of the reactor content after 15 hours would only show between 0 and 10 % conversion for all settings, but the high time resolution that is possible with *in situ* spectroscopy discloses that the final conversion is achieved after different reaction times, depending on the applied pressure. An analysis of the initial reaction rates also supports this, showing that a pressure increase of 40 bar more than doubles the reaction rate. The reaction time needed for full conversion and the initial reaction rate are important factors for the reaction optimisation and it is therefore a strong advantage of the *in situ* spec-

troscopy that it renders such data accessible.

A deeper look into the pressure variation experiments makes clear where the limitations of this measurement method lie. The dependence of the reaction rate on the pressure can have either of two reasons, an increase in the concentration of dissolved hydrogen and subsequent acceleration of the reaction itself or an increase in the mass transport from the gas phase into the liquid phase and thus a decreased transport limitation. It would of course be important to know whether the reaction is transport limited, but the data available from these experiments are not sufficient for a distinction of the two cases. This is due to the fact that only concentrations of glucose in the liquid phase are available. In order to find out if there is a transport limitation, concentration data of the dissolved gas in the liquid phase are necessary. If this data shows that the hydrogen concentration is constantly low during the reaction and only increases after full conversion is achieved, this strongly suggests a transport limitation, where the hydrogen is consumed quicker than it can be refurbished by transport from the gas into the liquid phase. In this case, if the hydrogen pressure is increased, the hydrogen concentration in the liquid stays low as long as the reaction is faster than the transport. If on the other hand, the reaction is not transport limited, the hydrogen concentration in the liquid phase should always match the solubility of hydrogen in water at the applied conditions.

To sum up, in order not only to monitor the course of the reaction, but to understand how it is influenced, additional information would be needed. This can be achieved either by replacing or by supplementing the applied analytics by a technique that can measure the dissolved hydrogen without losing information about the conversion. Either approach will necessitate a further modification of the reactor set-up and so result in an assembly that is not quite as similar to the single sample measurement arrangement, but that is more flexible to incorporate any required analytical techniques.

3. Hydrogenation of glucose: combination of mIR and Raman in the liquid phase

3.1. Context

As was illustrated in the previous section, every component of a high pressure two-phase reaction should be detectable in at least one of the phases. For the monitoring of the hydrogenation of glucose with mIR, this was not the case for hydrogen. Its concentration is neither detected in the gas phase, nor in the liquid phase. The use of alternative or additional analytical techniques can present a solution in such cases, if an appropriate technique for the analysis can be found. In two-phase reactions, the analysis of each component can be carried out in either phase, since the concentration values for the other phase can be calculated. So if a measuring technique for all components in one phase can be established, the whole two-phase system can be comprehensively characterised with this one technique. The implementation of only one technique leads of course to lower costs and a simpler installation. Depending on the components in the system, this is not always possible.

For the hydrogenation reaction, a possibility for the simultaneous analysis of all components with one technique is Raman spectroscopy. If the hydrogen content is measured in the liquid phase, the carbohydrates present in the aqueous phase can be monitored simultaneously with the

same probe[43]. Even though Raman spectroscopy is more difficult to handle and more affected by turbidity due to scattering, it benefits from the lower sensitivity towards water.

The test run will show whether Raman is suitable for the comprehensive monitoring of the reaction. If this is the case, then future experimental analysis can be based on Raman alone, suspending the need for additional mIR analysis. Ensuing experiments can then clarify the role of mass transport from the gas to the liquid phase and the limitations of the reaction.

3.2. Introduction

The adoption of Raman spectroscopy affords many advantages for the analysis of the hydrogenation system when compared with IR. In the first place, Raman is far less sensitive to water and since the reaction is carried out in aqueous phase, this means a major benefit. Due to this lower sensitivity, the technique has the potential to give better quantitative data for the carbohydrate concentrations, since their signals are more distinct when not overlapped by the water signals. In consequence, the choice of quantification method is not as restricted and good quantification results can be obtained with a lower number of calibration samples. These two facilitations were exploited for the quantification of the glucose and sorbitol concentrations with Raman, where an IHM rather than a multivariate method was chosen. The number of samples was subsequently reduced to six, which is high enough to get a first impression of the reaction course when working with this model and less complex spectra. Apart from this reduction of required calibration and quantification work, the use of Raman offers the second advantage that hydrogen can be detected by this method. While hydrogen does not possess a changing dipole moment and is therefore IR inactive, it shows a changing polarisability, leading to its Raman detectability[44]. Litera-

ture studies show that even small amounts of gaseous hydrogen of about 2 % at ambient pressure can be detected [45], so the concentration of the hydrogen dissolved in the aqueous phase may indeed be monitored qualitatively. The feasibility of the hydrogen detection is of course dependent on several factors, some of which cannot be influenced within the scope of this study. The intensity of the hydrogen signal is a function of the excitation energy of the employed laser light. The signal intensity also depends on the hydrogen concentration. For a good signal-to-noise ratio, these factors are completed by the detection time. While the radiation density of the laser is defined by the apparatus, the hydrogen concentration and the detection time are limited by the reactive system. The hydrogen concentration is determined by the pressure that can be applied to the set-up, which was in this case 30 bar. The detection time defines the time resolution of the analysis, so it has to be adapted to the reaction speed, as demonstrated for the IR measurements before.

Information on the hydrogen concentration could help to elucidate the reason for the pressure influence observed in the previous experiments and whether the reaction is transport limited, which is why the use of Raman is so promising. Still, if additional Raman analysis is implemented, the reactor set-up will have to be altered. This alteration will cause an increase in reaction volume to provide enough space for two different spectroscopic probes. As already mentioned, the installation of the Raman probe necessitates a pressure reduction, so the results will not be quantitatively comparable to the previous results. Also, it is not yet clear if hydrogen can be detected under the chosen conditions and with the available settings.

So this section will investigate whether the analysis of the hydrogenation can benefit from the application of Raman spectroscopy and whether this will enable the comprehensive monitoring of the reaction.

3.3. Outline

As for the analysis of the IR measurements, an intensive study of the spectra of glucose and sorbitol will be carried out for Raman, too. This includes a comparison of the positions of the signals with the highest intensity to see if the two substances can be distinguished spectroscopically. Again, the data of both substances are gained in water as a solvent. Although the water signals are much less pronounced for Raman, they still have to be considered when choosing the integration areas of the quantification model. The same holds true for the catalyst signals, which will be checked for in a separate step. The areas will be adjusted to include the main signals of glucose and sorbitol and exclude the main disturbances. After the integration areas are established, the model peaks for the IHM will be fitted to the component spectra. The subsequent calibration will be based, as already mentioned, on only 6 calibration samples and on a ratiometric method. This will lead to a rough quantification model, but will be sufficient for a first impression of the reaction course obtained from Raman measurements.

After the quantification model is built, it will be applied to a reaction run of the hydrogenation of glucose. This reaction will also be analysed by IR spectroscopy at the same time, so that this data can be used as a reference. This is possible since the IR data have already been evaluated in the previous section and have been shown to supply reliable concentration information. The reaction profile will then be compared with the profile gained from IR measurements to see whether the shapes match, the absolute values agree and which method delivers the best quality data.

Additionally, the obtained Raman *in situ* spectra of the hydrogenation can be analysed in more detail to determine the influence of hydrogen on the signals. Since no hydrogen pressure is applied for the calibration spectra, this is the first set of data for which the state before and af-

ter pressurisation, so with and without hydrogen in the system can be compared. Special focus will be given to the area that was described as characteristic for the hydrogen signal in literature. This evaluation will settle whether hydrogen can be detected under the applied conditions and whether the system is comprehensively characterisable by Raman spectroscopy, which could open up new conclusions on the limitations and transport behaviour of the system.

3.4. Comparison of spectra

The Raman spectrum of pure water consists mainly of the strong stretching signals ν(OH) above 3000 cm^{-1} and the intermolecular librational modes between 200 and 300 cm^{-1}. The bending signal δ(OH) at 1600 cm^{-1} is smaller. To exclude these signals from the calibration, the integration areas were limited to 300 to 1000 cm^{-1} and 2600 to 3020 cm^{-1}. This will reduce any influence of the water to a minimum.

With this knowledge about the water spectrum, the spectra of the components dissolved in water can be analysed. For glucose (fig. 3.1) with a concentration of $1.45 \cdot 10^{-3}$ mol/g, the most distinct signal is a doublet at 2780-3020 cm^{-1}, which is not overlapped by any other signals. This spectral region is dominated by ν(CH) and ν(OH) signals. The region 300-1515 cm^{-1} is composed of many sharp peaks. The region above 1000 cm^{-1} is excluded from the quantification model, but the triplet at 477-557 cm^{-1} caused by skeletal vibrations of δ(CC) and δ(CO), the broader band at 855 cm^{-1} and the doublet at 882-946 cm^{-1} which can most likely be attributed to ν(CC) vibrations are within the integration range.

The spectrum of sorbitol (fig. 3.1) with a concentration of $1.46 \cdot 10^{-3}$ mol/g is very similar to that of glucose, the region at 2780-3020 cm^{-1} is again dominated by a strong doublet signal. The two peaks have nearly the same height, with the peak at 2946 cm^{-1} slightly

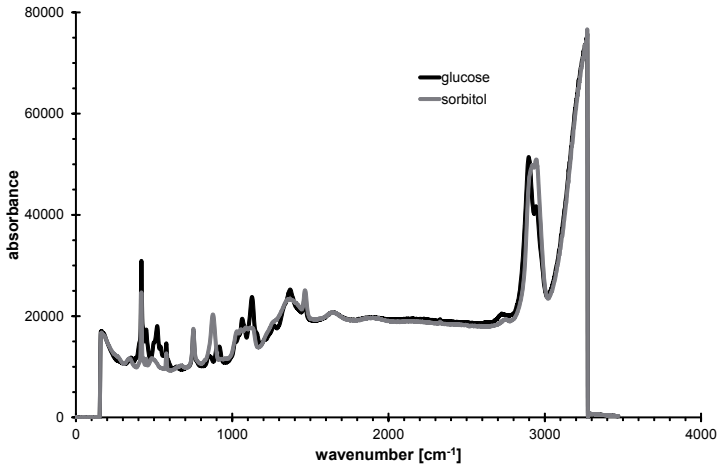

Figure 3.1.: Raman spectra of glucose and sorbitol in water as a solvent

above that at 2920 cm^{-1}, whereas the glucose signal at lower wave numbers of 2896 cm^{-1} is much higher than the peak at 2945 cm^{-1}. So with increasing sorbitol content, the peak at lower wave numbers should diminish while the peak at higher wave numbers grows. Again, the region between 300 and 1515 cm^{-1} shows many distinct peaks. The only peak that does not appear in the glucose spectrum and which is therefore characteristic for sorbitol is located at 875 cm^{-1} and can be attributed to ν(CO) stretching.

By analysing the concentration dependence of the glucose and sorbitol spectra (fig. C.5), the positions at 477-557 cm^{-1}, 875 cm^{-1} and 2780-3020 cm^{-1} are identified as the regions with the largest deviations. They will probably contribute most to the quantification of the two substances.

In a last step, the influence of the catalyst on the spectra was verified. The comparison of glucose spectra with and without the presence

of ruthenium reveals a very broad signal between 1840 and ca. 2500 cm^{-1} with a low intensity (fig. 3.2). There are no other signals detectable and since this area is not included in the integration range, the presence of the catalyst does not pose a problem for quantification. The whole defined integration range of 300 to 1000 cm^{-1} and 2600 to 3020 cm^{-1} can be used for the model building.

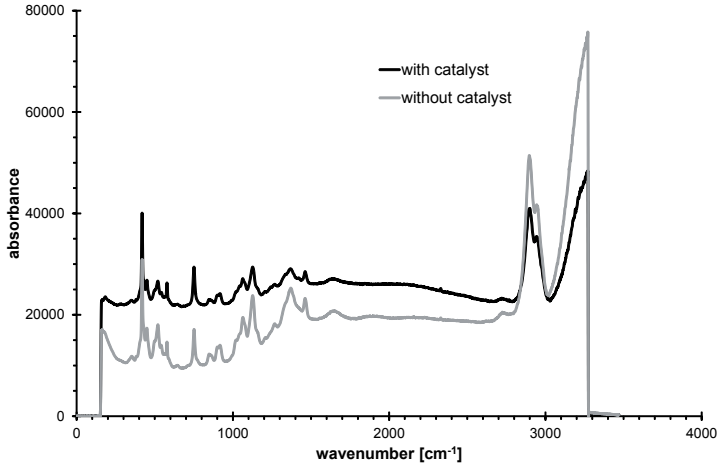

Figure 3.2.: Raman spectrum of glucose in water with and without catalyst

3.5. Quantification model

For IHM, the quantification process is not as dependent on the choice of the integration area as for the multivariate model, but is strongly influenced by the peaks used fitting the model to the spectra. The main parameters are the peak type, the peak amplitude and half-width at half maximum, the peak positions and the number of peaks.

Each mixture component was first modelled separately, but all models were based on a linear baseline and pseudovoigt type peaks. The model for water contains eight peaks, since it models the simplest spectrum. For sorbitol, nine peaks were used during fitting and for glucose, 16 peaks are necessary to simulate the original spectrum satisfactorily. The number of peaks is always chosen to accommodate each existing signal of the original spectrum in the model but to avoid fitting noise or unspecific signals. During this process, the root mean square (RMS) residuals are a measure of how well the model fits the spectral data. With eight peaks, the final model for water shows an RMS residual value of 1116, but the residuals for glucose with 16 peaks of 301 and for sorbitol with nine peaks of 357 are much smaller. Since water will not be quantified later on, this is a sensible approach to keep the final model as simple as possible. As an additional aspect, the distribution of the residuals over the spectral range should be considered (fig. 3.3). If the residual value is significantly higher for one region, it is highly likely that a signal of the original data is still unfitted. If on the other hand the residuals show a uniform distribution, the main signals are probably already incorporated into the model.

The final quantification model is made up of all three component models and the integration ranges determined by comparison of the spectra are transferred to the mixture model. The following calibration is based on the mentioned six spectra with different glucose and sorbitol fractions. The combined total molar amount of glucose and sorbitol is not varied in this calibration and the water amount is kept constant. This means that only the fractions of glucose and sorbitol are calibrated in the model. Neither the water content nor the absolute concentrations of glucose and sorbitol are calibrated and so they cannot be predicted later. This leads to a ratiometric model. The advantage of this approach is that with a low number of calibration samples, the adopted simplifications and additional information of the boundary conditions can help to still provide a satisfactory model. The concentration of water does not

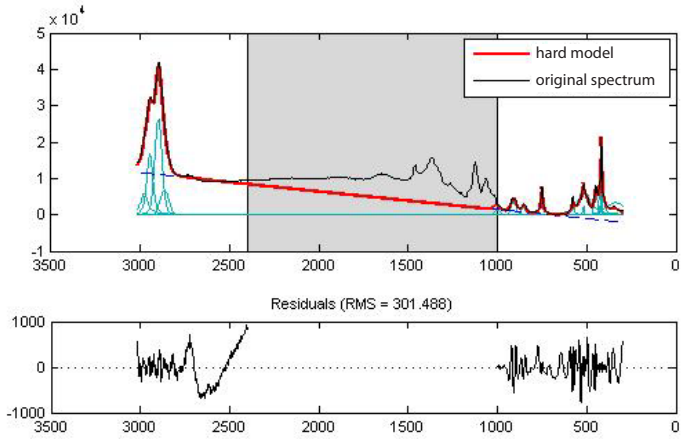

Figure 3.3.: IHM data of glucose including residual plot (bottom)

change during the reaction, so this information is less important and can conveniently be discarded in favour of more essential data. The same holds true for the absolute concentration values. Since the reaction is known to produce no side or secondary products, the sum over the molar amounts of glucose and sorbitol can be assumed to be constant, allowing a ratiometric calibration method to be employed.

With this rough calibration, an error value R^2 for the cross validation of 97.69 % is achieved. This is an acceptable error for a quantification model based on a small calibration set and should deliver reliable results for the *in situ* reaction monitoring.

3.6. Comparison of IR and Raman results

The Raman measurements of the hydrogenation reaction at 60 °C and a pressure of 33 bar (appendix A.2.1) were analysed with the IHM quantification model. The settings for the *in situ* measurements were exactly the

same as for the calibration spectra, since these showed good intensities of the signals. The time resolution was adapted to the reaction course, with a higher resolution at the beginning of the reaction, where a fast conversion can be expected, and a lower resolution towards the end of the reaction, where the change in concentration per time is expected to be smaller.

The first data point taken at room temperature gives a value of 0.98, which corresponds to a deviation of 2 %. This suggests a very good quality of prediction and is a good reference point, since the composition of the mixture before the start of the reaction is well known. When the reaction mixture is heated during the first 40 minutes without addition of hydrogen, the predicted fraction of glucose drops to about 0.89 (fig. 3.4). This behaviour of the quantification method can be attributed to the fact that the calibration spectra were recorded at ambient conditions and therefore only give accurate results at these conditions. If the temperature is set higher, the spectra are influenced and the method predicts lower glucose values, even though no reaction has actually taken place yet. If absolute conversion values are required, the calibration will of course have to be adapted by adding calibration samples recorded at the reaction temperature. In the present case, only the curve shape of the reaction profile will be considered and compared later on to that of the IR measurements.

Since the reaction only starts when hydrogen is added to the system, the time at this point was set to zero, creating a common time axis for both spectroscopic methods. From the point of hydrogen addition, the glucose fraction predicted by the Raman data stays almost constant. Starting from an average value of 0.89, the glucose content decreases only to about 0.83 during nearly three days of hydrogenation. Within the assumed error range at elevated temperatures, this data could indicate very low conversions or no conversion at all. Both scenarios are possible. Very low conversions could be owed to the much lower pres-

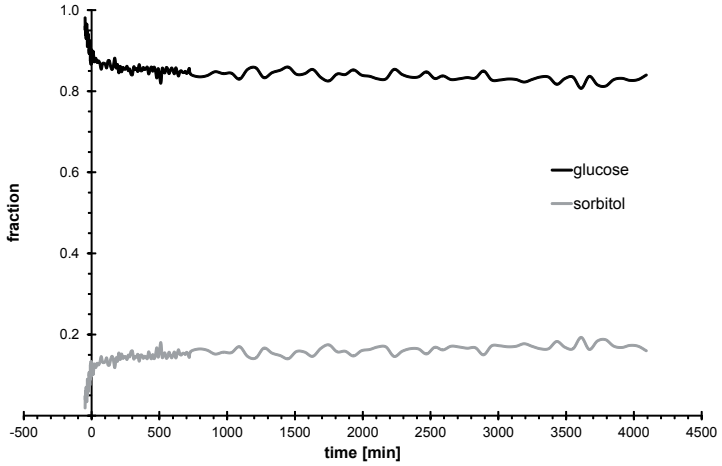

Figure 3.4.: Raman profiles of glucose and sorbitol during the heating period and hydrogenation at 60 °C and 33 bar

sure compared to standard experiments. Together with the low reaction temperature, this leads to a slow reaction and a high moiety of glucose in the reaction mixture. The absence of any conversion could be caused either by a deactivation of the catalyst or by the fact that the conditions are too mild.

To find out if this trend predicted by the Raman quantification method can be confirmed, the IR results are consulted. These can be applied as reference analytics since they have been previously confirmed by comparison with HPLC. The IR results show no conversion for this reaction run either, they even overestimate the glucose content to give fractions higher than 1 (fig. 3.5). So the Raman reaction profile seems to be predicted correctly by the Raman quantification method.

Even though no conversion is achieved in this reaction, the results still give important information on the behaviour and reliability of the Raman

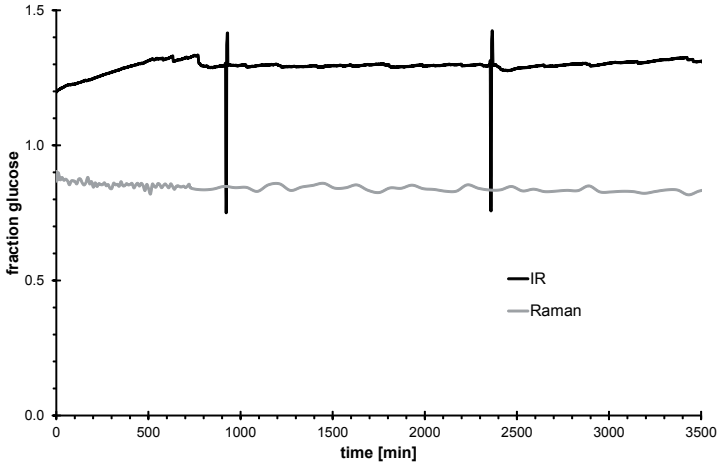

Figure 3.5.: Comparison of IR and Raman profiles of glucose during hydrogenation at 60 °C and 33 bar

data. In addition to the strong temperature dependence that can be observed during the heating period, the reaction course can be predicted by the Raman quantification method and matches the prediction of the IR quantification method. Both profiles show little noise and Raman has the additional advantage that no external cooling is necessary, so that the signal is not influenced by the cooling peaks as is IR. These are very promising results, illustrating that Raman has a high potential for the monitoring of carbohydrate hydrogenations and can possibly deliver even better results than IR if the calibration set is expanded and recorded at the reaction temperature.

3.7. Hydrogen detection

After 40 minutes, the reaction temperature of 60 °C is reached, so that the spectra are not influenced by the increasing temperature any more. To find out if hydrogen dissolved in the aqueous phase can be detected

by Raman spectroscopy, a spectrum from this stage in the reaction is compared to one recorded just after the addition of hydrogen. In both cases, the temperature is the same and the conversion should be negligible. If a difference between these two spectra is found, this should be solely due to absorptions caused by the hydrogen.

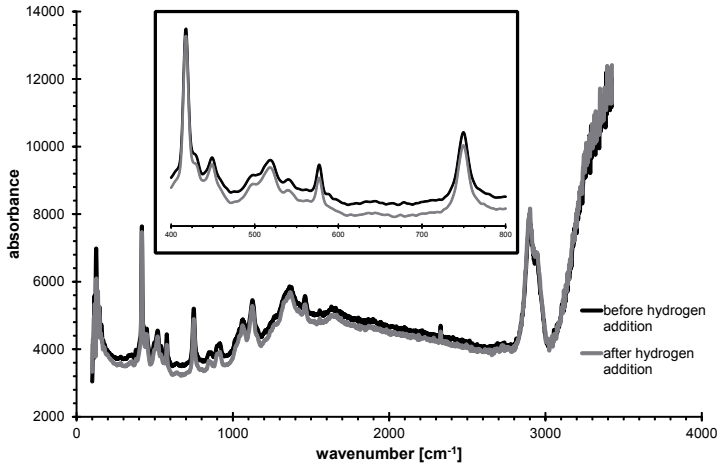

Figure 3.6.: Raman spectra before and after hydrogen addition

Unfortunately, no deviations of the spectrum after hydrogen addition from that before hydrogen addition can be identified (fig. 3.6). The spectra both show only the characteristic glucose signals. Special attention was given to the area around 600 cm^{-1}, because literature reports that the most intense rotational hydrogen signal can be found here[46,47]. Again, no deviations are observed, leading to the conclusion that the hydrogen which is dissolved in the water cannot be detected at the used conditions. A comparison with the measurements carried out in literature shows that hydrogen detection at low concentrations and ambient pressure was only realised in the gas phase, whereas the signals are significantly broadened in the case of dissolved hydrogen in water and are therefore far more

difficult to distinguish. Detection of hydrogen dissolved in water was achieved at higher pressures of 138 bar and very long scanning times of six hours. Even at these conditions, the peak width adds up to more than 150 cm^{-1}. Such a broad signal is very probably not distinguishable if the intensity is lowered significantly. The reaction conditions for the hydrogenation of glucose feature a pressure reduction of more than four times and a scanning time reduction of more than 700 times compared with the literature experiments, which illustrates well why the detection was not successful for the present reaction. Only a significant pressure rise can increase the solubility of hydrogen in water, and therefore its concentration, sufficiently to enable reaction monitoring with an acceptable time resolution. The required pressures would clearly necessitate a more sophisticated set-up and equipment including probes that can withstand these conditions. Within the scope of the present work, this was unfortunately not feasible.

3.8. Summary

The analysis of the Raman spectra of glucose and sorbitol showed that the two substances can be very well distinguished spectroscopically. Since all spectra were recorded in water as a solvent, the main absorption areas of water were excluded from the integration range, but because water has far weaker absorption in the Raman spectrum than in mIR, most of the characteristic carbohydrate signals are not overlapped by the water signals and can be used for analysis. Within the integration range that is left, the signals and deviations of the signals of the two sugars are far more distinct than in the IR spectrum, which facilitates the quantification and allows the use of an IHM instead of a multivariate method. The obtained error value R^2 of 97.69 % could be achieved with only six calibration samples and the use of a ratiometric calibration.

The analysis of an *in situ* hydrogenation showed that the quantifica-

tion method delivers realistic values that match the observations gained from the IR analysis, but the absolute values for glucose are underestimated due to the temperature increase that was not considered in the calibration. A more detailed calibration could lead to a quantification that is superior to the IR technique, since the spectral differences between the sugars are more distinct and the temperature effect on the spectra is not as strong as was expected. Raman can therefore be regarded as an alternative to IR for the sugar quantification.

To find out if Raman can bring the additional advantage of detecting the hydrogen component that is dissolved in water and is the only substance that could not be detected before, the spectra of the reaction mixture before and after addition of 30 bar of hydrogen were investigated. Even a more detailed examination of the main hydrogen absorption area at 600 cm^{-1} yielded no recognisable deviations between the spectra, leading to the conclusion that with the given settings for pressure and scanning time hydrogen cannot be detected by Raman spectroscopy.

All in all, Raman spectroscopy is a good alternative to IR for the analysis of carbohydrates and because the obtained signals are very distinct and less perturbed by the water signals, it might even be a better choice if a further calibration can increase the quality of the absolute values. Still, it does not add any extra information concerning the hydrogen concentration in water and so the comprehensive monitoring of all components of the reactive two-phase system is not possible with this set-up.

3.9. Conclusions

The combination of mIR and Raman in one set-up is generally desirable because the two methods give complementing information of the vibrational behaviour of molecules. In many cases, groups and molecules that are IR inactive are Raman active and the other way around, so

the combination of both gives a more complete picture. This also holds true for hydrogen, since it is not IR active, but has been shown to be detectable by Raman. Supplementing the existing IR measurements by Raman could therefore give more information on the system and help to understand transport limitations.

For the presented reaction conditions, the detection of hydrogen is not possible, but implementation of Raman still proved helpful for a better analysis of the product and substrate in the liquid phase. Raman often suffers from a higher noise level in the spectra and needs higher detection times, making it less applicable for the monitoring of fast reactions, but in this case, the benefit of a much smaller disturbance by the water signal outweighs this handicap. The sugar signals have a higher intensity and are much more distinct than in the IR spectra. Raman might therefore be used to develop a quantification method with much higher quality.

For the development of a more comprehensive analytical two-phase reactor design, the combination of the two spectroscopic methods provides no progress since one component of the system is still undetectable. No further advance to the understanding of the pressure influence and the transport effects in the system can be made on the basis of the gained data. With this analytical method, only a strong increase in hydrogen pressure could render the detection of hydrogen possible. Alternatively, a different analysis has to be applied, but the choice of hydrogen detecting systems is very limited. In both cases, the set-up would have to be changed significantly.

With the available means, the alternative is to switch to a different reactive system in which all components can be detected with the techniques and under the conditions applicable in this set-up. This approach will be pursued in the following chapter, where a different reactive system will be introduced into the modified existing set-up to verify the concept of a comprehensive quantification of all compounds of a two-phase high

pressure reaction.

4. Switchable solvent synthesis: two-phase analysis towards a total mass balance

4.1. Context

The analysis of all the systems described before suffers from a lack in information, especially on the gaseous component of the reaction. Even if the dissolved gas can be detected and quantified in the liquid phase, this would not remedy the complete void of knowledge concerning the composition of the gas phase. In the presented examples as well as in literature, the gas phase is mostly characterised by pressure measurements, which have the advantage of being easily integrable and requiring simple equipment. The downside is that any pressure change cannot be ascribed directly to one event in the system, because it can have multiple reasons. The pressure in the gas phase consists of the partial pressures of the solvent and all liquid substrates as well as the gaseous substrate. When a pressure change is observed, its cause can be the drop of any of the partial pressures and can therefore be reaction or temperature related. In short, a pressure decrease is not necessarily connected to the consumption of the gaseous substrate by the reaction and the information cannot be used for gaining kinetic information without the consulting of additional data.

The compositional analysis of the gas phase seems therefore desirable and will be implemented into the existing set-up. This will be combined

with a complete analysis of the liquid phase including the dissolved gas. The collected data will then be quantified and used to create a total mass balance of the reactive system. From this mass balance, information on the depletion of the substrates and the transport processes between the two phases can be extracted. Additionally, the area in which the mass balance is valid can be identified, which does not include fast reactions with low pressure or low stirring rates. The influencing parameters and reasons of the concentration fluctuations that disturb the mass balance can be analysed and explained, helping to create a more complete picture of the processes occurring in the reactor.

4.2. Introduction

Solvents are frequently used to facilitate chemical reactions. After the reaction is completed, they are often removed from the product by distillation. Due to the high energetic demand of distillations and their resulting negative environmental impact, an alternative separation technique would be very favourable. Currently, switchable solvents and membrane processes are the most promising candidates for a more energy efficient coupling of reaction and separation. Switchable solvents offer new possibilities for a "greener" process design. Their ability to readily switch between different solvent properties can eliminate the need for a solvent separation by distillation. Switchable solvents have therefore received growing attention in the past decade, both in academia and for industrial applications[48–50].

The concept of solvents with switchable properties was first reported in 1989, when the reversible reaction of the gases dimethylamine and CO_2 to a liquid carbamate and its potential use as solvent and extraction medium were described[51]. In 2005, the reaction of an amine and an alcohol with CO_2 to an IL presented the first fully liquid switchable solvent system[52], with CO_2 as a switch. The development of one-component

switchable solvents[53] and chiral systems[54] followed. Current publications mostly focus on exploiting the wide range of applications from extractions[49,50,55,56] to coupled reaction and separation tasks[57].

The synthesis of a two-component switchable IL[52,58] from 1,8-Diazabicyclo[5.4.0]undec-7-ene (DBU), 1-hexanol (hexanol) and CO_2 (fig. 1.5) was chosen as a case study of a reactive multiphase system. The reaction is reversible and can be carried out at room temperature under CO_2 atmosphere. An equimolar mixture of DBU and hexanol reacts with CO_2 to form the $[DBUH][O_2CO(CH_2)_5CH_3]$ IL. This switch from molecular liquid to IL affects many solvent properties such as polarity, conductivity and viscosity. The advantage of this switchable solvent for applications is that the reaction can be easily reversed by treatment with inert gas or mild heat, so that the system can be used for separation processes[57]. Due to the reversible nature of the reaction and the strong dependence on temperature and pressure, it is necessary to use an *in situ* analysis under reaction conditions to monitor this reaction. The use of CO_2 as a gaseous substrate has the benefit that it is IR active and can be easily monitored in the gas phase as well as in its dissolved form. The substrate mixture and the IL show intense signals in the IR spectrum that overlap only slightly. So all substrates and the product are very well detectable with the same spectroscopic method.

A disadvantage for the monitoring of this reaction is that it is a very fast reaction, so the time resolution of the spectroscopic measurements has to be kept as high as possible and transport limitations become more likely. So this work will have to show if a total mass balance can be achieved for this reaction and at which conditions this mass balance is valid.

4.3. Outline

A detailed analysis of the spectra of all components of the reaction mixture will be used to identify the positions of highest deviation. Since the reaction is carried out solventless, the intensity and concentration dependence of the signals will be much stronger, making the calibration and subsequent quantification easier and again allowing, as demonstrated for the Raman measurements, an IHM approach for the substrates and the product. CO_2 has a sharp and non-overlapped signal, so its content will be quantified separately by a simple univariate method.

The next step will be to show on a model system of CO_2 and hexanol how quantitative concentration data can be obtained for CO_2 in both gas and liquid phase and how these can be used to establish a total mass balance. This simple absorption system can act as a first test for the CO_2 quantification before a more complex reaction with an increased number of species can be tackled.

Afterwards, the same approach will be applied to the two phase IL synthesis reaction of DBU and hexanol with CO_2 as an example of possible applications. In this system, all components will be quantified and the CO_2 mass balance includes an additional term of the CO_2 that is incorporated in the IL. For this reaction, a total mass balance will be carried out and checked for its validity.

Since performed experiments at low stirring rates and low pressures suggest that the mass balance the time scale of the switch is dominated by transport limitations, mainly due to the high viscosity of the formed product that hinders good contact between the CO_2 and the substrates, this aspect will be enlightened further. The first aim will consequently be to find out which limitations influence the reaction time. Afterwards, the different reaction parameters and their effects will be analysed and assembled in a parameter map. This allows improving the reaction con-

ditions and predicting the behaviour of future experiments. Finally, to understand not only how, but why certain parameters influence the synthesis reaction, a descriptive model for the parameter dependence will be developed.

4.4. Comparison of spectra and quantification

An IR spectrum of dissolved CO_2 in hexanol (fig. 4.1) shows the strong C=O stretching vibration at 2330 cm^{-1} of CO_2 and the bands of hexanol which do not superimpose this area, so that it is suitable for a univariate integration method. The same is true for the reactive system.

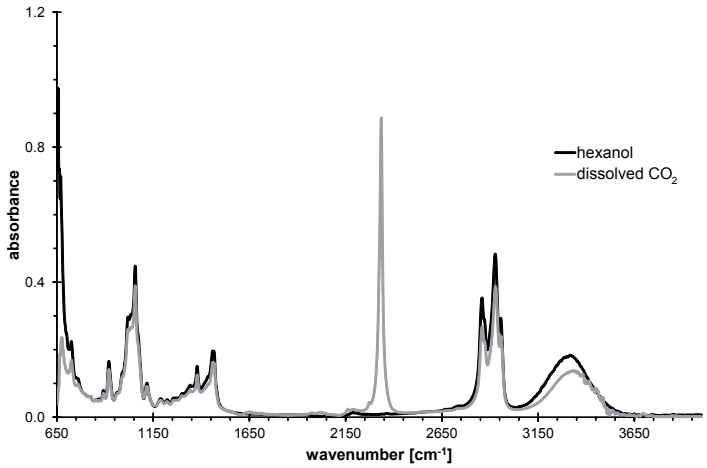

Figure 4.1.: IR spectra of hexanol with and without dissolved CO_2

The bands of the substrate mixture containing DBU and hexanol on the other hand are largely superimposed by the bands of the IL, due to their similar structure and resulting vibrations (fig. 4.2). The most prominent absorption bands of hexanol are a broad O-H signal at

3300 cm^{-1} and the multiple C-H signals between 2800 and 3000 cm^{-1}. The latter are overlaid with the C-H bands of DBU between 2700 and 3000 cm^{-1}. Apart from these and the multiple signals in the fingerprint region between 800 and 1500 cm^{-1}, DBU shows a strong C=N absorption band at 1610 cm^{-1} which is only partly superimposed by the band of the IL at 1630 cm^{-1}. The latter signal is comparable to literature data[58]. The IL shows a second characteristic signal at 1270 cm^{-1}, but because it lies in the fingerprint region, it is superimposed by many DBU and hexanol signals. Therefore, an IHM model rather than a univariate method was chosen for the analysis of the composition of the liquid phase.

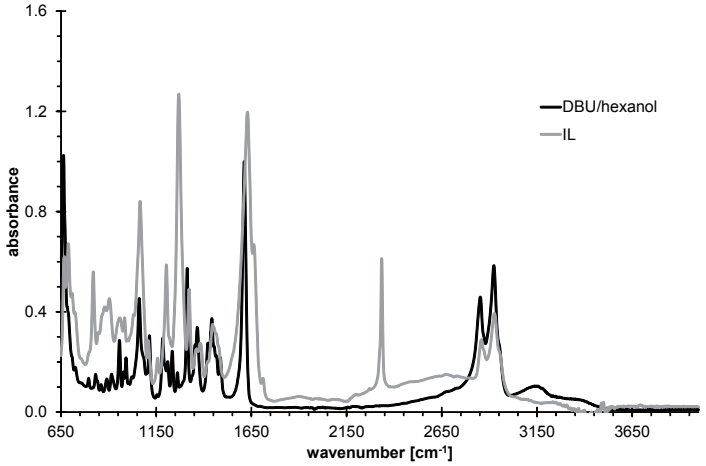

Figure 4.2.: IR spectra of a DBU/hexanol mixture and the IL with dissolved CO_2

The CO_2 quantification is based on a calibration set of 26 samples with concentrations between 0.08 and 20.56 mol/L. The integration is carried out from 2225 to 2500 cm^{-1} with a baseline based on four interpolation points at 1800-2700 cm^{-1}. The method is applicable to gaseous CO_2 as well as dissolved CO_2 present in the liquid phase. The detection limit of

CO_2 in the gas phase is below 1 bar. The validation gives an error R^2 of 99.99 %.

The IHM model for the prediction of the DBU/hexanol mixture and the product concentration is based on a spectral range of 778 to 2000 cm^{-1} and a calibration set of 104 samples. As the reaction is carried out neat, molar fractions of the components were calibrated for the whole range from 0 to 1 with an error R^2 of 64.23 %.

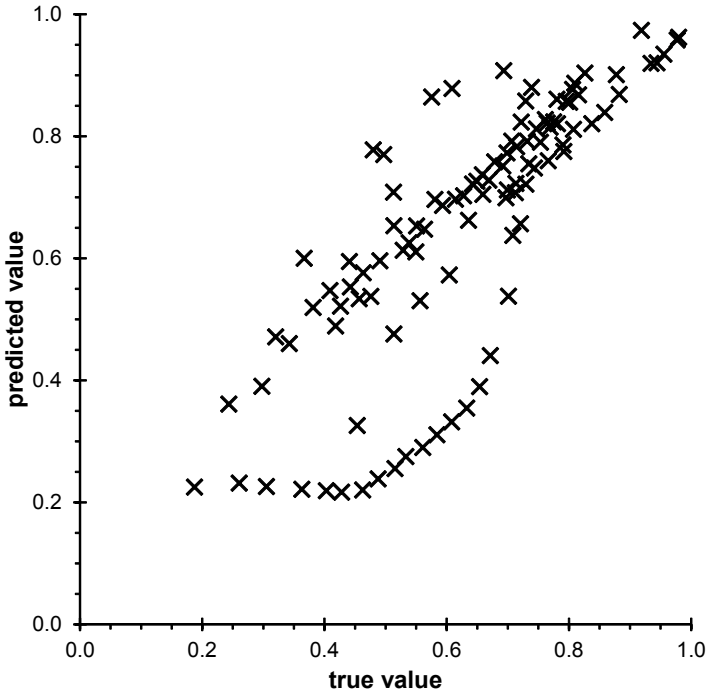

Figure 4.3.: Results of IHM validation, comparison of calibration data (true value) and prediction of the model

A parity plot of the predicted and true molar fraction values (fig. 4.3) shows that the comparatively low coefficient of determination is mainly

due to the high scattering of the calibration measurements rather than the quality of the model.

4.5. Model system: absorption of CO_2 in hexanol

As a non-reactive model system, the dissolution of CO_2 in hexanol was investigated and a total mass balance of CO_2 was formed. The concentration of CO_2 was measured with mIR both in the gas phase and in the liquid phase. The major advantage of this system is that a known volume of hexanol is pressurised with CO_2 and no reaction takes place. Accordingly, the concentration of CO_2 in the liquid can be compared to literature data for the solubility and the concentration in the gas phase can be compared to the recorded pressure. The sum over both phases should stay constant over time. This makes it easy to check the correctness of the quantification method via the mass balance.

A qualitative evaluation of the spectra shows that while the amount of CO_2 in the gas phase increases immediately after pressurisation and afterwards slowly decreases, the amount in the liquid rises slightly later and slower until it approaches its final value of 3.77 mol/L (fig. 4.4). Calculating the molar fraction from this concentration gives a value of 0.32 at room temperature and 32-33 bar, which agrees well with the literature data for the solubility of CO_2 in hexanol of 0.2974 at 293.15 K and 31.5 bar (0.4655 at 45.8 bar)[59]. The equilibrium gas phase concentration of 1.53 mol/L corresponds to an amount of 0.04 mol of CO_2, while calculations from the pressure measurements yield values between 0.035 and 0.038 mol.

The resulting mass balance for CO_2 reveals a constant value of 0.067 mol with a deviation of only 4 % during the experiments. This shows that the

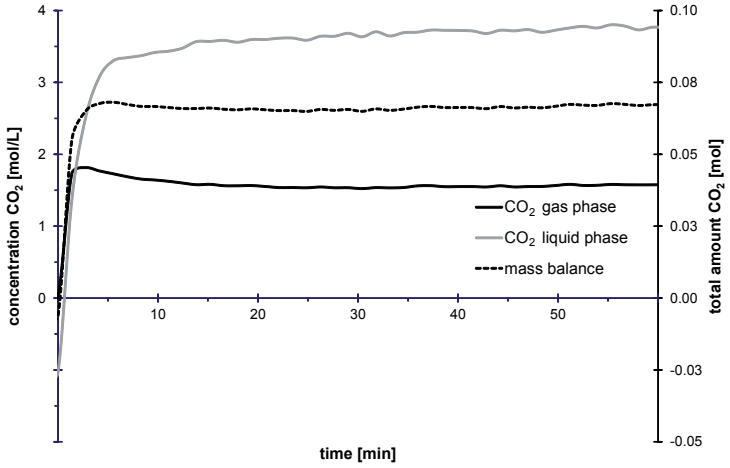

Figure 4.4.: Concentration of CO_2 in the gas and liquid phase during dissolution in hexanol and mass balance

quantification in both phases and the total mass balance are consistent and that this approach is legitimate. The next step is the application of this principle to the reactive system.

4.6. IL synthesis and total mass balance

The IR signals of the IL in the liquid phase show a fast increase in the beginning of the reaction and the signals of DBU and hexanol decline rapidly while no CO_2 signal is detected. After 10 minutes, the CO_2 signal slowly starts to increase, the DBU and hexanol signals have completely disappeared and the IL signals stay constant. This indicates the end of the synthesis reaction. In the gas phase, only traces of DBU and hexanol are detectable. The CO_2 signal displays a leap during pressurisation and afterwards diminishes.

A look at the concentration profiles of the DBU/hexanol mixture and

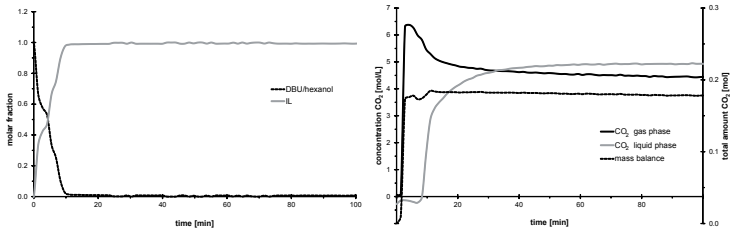

Figure 4.5.: Left: concentration profiles of IL and DBU/hexanol during reaction in the liquid phase; right: corresponding CO_2 concentrations in the liquid and gas phase and mass balance

the product reveals that the reaction is very fast with a reaction time of only just over 10 minutes (fig. 4.5).

Experiments with different stirrer settings showed that the reaction time is highly dependent on the mass transport of the CO_2 into the liquid phase and hence varies greatly with the stirring mode and speed. The CO_2 concentration profiles of the gas and liquid phase strongly resemble those of the dissolution experiments. The gas phase concentration rises abruptly when the autoclave is pressurised and then slowly decreases over time until it reaches the equilibrium value. In the liquid phase, no CO_2 is detected within the first 10 minutes, which reflects exactly the reaction time and suggests that all the CO_2 that is transported into the liquid phase within the first 10 minutes instantaneously reacts with DBU and hexanol to form the IL. This strongly points towards a transport limitation of the reaction and suggests that the reaction time can be decreased by an improved phase contacting between the gas and liquid phase.

An increase in the concentration of dissolved CO_2 can only be detected after the reaction is finished. At this point, CO_2 is taken up by the liquid phase and dissolved until the equilibrium between the two phases is reached. Sadly, no literature data is available for direct comparison

in this case. However, the concentration of absorbed CO_2 in the liquid phase is anticipated to be in the same range as for hexanol (3.77 mol/L), but should have a higher value due to the higher polarity of the IL[52]. The liquid phase concentration of 4.93 mol/L matches these expectations.

The mass balance of this reaction not only contains the substance amounts of CO_2 in the gas and liquid phase, but also includes the amount that is chemically incorporated in the IL. Only traces of hexanol and DBU were detected in the gas phase, which can be neglected. The IL is not present in the gas phase at all as was expected, so this does not have to be taken into account for a mass balance either. DBU and hexanol are completely converted to the IL in the liquid phase. As was expected, the derived mass balance is constant, varying slightly during the pressurisation and afterwards showing a deviation of less than 3 %. It thus confirms the results of the quantification method

Clearly, the obtained liquid phase concentrations of CO_2 are in good agreement with solubility data, the concentration profiles are consistent and a total mass balance of the reaction system can be drawn up.

4.7. Assessment of limiting factors

While the previous results showed a fast and easy switch, reaction times for the synthesis of the IL often take one hour. This may be an acceptable time span for small scale laboratory reactions, but since the main aim of this concept is large scale industrial applicability, these times are much too long. An important question must therefore be why such long times are required and whether they can be shortened significantly.

So the synthesis of a two-component reversible IL from DBU and hexanol under CO_2 was exemplarily investigated. It is an exothermal equilibrium reaction that is reversed at elevated temperatures[57,58]. In

addition to this temperature dependence, the reaction is also pressure dependent since one of the reactants is gaseous CO_2. The two substrates and the product are fully miscible. During the reaction, there is a density change when going from the reaction mixture (measured as 0.92 g/mL; 0.814 g/mL from hexanol and 1.018 g/mL from DBU) to the product [DBUH][$O_2CO(CH_2)_5CH_3$] IL (1.06 g/mL) and due to the CO_2 dissolved in the reaction mixture (0.5-5.5 mol/L). The reaction is also accompanied by a change in viscosity between the equimolar substrate mixture (5-6 mPa s) and the resulting product (ca. 400 mPa s). In order to evaluate which of these parameters has an influence on the reaction, a well-defined set-up is needed (appendix A.3.3). This consists of a high pressure autoclave with an inner diameter of 30 mm and a 45°pitched 4 blade turbine shaft drive stirrer with an impeller diameter of 18 mm and agitator speed control. The gas is added into the system through an inlet valve at the top of the reactor, so that the reaction only occurs at the liquid surface. The gas pressure can be monitored spectroscopically with ATR-mIR and with a standard pressure sensor.

To investigate the temperature influence, the IL synthesis was carried out and high resolution temperature measurements were recorded. As discussed above, the reaction is exothermic and the released heat can cause a shift of the reaction equilibrium towards the molecular liquids. If one of these counteracting effects is delayed, this could cause thermokinetic oscillations detectable in the temperature measurements. This was however not the case. Instead, the temperature showed a linear trend and this parameter can hence be ruled out. Pressure measurements showed that while the pressure sinks steadily during the reaction, it does not drop below 3 bar, so the reaction is not limited by the amount of CO_2 available at the surface. Of course, a higher partial pressure will still lead to a slightly faster reaction, but the effect is minor.

Transport inside the reaction mixture of the product away from the interface and of fresh reactants to the surface is most likely the limiting

factor of the reaction. The Reynolds number for stirred vessels is defined as:

$$Re = \frac{\rho N D^2}{\mu} \tag{4.1}$$

with the density of the stirred liquid ρ, the stirring speed N, the diameter of the stirrer D and the dynamic viscosity of the liquid μ. For the presented reaction, both the density and the viscosity of the stirred liquid change during the reaction, so that a Reynolds number can be calculated for the start of the reaction using the parameters of the substrates and for the end of the reaction using the parameters of the product. These can then be used as upper and lower limits of the Reynolds number. For typical stirring speeds of 50 to 400 rpm, the resulting Reynolds numbers range from 45 to 360 at the beginning of the reaction and 0.7 to 5.6 for the pure IL at the end of the reaction. The flow regime is thus laminar and a laminar mixing model should be considered not only for the micromixing process[60], but also for macromixing. According to two different approaches, either using the impeller discharge flow rate or the mixing rate constant, the standard blend time of the reaction is 2 to 20 seconds, but if corrections for the Reynolds number, the density difference and the viscosity difference are applied, the theoretical blend time t_{99} rises to 80 to 800 minutes. If the actual blend times lie in the same range, mixing problems are clearly the major limitation of the synthesis reaction and should be addressed experimentally.

At low Reynolds numbers, convection induced by stirring is so low that it is not dominating anymore and natural convection gains importance. Natural convection can be based either on Rayleigh convection caused by a density gradient or on Marangoni convection caused by a difference in surface tension. They are characterised by the Rayleigh (Ra) or Marangoni (Ma) number respectively and can be induced either by temperature or by concentration gradients. The temperature at the bottom of the vessel is not higher than at the top, so that the natural convection

is not caused thermally. The Rayleigh number is defined as the product of the Grashof (Gr) and the Prandtl (Pr) number (eq. (4.3)).

$$\mathrm{Ra} = \mathrm{Gr} \cdot \mathrm{Pr} = \frac{g \cdot L^3}{\nu \cdot a} = \frac{\Delta\rho}{\rho_l} \qquad (4.2)$$
$$\text{with} \quad \Delta\rho = \rho_{surface} - \rho_{bulk}$$

In this equation, g is the acceleration due to gravity, L the characteristic length, ν the kinematic viscosity, a the thermal diffusivity, $\Delta\rho$ the density difference and ρ_l is the quiescent density of the liquid. All parameters in this equation are positive except for the density difference, which can assume either sign and therefore determines whether Ra is positive or negative. Since the IL has a higher density than the substrate mixture, the concentration-driven convection is caused by a density difference where $\Delta\rho > 0$ and hence, $\mathrm{Ra} > 0$, so the system is Rayleigh-unstable. Since Rayleigh instability is dominant compared to Marangoni instability[61], the reaction system experiences additional convective mixing irrespective of Ma. Although the effects cannot be observed in the high pressure set-up, literature[61] suggests that the heavy top phase sinks to the bottom of the reactor in plumes along the reactor walls while the substrate ascends at the surface centre. The additional mixing effect might shorten the effective blend time compared to the theoretical value of t_{99}, but does not eliminate the mixing problems significantly.

4.8. Analysis of reaction parameters*

A first evaluation of the concentration profiles of the reaction confirmed that fluctuations in the concentration can be detected (fig. 4.6). While it takes only 3 minutes for the first 75 % of conversion at 25 bar and

*Measurements of the pressure and stirring speed dependence were carried out by Robin Heedfeld as part of his research studies.

100 rpm, the total reaction time is approximately an hour. After the first steep increase in IL, the fraction drops again to a value of 25 % and shows a second dip after 30 minutes. These signal fluctuations are very distinctive and could be connected to an imperfect mixing, causing fluid aggregates of different composition to pass the probe's detection surface consecutively.

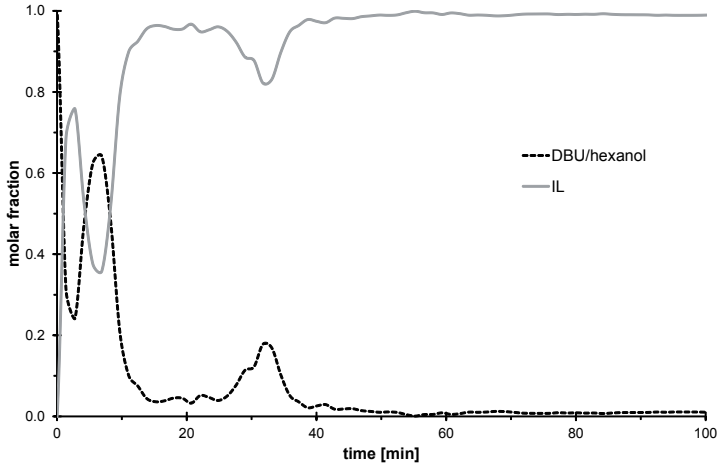

Figure 4.6.: Concentration profiles of IL and DBU/hexanol in the liquid phase during reaction at 25 bar and 100 rpm

At approximately the same pressure (27 bar) and higher stirring rates (300 rpm), no pronounced fluctuations are detectable (fig. 4.7).

When repeating experiments at exactly the same conditions to check the reproducibility, fluctuations are again observed and their intensity is the same, while the profile shape is not reproduced exactly. As may already be suspected from visual inspection of the profiles, a proper analysis confirms that the system displays no low-dimensional dynamic behaviour.

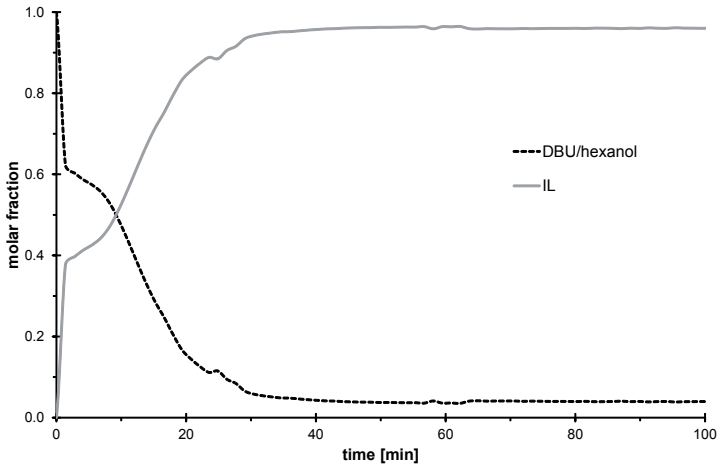

Figure 4.7.: Concentration profiles of IL and DBU/hexanol in the liquid phase during reaction at 27 bar and 300 rpm

In order to verify whether the observed fluctuations are really mixing induced or related to the reaction, a control experiment was conducted in which the substrate mixture was first filled into the reactor and afterwards preformed IL was added while stirring. This procedure eliminates all reaction related concentration changes and is reduced to pure mixing phenomena. Again, strong fluctuation behaviour is observed (fig. 4.8), confirming the previous surmise.

The reaction procedures for the synthesis of the IL found in literature[57,58,62] are all alike and differ from the approach presented here. They are carried out in a glass tube filled with the premixed substrates under inert gas by bubbling CO_2 through the substrate solution via a narrow steel tube at one atmosphere. The long reaction times reported for this procedure suggest that this approach is also accompanied by mixing problems. Although the sparging causes convection in the reaction mixture, the bubbles cause only very little mixing near the walls and at

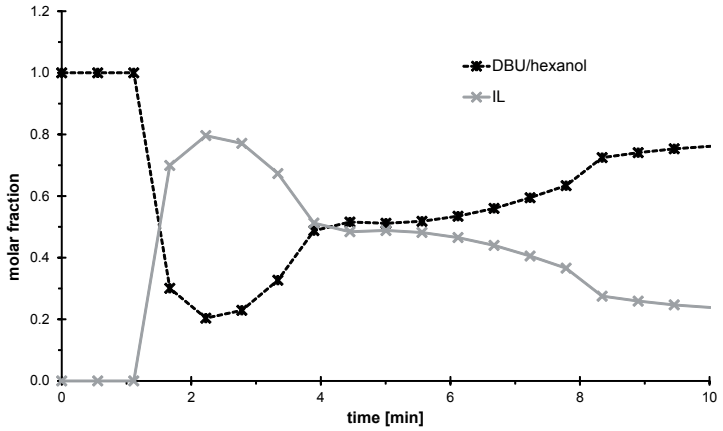

Figure 4.8.: Concentration profiles of IL and DBU/hexanol in the liquid phase during mixing experiment at 100 rpm (no reaction)

the bottom of the tube at higher viscosities.

Although the stirring speed is the most apparent parameter when mixing problems are considered, the influence of the pressure was also investigated to get as complete a picture of the mixing behaviour as possible. At low pressures of 15 bar, the fluctuation profile is stronger than at 40 bar and the reaction time is up to 10 times longer at lower pressures.

The results of the stirring speed variation (50-400 rpm) and the pressure variation (15-60 bar) were analysed and classified into three groups of different fluctuation strength. The curvature strength of each concentration profile can also be used as an objective measure of the fluctuation strength. Since the concentration of the product during a reaction that shows no fluctuations increases monotonously, the curvature of its profile should be negative. If the concentration fluctuates during the reaction, the curvature of the profile varies and can assume positive values. The sum over all positive values of the second derivative of the reaction profile

was introduced as a measure of the fluctuation strength. This parameter was calculated as follows:

$$S_{curvature} = \sum_{t=0}^{t_e} \frac{d^2 c_p(t)}{dt^2} \cdot \delta(t) \tag{4.3}$$

$$\text{with} \quad \delta(t) = \begin{cases} 0, & \left(\frac{d^2 c_p(t)}{dt^2}\right) \leq 0 \\ 1, & \left(\frac{d^2 c_p(t)}{dt^2}\right) > 0 \end{cases}$$

where $t = 0$ is the starting point of the reaction, t_e is the time until full conversion is reached and c_p is the concentration of the product. The obtained values vary from 0 to 1.5, where values up to 0.3 were categorised as weak fluctuations and values above 0.7 represent strong fluctuations. Assessing the curvature strength accordingly confirmed the validity of the three previously used groups.

A statistical evaluation of all reaction parameters with Design-Expert confirmed that the stirring speed and the pressure with probability values of 0.001 and 0.013 respectively are the significant parameters influencing this fluctuation strength. These parameters were therefore used as dimensions of a parameter map and all experiments transferred to this map according to their fluctuation strength (fig. 4.9). They show clearly that at high stirring speeds and pressures, the experiments show very little fluctuations while for low stirring speeds and pressures, the measurements always show distinct fluctuating behaviour.

To improve the reaction conditions and avoid mixing problems, stirring speeds above 200 rpm and pressures above 25 bar should be applied. This area where fluctuations can be reliably avoided is marked in the parameter map. In the transition area at high stirring speeds but low pressures, the behaviour of the reaction is hard to predict, since very small changes in the conditions cause large changes in the mixing behaviour and thus

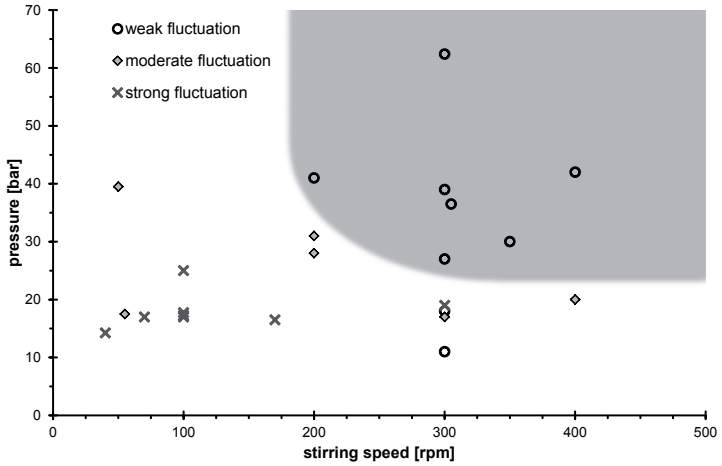

Figure 4.9.: Parameter map of fluctuation strength as a function of stirring speed and pressure for all performed experiments

in the fluctuation strength.

The influence of the pressure and of the stirring speed on the quality of mixing in the reactor was shown and analysed. In order to understand the reason for these influences, their mechanism should be further elucidated. When the stirring speed is increased, so is the energy input into the system via the stirrer. This is reflected in a higher Reynolds number. In this case, the mean aggregate size becomes smaller, the macromixing is better and a 99 % mixing degree is achieved faster. Consequently, the amplitude of the fluctuations becomes smaller, as was detected with the IR measurements. In addition to this effect, a higher stirring speed also leads to a faster renewal of the interphase. The improved phase contact produces a faster reaction, which is apparent in the reduced time it takes to achieve full conversion.

When a higher pressure is applied to the reaction, the most obvious

consequence is a rise in CO_2 solubility[59], which most likely causes the fluctuation reduction. The increased amount of dissolved CO_2 decreases the viscosity of the reaction mixture[63], so that the effective Reynolds number, which is inversely dependent on the viscosity, is raised, causing better mixing and less fluctuations. Also, in consequence of the higher supply, the CO_2 may not be completely consumed at the surface, but a fraction of it may reach the substrate bulk, where it can now react. In this way, the IL is formed everywhere in the bulk, the concentration gradient in the reaction mixture is smaller and the mixing phenomena become less pronounced.

An additional effect when a higher pressure is applied to the reaction is that the CO_2 concentration at the surface increases and the reaction becomes faster. This however would not lead to a diminished fluctuation strength, but only to a shorter reaction time.

As a last feature, the shape of the observed mixing profiles will be addressed. If the fluctuations in the signal are caused by aggregates of different composition passing the probe head, a sharp change in signal with a characteristic time for spectral changes of a few seconds is to be expected when a different aggregate hits the detection surface. The IR signal however shows a damped curve shape with a characteristic time of several minutes. This is caused by the detection principle of the ATR probe. The penetration depth in which the IR measurement takes place is 1-10 μm and the thickness of the boundary layer around the probe is in the range of 20-30 μm. This means that the concentration is only detected inside the boundary layer of the probe. So for a substance to be detected, it has to cross the boundary layer, which is only possible by diffusion. This causes a delay in the detection compared to the bulk and the concentration gradient dependence of the diffusion causes the damping effect that is observed. This principle has already been described in literature, where the interaction of a sharp concentration signal with the boundary layer to create a damped detection signal was

characterised[64]. The same principle holds true at lower stirring speeds, where natural convection occurs. In this case, fluid aggregates are not transported to the probe by the stirrer, but plumes of high IL content are formed and spread down the reactor walls[61]. The probe head does not emerge very far into the reactor, but is installed in proximity to the wall, so that the plumes flow over the probe head consecutively and there again interact by diffusion with the boundary layer of the probe.

4.9. Summary

Experiments with hexanol and CO_2 as a model system showed that CO_2 can be measured with mIR both in solution and in the gas phase. The advantage of the spectroscopic gas phase analysis over a simple pressure sensor is that for gas mixtures, not only the total pressure but the amount of each spectroscopically active component are available. The obtained concentration profiles are consistent and a total mass balance of the reaction system can be established. This confirms that the quantification methods are applicable. The same principle was applied to a reactive system, where the synthesis of a switchable solvent was carried out. At any reaction time, a closed mass balance over all phases can be achieved for every component in the reaction system. This constant total mass balance again confirmed the results of the quantification method.

The results indicate that with this system, several substances in a multiphase multicomponent reaction can be quantitatively analysed. The drawing up of a total mass balance from the quantification results and the knowledge of the composition of each phase present in the reactor give a further insight into the reaction. As shown, it is now possible to attribute different phenomena to different stages during the reaction or to the transport between the phases. The results thus permit to ascribe the reaction time mainly to a rate-determining mass transport of the CO_2 from the gas phase to the liquid phase rather than to the reaction

rate itself.

If a systematic study of the synthesis of a switchable solvent from DBU and hexanol is carried out, it is possible to understand which parameters determine the reaction time. Calculations on the flow regime, the Reynolds numbers and the resulting theoretical blend times hinted at mixing problems as a main influence. Other possible factors such as temperature and limitations due to a pressure drop could be ruled out.

A well-defined experimental set-up where transport of the gas into the reaction mixture only occurs at the liquid surface was used for a practical evaluation of the system's behaviour. Composition measurements of the reaction mixture were carried out with an mIR probe and showed that fluctuations in the concentration can be detected. This confirms the assumption of mixing problems. The fluctuations are likely caused by fluid aggregates of different composition that pass the probe head in turns. An investigation of the influence of stirring speed and pressure showed that the increase of either parameter can shorten the reaction time significantly and reduce the fluctuations. For a better overview, all experimental results were classified as to their fluctuation strength and depicted in a parameter map. In this map, the parameter range can be divided into areas at high stirring speeds and high pressures, where little to no fluctuations occur, areas at low stirring speeds and low pressure, where strong fluctuations are visible and a transition area, where the behaviour is strongly parametrically sensitive.

The influence of the stirring speed can be assigned to the increased turbulence of the system, the subsequent decrease in aggregate size and the shortened blend time. A pressure rise enhances the gas solubility, so that the viscosity of the system is reduced by the dissolved CO_2, improving the diffusivity and hence the mixing.

In addition, the gas is not completely consumed at the surface, dimin-

ishing the concentration gradient throughout the system and the transport problems. Overall, it could be shown that mixing problems can be avoided and the reaction time shortened by applying stirring speeds above 200 and pressures above 25 bar. So a total mass balance of the reaction is possible for conditions where mixing is not limiting and the conditions at which mixing becomes limiting could be identified and explained.

4.10. Conclusions

For a reaction system where all components are spectroscopically detectable, a total mass balance over both phases is achievable. Several conditions had to be satisfied to realise this concept. Most importantly, spectroscopic measurements have to be carried out simultaneously in both phases, so an installation of two probes, one in each phase, was necessary. These can deliver information on the composition of each phase if all the substances present in the phase are not only detectable, but quantifiable.

So the use of at least one detector per phase, the detectability and the quantifiability of each substance present in a phase are the basic conditions for the total mass balance. The example in this chapter shows that these requirements are indeed sufficient.

Since concentrations of the gas are now available which were not available for the hydrogenation reaction, transport of the gas into the liquid phase could be assessed and was even identified as limiting during the reaction. To accelerate the overall reaction, transport between the phases has to be improved.

For regimes where the system shows distinct inhomogeneity, the measurement of both phases allows to distinguish between pressure or tem-

perature effects causing fluctuations and mixing effects. Any effects that affect the whole reactor set-up, such as temperature or pressure changes, would always affect the gas phase as well as the liquid phase. The absence of fluctuations in the gas phase measurements helps to identify mixing as the true limiting factor. So with the new set-up, more information on the reaction system is available and hence, more conclusions on limiting factors and transport inside the reactor can be drawn.

The investigated system has the advantage of being completely detectable and quantifiable with only one spectroscopic technique, making the installation and realisation of the total mass balance easier. If however not all substances can be detected with the same method, a combination of several spectroscopies in one set-up and even in one phase is necessary. In the presented reactor, up to two spectroscopic methods per phase can be installed, keeping it applicable even for the analysis of more complex reactive systems.

5. Switchable solvent synthesis: two sensors in one for space-dependent analysis*

5.1. Context

As the previous chapter has shown, poor mixing and fast reactions can lead to concentration fluctuations that are caused by local inhomogeneities. This is especially relevant for analytical techniques with small sampling volumes. Transmission techniques give an average over the measurement distance and thus may reduce the error caused by concentration deviations along this path, although deviations perpendicular to this transmission axis are not captured in this average. The error made by the smallness of the sampling volume is very pronounced in ATR spectroscopy, where the pathlength inside the sample is very short. The disadvantage can be that the mass balance over several phases is invalid and that the concentrations of different compounds are either overrated or underrated.

If these mentioned concentration deviations are taken into account and averaging over longer times is carried out for slow reactions to receive more exact information, this disadvantage can be partly avoided. This is of course more difficult if several phases are present and all measurements are error prone.

*Measurements of composition dependent conductivity were carried out by Sören Lehmkuhl as part of his research studies.

The errors due to fluctuation present an even greater problem where several analytical techniques are combined. As previously discussed, the combination of different techniques broadens the information available and can often be combined to give a fuller picture of the molecular changes involved. The different techniques are normally introduced by using different sensors, which are installed in different places of the reactor. If spatial inhomogeneities are present, this means that different volume elements are detected by the different techniques. These do not have the same composition and therefore the data of the analytics do not match. Data collected under these conditions must not be compared or even combined for analysis, so the advantages of introducing several techniques in one reactor are lost.

In order to reduce the number of installations and ensure the measurement with different techniques at the same point inside the reactor, the sensors have to be installed as close to each other as possible. This ensures that they measure the same volume element, in which case they gather matching information, if not information that is representative of the whole bulk. The closest possible installation is to use one sensor for several measurement techniques. This is difficult where several spectroscopic regions are concerned that require differing fibre and IRE material, so for this demonstration, a spectroscopic method and an electricity based measurement will be combined.

5.2. Introduction

The combination of two analytical techniques in one sensor will be carried out for mIR spectroscopy and electrical conductivity measurements. While the light is conducted through an optical fibre inside a metal probe shaft and the measurement is carried out at a diamond reflection element, the electrical measurement makes use of the shaft itself, which is made

from gold-coated stainless steel and is therefore highly conductive. So the probe shaft serves as an electrode for the conductivity measurement (appendix A.3.4). The second electrode which is needed for the conductivity measurement can be either a second probe, i.e. for a further spectroscopic analysis, or any standard electrode.

The switchable solvent synthesis is again chosen as an example reaction. Due to the high increase in ionic strength during the reaction, the substrates and product should be easily distinguishable by conductivity measurements. While the substrates are not ionic and have a low polarity, the IL is made up of ion pairs that can act as charge carriers, albeit not fully independently. The mechanism of the conductivity in ILs in general is different from the mechanism in salt solutions. This is mainly due to the formation of nanodomains within the IL[65]. Parts of the IL that show strong interactions build a three-dimensional ionic network while parts with weak interaction forces form non-polar domains embedded into this ionic network. This structure changes the conductivity behaviour of the IL considerably, since the charge carriers are no longer made up of free single ions, as is the case in salt solutions.

So the mechanism of the conductivity in ILs in general has been thoroughly investigated[65,66] and conductivity measurements have even been conducted with switchable ILs[58], but until now they have only been applied to show qualitatively that a switch has been performed. They have never been used for a quantitative analysis of the composition or for reaction monitoring, which will be aimed for in this chapter.

Hence, the task is to show whether conductivity and IR measurements can be combined without disturbing each other, how the sensor has to be adapted and if the combination is feasible and delivers complementary information. The results will show whether a quantitative analysis is possible.

5.3. Outline

Since the spectroscopic analysis of the switchable solvent synthesis has already been validated and used for the monitoring of the reaction under various conditions, the main task will be the identification of influencing parameters, the subsequent choice of conditions for reaction and the detailed validation of the conductivity measurements.

In a first step, the conductivity of the substrates and product will be measured in the adopted set-up and compared with literature data. An evaluation of the difference in conductivity between substrates and product will then show if the change in conductivity during the reaction is large enough to obtain a quantifiable signal. If this is the case, then the conductivity data can be used for monitoring the reaction.

Afterwards, the various parameters influencing the conductivity measurements will be identified and their influence analysed. Using this information, the parameters of the set-up and the reaction can be improved to obtain the best signals possible and to reduce the influence of disturbing interferences. Two of the parameters, namely the temperature and the viscosity, are intrinsically affected by the reaction course itself and their change during the measurements therefore cannot be avoided. The temperature influence can be minimised by the reaction procedure, as will be demonstrated, and the viscosity influence can either be decreased or utilised to gain additional information on the reaction mixture. These two possibilities will be discussed and evaluated according to the aim of the analysis and the reaction characteristics.

The third step will be the comparison of the data obtained from the spectroscopic analysis and that from conductivity measurements. If these data are combined, the conductivity measured at different times can be clearly correlated to the composition at that moment to give concentration dependent conductivity data. For systems where these factors

are linearly dependent, the conductivity measurement is a simpler and more economical alternative for the composition analysis compared to IR spectroscopy. If the factors however are not linearly dependent, then the conductivity measurements are probably influenced by an additional factor and can give additional information on the state of the reactor content, depending on which parameters influence the conductivity apart from the composition. In this case, conductivity measurements are not an alternative, but a complementary technique to IR spectroscopy.

In the end, an exemplary study of four reaction mixtures with different compositions will demonstrate how frequency dependent conductivity measurements can be used to gain impedance spectra of the solutions in order to derive further information on the resistance characteristics of the mixtures.

5.4. Evaluation of conductivity values

Conductivity measurements in a similar switchable solvent system of N,N,N',N'-tetramethyl-N"-butylguanidine (TMBG) and methanol with CO_2 to the IL N,N,N',N'-tetramethyl-N"-butylguanidinium methylcarbonate conducted in chloroform as a solvent gave conductivity values of $\sim$0 μS/cm for the equimolar TMBG/methanol mixture and 250 μS/cm for the IL[57], which points towards a strong difference in conductivity for these kind of systems.

The conductivity determined in literature of the neat, equimolar DBU/hexanol mixture is stated to be 7 μS/cm and that of the IL 187-189 μS/cm[58]. The conductivity of the IL with a rest content of below 2 % substrate at 18 bar measured in the combined conductivity and spectroscopy analytical cell has a value of 49 μS/cm. The deviation between this value and the literature data might be either due to the difference in the reactor and electronic set-up or due to the differ-

ence in CO_2 pressure and substrate content. For the present set-up, the difference between the substrates and the IL is smaller, but it is still high enough for quantification, especially since the error is mainly dependent on the consistency of the applied voltage and the temperature of the reactor content. These result in an error of only 3 %, so that the signal-to-noise ratio justifies the hope of monitoring the reaction with conductivity measurements.

5.5. Analysis of conductivity parameters

Several aspects of the reaction set-up (appendix A.3.4) and the reaction conditions can influence the conductivity. The electrode geometry and material is an important factor, but this is mainly dictated by the shape of the spectroscopic probes and is therefore fixed. The distance between the two electrodes however is flexible and can be adapted to maximise the conductivity signal. A variation of the distance between 4 and 28 mm clearly shows a linear correlation between the distance and the conductivity in this distance range, where the conductivity of course decreases with increasing distance (fig. 5.1). So for a high signal, the distance between the electrodes should be chosen as small as possible. This will lead to smaller errors. On the other hand, a small space between the electrodes does not allow for good mixing, so the measured substance between the electrodes is not representative of the bulk. The distance should therefore be wide enough to permit convection. Following the aforementioned arguments, an electrode distance of 20 mm was chosen for the reactive experiments.

Similar arguments hold true for the stirring speed inside the reactor vessel. To ensure good mixing and the highest possible homogeneity of the reactor content, high stirring speeds are advantageous, but at very high stirring speeds, the liquid can splatter and adhere to the walls. In order to investigate the exact influence of the stirring speed, a varia-

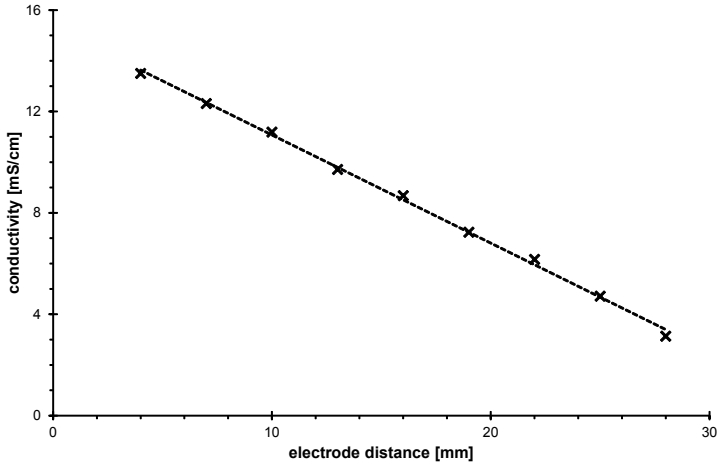

Figure 5.1.: Electrode distance variation and resulting conductivity

tion between 0 and 500 rpm was carried out and the conductivity values analysed. The resulting diagram (fig. 5.2) displays a constant conductivity value for stirring speeds up to 200 rpm which rapidly decreases at higher stirring speeds. Observations can easily explain this behaviour, since at higher stirring speeds, a vortex is formed in the middle of the reactor, causing increasing amounts of air to be entrapped between the electrodes. Since air has a much negligible conductivity, the conductivity accordingly drops. To keep up the best possible mixing and the highest possible conductivity, a stirring speed or 200 rpm was accordingly adopted as the ideal setting during all following experiments.

The influence of the temperature on the conductivity was tested for the IL. Generally, an increase in temperature leads to a decrease in viscosity, which raises the conductivity according to the Walden rule

$$\eta \cdot \Lambda = const. \tag{5.1}$$

where η is the viscosity and Λ is the molar conductivity. The reason is

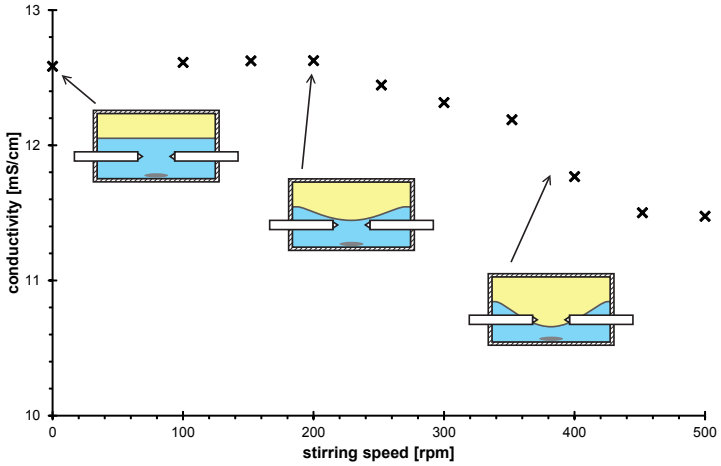

Figure 5.2.: Stirring speed variation and resulting conductivity

that at lower viscosities, the mobility of the charge carriers is increased. The stronger the influence of the temperature on the viscosity of the substance investigated, the more pronounced the change in conductivity. The substrate mixture has a low conductivity, but also a low viscosity (5-6 mPa s), so that the impact of the temperature is not as high. For the IL however, the impact is very large, since the IL has a high viscosity at room temperature (∼400 mPa s) which decreases strongly with temperature. Therefore, the temperature dependence of the IL was analysed. Starting from 21 °C, the temperature was increased to 80 °C and the conductivity recorded during the heating period until a constant value was reached (fig. 5.3).

A fourfold higher conductivity is detected, confirming the strong influence already anticipated. The IL synthesis reaction is known to be very exothermic, leading to a high temperature increase for adiabatic reaction procedures. Accordingly, the composition dependent conductivity signal will be superimposed by the conductivity change due to the

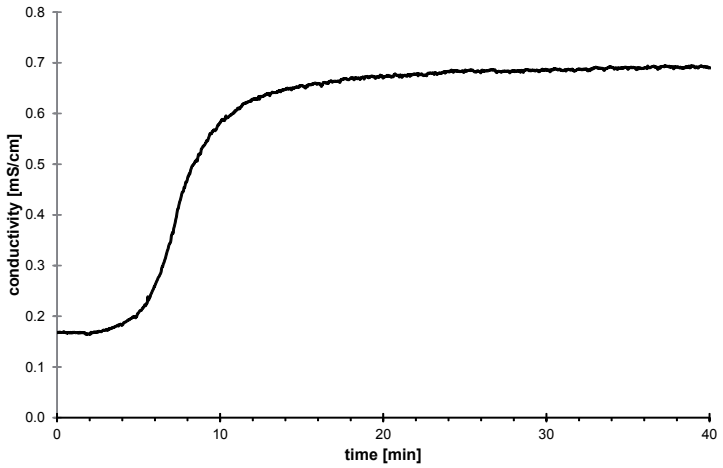

Figure 5.3.: Temperature dependence of IL conductivity during heating from 21 °C (0 min) to 80 °C (40 min)

temperature rise of the reaction. This superposition makes an attribution of the conductivity with the composition of the reaction mixture for monitoring purposes impossible. In order to obtain useful conductivity data, the temperature rise has to be inhibited. Two different methods can be adopted for this purpose. The first is based on a temperature control with high volume flows outside the reactor while the reaction is slowed down to diminish the heat formation inside the reactor. With this concept, the heat released per time unit is restricted to an amount that can be dissipated, so that the temperature inside the reactor should stay constant. A disadvantage of this method is that the reaction takes long and the conversion is lower due to the lower pressure that is applied. The second method is based on a stepwise addition of CO_2. After each addition, the temperature equilibration is waited for and the value for the constant conductivity at the equilibrium is recorded. A drawback is that only a limited number of compositions can be measured with this method, so that the dynamic behaviour of the reaction is not detected.

Both methods were carried out for the IL synthesis and will be compared in the following chapter.

5.6. Comparison with IR spectroscopy

During all synthesis reactions conducted with either of the methods with reduced temperature influence, the composition of the reactor content was monitored and analysed with IR spectroscopy, so that each conductivity measurement can be related to a composition. Comparing the IR spectra of these measurements with those obtained during experiments without additional conductivity measurements, neither the signal intensities nor their positions show any deviations (fig. C.6). So the spectroscopic measurements are undisturbed by the current applied to the system.

If the conductivity is now plotted against the composition, their dependency can be determined. This was first carried out for the stepwise experiments which cover the whole compositional range from 8 to 89 % conversion (fig. 5.4 measurement 1). The most obvious aspect is that the dependence is not linear at all, but that the conductivity reaches a maximum of 200 μS/cm at an IL content of 28 %. At higher IL ratios, the conductivity decreases perceptibly until a value of approximately 40 μS/cm is reached. This trend does not fit the expectation of a linear correlation between the composition and the conductivity at all.

Before drawing further conclusions, the experiment was carried out again to check the reproducibility of the measurements and to narrow the step width by adding further compositions (fig. 5.4). The same trend is observed for this second experiment and the values at similar compositions only vary by less than 20 μS/cm, which is small compared to the composition dependent effect. A comparison with the continuous experiment at mild reaction conditions and longer reaction times confirms

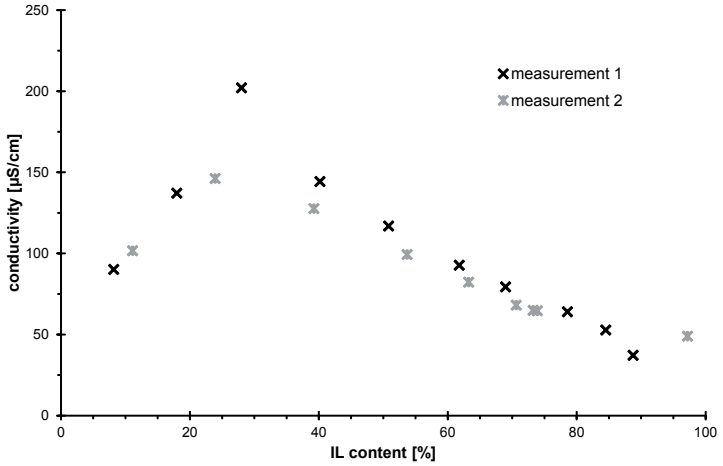

Figure 5.4.: Reproducibility of conductivity measurements of IL synthesis reaction (stepwise)

the trend derived from the stepwise experiment (fig. 5.5). The deviation between these values is higher than between the reproducibility experiments, which is probably due to a small temperature effect that could not be completely suppressed and is still present in the continuous experiments. The major trend rests the same however.

To explain this trend, not only the increase in ionic strength during the reaction, but also the increase in viscosity has to be taken into account. When the pure substrates and the pure IL are compared, the effect of ionic strength prevails. Due to the higher ionic strength of the IL, the conductivity increases. This effect can also be observed at low conversions. When comparing mixtures with an IL content of 30 and 97 %, the effect of viscosity increase dominates. While the ionic strength of the mixture still rises, this positive influence on the conductivity is more than compensated by the conductivity reducing influence of the viscosity caused by the reduced mobility of the ions. Accordingly, the conductiv-

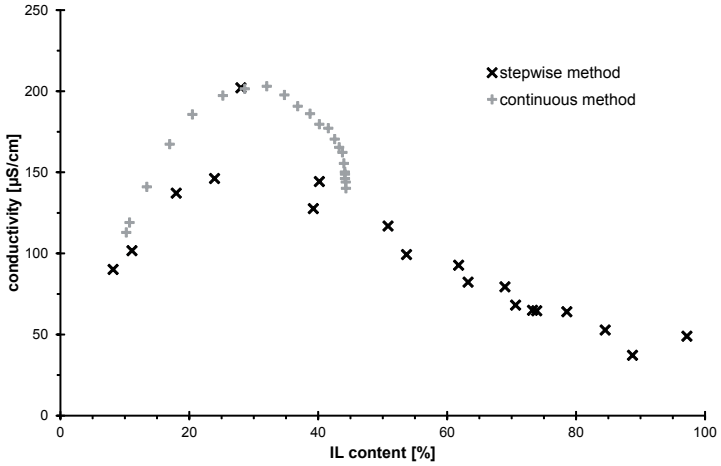

Figure 5.5.: Comparison of conductivity measurements with different methods during IL synthesis reaction

ity drops at higher conversions. The superposition of the two influences results in the existence of a maximum conductivity. Similar trends were observed in literature[65]. For applications where a high conductivity of the IL is required, i.e. as electrolyte in batteries[66,67], this also means that the conductive properties can easily be improved by adding any low viscous solvent up to the optimum composition deduced from a similar binary compositional investigation.

The conductivity measurement cannot be used as an alternative to IR spectroscopy for the analysis of the composition without using additional information. If the system is however calibrated more accurately and information is available on whether the conversion is above or below 30 %, a quantitative analysis of the composition may still be possible. Alternatively, the conductivity measurements can be combined with the IR spectroscopy to gain information on the viscosity as well as the composition of the system. The performed study shows that the two techniques

can be combined in one sensor, presenting a valuable tool for confined sampling spaces as well as for space-dependent systems.

If the reaction is carried out in a solvent rather than neat, the influence of the viscosity is lowered considerably[57], so that the conductivity is proportional to the composition and the conductivity measurements can indeed be used for a compositional analysis without requiring additional information.

5.7. Impedance spectroscopy

To further exploit the possibilities of the conductivity measurements, frequency dependent conductivity measurements were carried out to gain impedance spectroscopic data. Since the conductivity of the reaction mixture is dependent on the frequency of the measuring voltage, the impedance was measured as a function of the frequency between 0.2 Hz and 250 kHz for different compositions with 0, 10, 50 and 90 % IL content. When the real and imaginary parts of the impedance are plotted against each other, the data result in a semi-circular trend for all compositions (fig. 5.6). The semicircles always start from 0 MΩ and again intersect the abscissa at different values between 3.8 and 17.9 MΩ. This trend matches the typical behaviour of a capacitor, so independent of the composition the reaction mixture always behaves as a capacitor.

The point of intercept with the abscissa represents the real part of the impedance and its value therefore corresponds to the Ohmic resistance R. Using the angular point of each semicircle, the capacity C can be calculated. Both values show opposite trends for the composition variation. The resistance drops from 17.9 MΩ for the pure substrates to 3.8 MΩ at 50 % conversion. Afterwards, it rises to a value of 17.0 MΩ at 90 % IL content. The capacity rises from 22 to 230 μF between 0 and 50 % IL content and then decreases to 26 μF at 90 % IL.

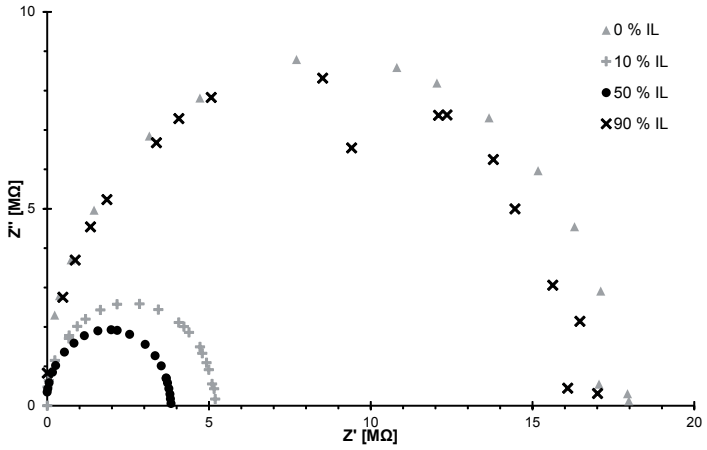

Figure 5.6.: Impedance spectra of binary mixtures of DBU/hexanol and IL

This trend where a maximum of the resistance or minimum of the capacity can be found for a medium IL content while the value for the pure IL is again nearer to the starting value of the pure substrates matches the trend for the conductivity measurements and can be attributed to the same reasons.

So for this experiment, the impedance behaviour of all mixtures can be described by a capacitor of varying capacity and resistance. For different reactions, it might be even more interesting to carry out impedance measurements to verify if the character of the impedance changes during the reaction.

5.8. Summary

The measurements of the conductivity of the switchable IL in an adapted reactor set-up yielded a value of of 49 μS/cm, which is seven times higher than the conductivity of the DBU/hexanol substrate mixture of the synthesis (7 μS/cm). Combined with the low error of the measurements of only 3 %, this change in conductivity could be estimated as sufficient for the quantitative monitoring of the reaction. Accordingly, the influencing parameters of the measurements were investigated. A higher distance between the probes used as electrodes was found to lower the conductivity, so that a minimisation of the distance seems desirable. On the other hand, small distances hinder convection and thus the mixing between the bulk and the sample volume between the probes. Hence, a distance of 20 mm was chosen as a good compromise.

Variations of the stirring speed showed that at high stirring speeds, a vortex is formed in the middle of the reactor that reaches the sample volume, at which point air is present between the electrodes and the conductivity drops strongly. At low stirring speeds however, mixing of the reactor content is insufficient. The highest stirring speed without vortex formation was therefore chosen as a setting, which is at 200 rpm.

A more complex influence is that of the temperature. This is small for the substrate mixture, since it has a low viscosity, but for liquids with high viscosities such as the IL, the temperature influence becomes very large. This is due to the lowered viscosity as higher temperatures and hence the increased mobility of the charge carriers. The conductivity was found to increase to fourfold its original value during a temperature increase of 60 K. Since the synthesis reaction is exothermic and will produce heat, a procedure has to be adapted to hinder a temperature rise. To that effect, two methods were adopted, one with strong cooling and a slow reaction, so that little heat is released per time, and one based on the stepwise addition of CO_2, so that after each step the acquisition

of the conductivity data can be conducted when the thermal equilibrium is reached again. Both methods were tested in the subsequent reactive experiments.

These were additionally monitored by IR spectroscopy to gain information not only on the conductivity, but also on the composition of the reaction mixture. In this manner, conductivity data can be correlated to compositional data for both reaction procedures and the results easily compared. Apart from minor deviations, both methods showed that for small IL ratios, the conductivity increases with increasing IL content until a content of ca. 30 % is reached. Afterwards, the conductivity decreases with increasing IL content. This trend could be explained by the counteracting effects of an increase in charge carriers when IL is formed, leading to higher conductivities, and an increase in viscosity, leading to a lower mobility of the charge carriers and thus to a lower conductivity. Both effects combine to give a maximum conductivity at an IL content of 30 %.

In the end, the same set-up was used for frequency-dependent conductivity measurements in order to find out more about the impedance behaviour of the substrates and product. The plot of the imaginary and real parts of the impedance showed that all investigated mixtures of different composition behave like a capacitor. The only difference lies in the resistance and capacity values. These behave similar to the conductivity in their dependence on the composition, with a maximum or minimum respectively at medium IL contents.

5.9. Conclusions

The concept of combining two different analytical methods in one sensor to minimise the distance between the two measuring points was shown to be feasible. Conductivity measurements and IR spectroscopy carried out

using the same probe as electrode and ATR sensor gave coherent results where none of the measurements was disturbed by the other.

In the neat switchable solvent synthesis where the conductivity is not only dependent on the composition, but also on the viscosity, the introduction of the second method does not deliver redundant information on the composition, but additional data on the state of the liquid. If the influence of the viscosity is eliminated, the conductivity measurement can of course be used as an alternative to the rather expensive spectroscopy, since it can then give information on the composition. In this case, the combination of both techniques is not as interesting.

A further advantage of the introduced concept is that the number of separate installations is reduced, which can be especially important for applications in small reactors or angled spaces.

For the analysis of multiphase reactions with an inhomogeneous concentration distribution the concept allows the measurement of the same volume element, ensuring that the analytical methods collect complementary data. Dynamic processes such as mixing can be analysed with space-resolved measurements employing several techniques simultaneously and effects such as the transient oscillation can be detected and interpreted.

6. Summary and Conclusion

On the basis of two different model reactions, the whole range of tasks for the adaption of spectroscopic analysis in high pressure systems could be shown. In this process, it is important to realise that the analytical solution always depends on the reactive system, the reaction conditions that have to be applied, the geometry of the reactor set-up and the question that is to be answered with the measured data. Comprehensive measurement arrangements are available, but very often, they are not used to full capacity and a simpler and cheaper solution would be possible. Very elaborate systems can even have a discouraging effect by giving the impression that the installation of spectroscopy is too complex and laborious to make its adoption attractive. The previous chapters have hopefully contributed to introducing the idea of a flexible, feasible and simple tool that can be adapted to the purpose rather than requiring the adaption of the process.

The most basic step and one that has a high impact on the quantity of information available is the change from single sample analytics to the use of spectroscopy as an *in situ* monitoring technique. This was accomplished for the hydrogenation of glucose, where the standard approach of taking one sample at the end of the reaction and analysing it by HPLC could be replaced by a quantitative spectral analysis, increasing the time resolution to 1.8 min^{-1}. This delivers a high amount of measurement date, which is essential for the use of an initial rates method [68] and thus makes an analysis of the observable concentration change and a kinetic evaluation of the reaction possible. A pressure dependence study of the reaction for example yielded very similar conversions after 15 hours re-

action time, but the initial rates taken from the slopes of the reaction profile measured with IR spectroscopy give a different picture, showing that the reaction rate is strongly influenced by the hydrogen pressure and that an increase in pressure of 40 bar can more than double the reaction rate. This information on the reaction rate and on the course of the reaction profile would not be available with standard single sample analysis, although such kinetic studies very often provide the basis for the understanding and improvement of reactions by chemists. The merit of the accessibility of such data is therefore inestimable.

As was demonstrated, the implementation of a single probe into the existing reactor is quite simple and requires little changes to the set-up. Probes are available in different sizes and can be installed with standard fittings. This approach helps to keep the results comparable to those before the installation and the reaction procedures do not have to be revised. The profit is the ability to quantitatively monitor the reaction online. This is however limited to reactions where all crucial reactants are spectroscopically active in the same wavelength region. Where this is not the case, important feedback can be missing. A typical case was demonstrated for the identification of a transport limitation, which cannot be clearly ascertained nor ruled out since no information on the hydrogen concentration in the liquid phase is available. If an identifiability analysis according to literature[68] is carried out, the measurement matrix clearly shows a rank-deficiency, so the system is not structurally identifiable.

Gases are often more difficult to detect since their concentrations are generally low and many gases are not detectable by standard spectroscopies. A solution was presented with the combination of several spectroscopic techniques. This broadens the range of molecular information as well as detectable components, leading to a more versatile analytical system. As a downside, the installation of several probes often means that the set-up has to be altered significantly where the standard reactor geometry does not allow enough room. Again, it depends on the infor-

mation that is needed whether a more complicated set-up is worthwhile or not.

In the case of the hydrogenation, supplementing or even replacing IR with Raman spectroscopy is interesting because Raman can also be used for the analysis of different sugars and has the advantage of detecting hydrogen. First studies showed that under mild conditions with up to 30 bar hydrogen pressure, the dissolved gas cannot be detected in the aqueous phase. This is mainly due to the low solubility of hydrogen in water and the accordingly low concentrations that lie below the detection limit. The analysis of the different sugars with Raman is however possible and could have even more potential than the IR analysis. Thanks to the lower sensitivity of Raman to the reaction medium water, the sugar signals are not as strongly superimposed so that the quality of the analysis is significantly enhanced. Hence, Raman holds the potential for improved quantitative data and the detection of hydrogen might still be possible at higher pressures.

Following the same idea of measuring both the liquid components and the gaseous substance with the same spectroscopic method, the synthesis of a switchable solvent from DBU, hexanol and CO_2 was investigated. In this case, the gas and the liquid components are all IR active and the detection limit of the gas is low enough for a detection under reaction conditions. Accordingly, the information that was missing for the hydrogenation reaction can now be gained and used for a comprehensive quantification of the reaction. As a consequence, an identifiability test now shows the measured system to have full rank. So the collected data are in principle suitable as a base for a kinetic model[68]. To prove the analytical concept, a total mass balance over both phases for all components of the reactive system was carried out. This serves as a check for the quantification approach, since the sum over the amount of one substance in all phases should be constant. To achieve this, probes have to be installed in both phases, again resulting in a need for two probes

rather than one, as was the case for the combination of two spectroscopic methods. This can of course cause the same disadvantages.

The results show that the mass balance is indeed constant and in addition to the conversion in the liquid phase, the gas dissolved in the liquid can be quantified. Consequently, the mass transport limitation of this component can now be investigated, leading to the conclusion that the reaction is limited by the amount of CO_2 available, which is not transported fast enough from the gas phase into the liquid. So for a different reaction system, the desired information on the transport limitation can be obtained, pursuing a similar approach to that in the hydrogenation reaction.

The transport issues of the reaction also show in a second aspect of the obtained data. Examining the reaction profiles, concentration fluctuations become apparent at lower stirring speeds. An analysis of the influencing parameters of the fluctuation strength and its causes showed that not only transport from the gas into the liquid phase is slow, but also mixing inside the liquid phase, leading to spatial inhomogeneities that are detected by the probes due to their small penetration depth. Both the Reynolds number and the pressure could be identified as relevant influences.

Based on these observations, a concept for a sensor combination that can be used in spatially inhomogeneous systems was developed and tested. Drawing on the initial claim for a simple analytical system that can be easily integrated into an already existing reactor and aiming for a detection system where the two analytical methods reliably measure the same volume element with the same composition, the combination of two analytical methods in one sensor is the most sensible solution. The approach was realised with a combined IR and conductivity sensor which can even be adapted to measure impedance spectra and could be shown to be feasible. The two methods do not disturb each other, but deliver coherent

results that can be compared and combined since they relate to the same sampling volume of the liquid. Thanks to the fact that the conductivity is not only dependent on the composition, but also on the viscosity of the reaction mixture, these measurements can give additional information on the state of the system which is not accessible with IR spectroscopy alone.

In total, four different analytical solutions were investigated that can be applied to four different tasks. While the choice of spectral range has to be adapted to the absorption behaviour of the substances present in the reaction and ideally covers a spectrum in which all substances present are detectable, the number of installations and combination of techniques depends strongly on the behaviour of the reactive system. For multiphase reactions where all phases are possibly mixtures, the installation of as many probes as phases is desirable to cover all mass transport effects. For inhomogeneous systems where mixing is imperfect, measurements from different techniques can only be combined if measured in the same volume element. For systems where not all components can be detected by the same technique, supplementing the main analytical method by a second technique is essential to gather all necessary information and can normally be achieved by the implementation of two probes. For simple systems with one pure phase where only information on the conversion is desired however, the analytical system should be kept as simple as possible, so that it can be well integrated into the existing set-up and thus minimising the changes made to the reaction procedure. The choice of the appropriate analytics can then help to gain crucial information on the reaction characteristics, as was demonstrated for both reactions, and deepen the understanding of the underlying processes involved.

7. Theory

7.1. Introduction

Analysis can be defined as the performance of a systematic study in order to find out specific features. In analytical chemistry, these studies can be generally grouped into qualitative studies aiming at the identification of substances in a sample and quantitative determinations[69,70] of the amount of a substance contained in a sample. The two are often combined, where a quantitative measurement follows the qualitative analysis of the substance. One of the first historic example of the use of analytical chemistry was an experiment conducted on a scale in 1756 by M. Lomonossow and in 1774 by A. L. Lavoisier on combustion and the weight change connected with it[71,72]. Since the set-up comprises the determination of a quantifiable observable, this can be classified as a quantitative study. Other major contributions to the field of analytical chemistry were made by J. von Liebig with his development of systematic elemental analysis and W. Ostwald in 1894 with his book "Die wissenschaftlichen Grundlagen der analytischen Chemie" [73].

Most of the early works in analytical chemistry until about 1920[74] were based on wet chemistry methods, which are accordingly referred to as "classical methods". These rely on chemical detection reactions and for quantification, volumetric and gravimetric measurements are used exclusively. The more modern method of instrumental analysis on the other hand depends on the measurement of physical quantities such as interaction with radiation, emission of radiation or interaction with elec-

trical systems[74]. The interaction of a sample with radiation is generally called spectroscopy and can be classified according to the type of radiation used, its wavelength and the type of interaction that occurs[70]. Depending on the spectroscopic method that is employed, different information on the investigated substance is available so that a combination of several methods is often desirable to expand the informational content[75].

The analytical methods used in this work will be described in the following sections, where special attention will be given to the properties that can be concluded from the measurements and the advantages and disadvantages of the instrumental techniques that are available.

7.2. Analytical methods

7.2.1. Mid-infrared

The IR region of the electromagnetic spectrum lies between 1 and 700 nm and is commonly divided into 3 different regions, namely the near, mid and far infrared. The mIR spectrum is defined by the International Organisation for Standardisation to contain wavelengths of 3-50 μm, which corresponds to wavenumbers of 200-3300 cm^{-1}. This light can interact with a molecule by changing the molecule's energetic state.

The mechanism of this interaction is based on the existence of the molecule in discrete energetic states[70]. A molecule can pass into a higher energetic level by absorbing energy. The energy needed to pass from one level to the next corresponds to the energy difference between these levels. According to $E = h\nu$, this energy can be supplied by an electromagnetic wave of the right frequency. Radiation in the frequency range of mIR can excite changes in the oscillatory energy of the molecule. While an interaction with the electromagnetic wave is only possible when a change in dipole moment occurs as a consequence of the vibrational motion, the

absorbed energy is characteristic of the vibration and its absence from the mIR spectrum can be used to identify the vibrating structural group [74].

The position of an absorption in the spectrum can therefore be used to gain structural information while the intensity of the absorption is proportional to the concentration of the absorbing substance according to Beer and Lambert

$$A = lg\frac{I_0}{I} = \epsilon \cdot c \cdot d \tag{7.1}$$

with the absorbance A, the light intensity I, the extinction coefficient ϵ, the concentraion c and the path length d. This relationship is used in chemometrics for the quantitative evaluation of the spectra as described in sections 2.5, 3.5 and 4.4. To gain the spectral information, there are several measuring techniques available. To record absorption spectra in the mIR region, transmission or ATR measurements can be carried out, depending on the nature of the sample. In transmission measurements, the incident light beam passes straight through the sample and is gathered at the opposite site of the sample. The absorbance of the sample can be varied by changing the pathlength of the light through the sample. For turbid or opaque solutions however, a high proportion of the light intensity is not lost due to absorption by the sample, but due to scattering, rendering transmission spectroscopy unfeasible for such samples. ATR measurements, on the other hand, make use of the interaction of an evanescent wave formed by total reflectance at an IRE/sample interface (fig. 7.1) with the molecules in the sample [76]. Since the electrical field amplitude of the evanescent wave decays exponentially

$$E(x) = E_0 \cdot e^{-x/d_p} \tag{7.2}$$

the penetration depth defined as

$$d_p = \frac{\lambda_1}{2\pi\sqrt{sin^2\theta - \left(\frac{n_2}{n_1}\right)^2}} \tag{7.3}$$

into the sample is short. Here, E is the electrical field amplitude, d_p is the penetration depth, λ is the wavelength of the incident light, θ is the angle of incidence and n_1 and n_2 are the refractive indices of the materials.

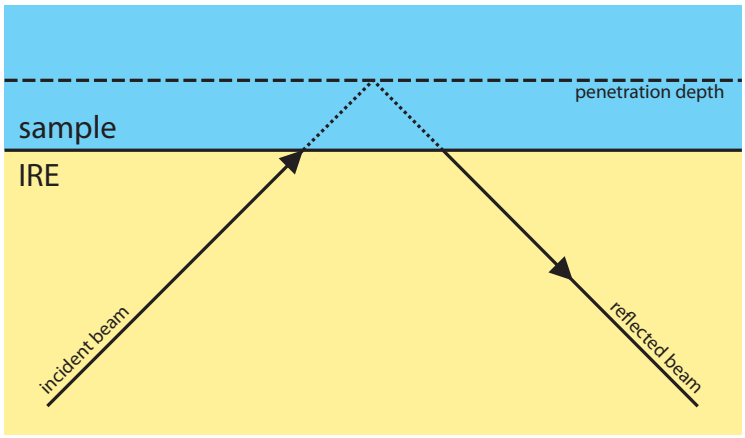

Figure 7.1.: Schematic of ATR measurement principle

For mIR light, the penetration depth is typically in the range of 1-10 μm. This reduces the interaction with particles contained in the sample, which have to penetrate the IRE surface layers convectively. As an additional advantage, the short light path length decreases the attenuation caused by strongly absorbing samples, making measurements possible even for high concentrations.

Since the spectral information of ATR measurements is contained in the reflected beam, which spreads at an angle to the direction of the incident beam, the use of a single shaft probe is possible by realising

multiple reflections and an adapted geometry of the IRE. This probe geometry allows for a simple single-port installation and has a low space requirement inside and in the vicinity of the set-up.

7.2.2. Raman

Raman spectroscopy, as opposed to IR spectroscopy, is based on scattering of incident light rather than its absorption. A very intense monochromatic light beam interacts with the sample by inelastic scattering and the scattered light is detected at right angles to the source[74]. Analogous to IR spectroscopy, the interaction of the electromagnetic wave with the molecule is connected to a change in the vibrational state of the molecule. The molecule absorbs and reemits energy. If the same vibrational state is assumed after this process, the frequency of the scattered light is the same as that of the incident light (Rayleigh scattering). If a different rotational state either higher or lower in energy than the original state is assumed, the frequency of the scattered light is shifted exactly by the corresponding energy difference between the two states (Raman scattering)[44]. A comparison between the incident and scattered light therefore delivers information that is very similar to the information obtained from an IR measurement. Interaction in this case is however only possible where a change in polarisability of the molecule occurs as a consequence of the vibrational motion[77]. This difference makes the two methods highly complementary, since certain molecules or vibrational modes are only Raman or IR active and only a combination of information from both techniques gives a full characterisation of the vibrational states of the molecule.

The implementation of Raman measurements in a single probe is straightforward. The monochromatic light beam is focussed on the sample through a window at the probe head (fig. 7.2). The scattered light is detected through the same window at a scattering angle of 180°. In this case, the focus of the illumination and collecting optics coincide[76]. Con-

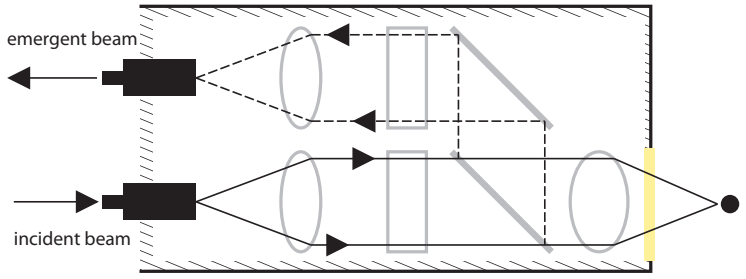

Figure 7.2.: Schematic of Raman measurement principle

tactless measurements are therefore possible and by changing the focal point, the measuring position can be adapted.

7.2.3. Conductivity measurement

The conductance L of a solution can be measured by applying an electrical force and measuring the arising current. The resulting conductance value is the reciprocal of the electrical resistance and a property of the measuring cell, since it is dependent on the cross sectional area A and the length l.

$$L = k \cdot \frac{A}{l} \tag{7.4}$$

If the conductance is normalized, i.e. by measuring between 2 electrodes with an area of 1 cm^2 each and a distance of 1 cm [74], the specific conductance or conductivity k of the solution is obtained as a property of the material. As this conductivity is achieved by mass transport of the charge carriers, it is dependent on their molar concentration C. The molar conductivity Λ has been introduced as a concentration independent property of the charge carrier.

$$\Lambda = \frac{k \cdot 1000}{C} \tag{7.5}$$

Apart from its concentration dependence, the conductivity is also influenced by the temperature, the electrical force that is applied and the frictional forces exerted on the charge carriers in the solution. To carry out conductivity measurements, also known as conductometry, the use of alternating current is preferable since it involves nonfaradaic processes and thus avoids electrolysis. The geometric dimensions and the measuring conditions should be kept constant to be able to trace the concentration change caused by the reaction progress[70].

In alternating current circuits, the resistance has to be substituted by the concept of impedance, which includes additional information on the phase shift occurring between the sine functions of the alternating voltage and current. Impedance is a complex quantity and can be divided into a real part representing the resistance and an imaginary part representing the reactance. Since the imaginary part of the impedance depends on the frequency, measurements based on a frequency variation of the applied alternating current can be carried out to gain additional information. Such measurements are commonly referred to as dielectric or impedance spectroscopy. The measuring circuit is similar to that of alternating current conductivity measurements, but the frequency of the applied current has to be tunable. The frequency dependent impedance of the system is recorded and the imaginary and real part can be plotted in a Nyquist diagram, with the real part on the x-axis and the imaginary part on the y-axis. For the evaluation of the data, the behaviour of the system is compared to and described by an equivalent circuit diagram consisting of parallel and series connections of simple impedance elements such as Ohmic resistors or capacitors[78]. Each of these elements can then be assigned a physical property of the investigated material. Ionic solutions behave as conducting dielectrics, since they contain charge carriers that cannot move completely freely, and can often be described by a combina-

tion of capacitor and resistor. The capacitive behaviour can be assigned to the formation of a double layer at the electrode surfaces while the characteristics of a resistor can occur due to the resistance of the solution to the transport of ions to and from the electrodes.

Bibliography

[1] B. Cornils, E. Wiebus, *Receuil des Travaux Chimiques des Pays-Bas* **1996**, *115*(4), 211–215.

[2] B. Chen, U. Dingerdissen, J. G. E. Krauter, H. Rotgerink, K. Möbus, D. J. Ostgard, P. Panster, T. H. Riermeier, S. Seebald, T. Tacke, H. Trauthwein, *Applied Catalysis A: General* **2005**, *280*(1), 17–46.

[3] S. Carra, E. Santacesaria, *Catalysis Reviews-Science and Engineering* **1980**, *22*(1), 75–140.

[4] B. Cornils, W. A. Herrmann, I. T. Horvath, W. Leitner, S. Mecking, H. Olivier-Bourbigou, D. Vogt, *Multiphase Homogeneous Catalysis*, Wiley-VCH Verlag GmbH & Co. KGaA, Weinheim, **2005**.

[5] J. J. M. de Pater, B.-J. Deelman, C. Elsevier, G. van Koten, *Advanced Synthesis & Catalysis* **2006**, *348*(12-13), 1447–1458.

[6] A. Behr, J. Leschinski, A. Prinz, M. Stoffers, *Chemical Engineering and Processing: Process Intensification* **2009**, *48*(6), 1140–1145.

[7] A. Z. Fadhel, P. Pollet, C. L. Liotta, C. A. Eckert, *Molecules* **2010**, *15*(11), 8400–8424.

[8] M. Irfan, T. N. Glasnov, C. O. Kappe, *ChemSusChem* **2011**, *4*(3), 300–316.

[9] F. M. A. Geilen, T. vom Stein, B. Engendahl, S. Winterle, M. A. Liauw, J. Klankermayer, W. Leitner, *Angewandte Chemie International Edition* **2011**, *50*(30), 6831–6834.

[10] A. M. Ruppert, K. Weinberg, R. Palkovits, *Angewandte Chemie International Edition* **2012**, *51*(11), 2564–2601.

[11] D. J. Cole-Hamilton, R. P. Tooze, *Catalyst Separation, Recovery and Recycling*, Springer, Dordrecht, **2006**.

[12] A. Mersmann, M. Kind, J. Stichlmair, *Thermal Separation Technology*, Springer-Verlag, Berlin Heidelberg, **2011**.

[13] B. Lohrengel, *Einführung in die thermischen Trennverfahren*, 2 Aufl., Oldenbourg Wissenschaftsverlag GmbH, München, **2012**.

[14] H. Schubert, *Handbuch der Mechanischen Verfahrenstechnik*, Bd. 2, Wiley-VCH Verlag GmbH & Co. KGaA, Weinheim, **2003**.

[15] G. E. Weismantel, *Encyclopedia of Chemical Processing and Design*, Bd. 52, Marcel Dekker, Inc., New York, **1977**.

[16] W. A. Cunningham, *Encyclopedia of Chemical Processing and Design*, Bd. 28, Marcel Dekker, Inc., New York, **1988**.

[17] W. A. Cunningham, *Encyclopedia of Chemical Processing and Design*, Bd. 24, Marcel Dekker, Inc., New York, **1986**.

[18] P. A. Lovell, M. S. El-Aasser, *Emulsion Polymerisation and Emulsion Polymers*, John Wiley & Sons Ltd., Chichester, **1997**.

[19] P. Harriott, *Chemical Reactor Design*, Marcel Dekker, Inc., New York, **2003**.

[20] E. L. Paul, V. A. Atiemo-Obeng, S. M. Kresta, *Handbook of Industrial Mixing*, John Wiley & Sons, Inc., Hoboken, **2004**.

[21] A. L. German, H. W. G. Heynen, *Journal of Physics E: Scientific Instruments* **1972**, *5*(5), 413–414.

[22] G. Dünnebier, A. Bamber, *Chemie Ingenieur Technik* **2004**, *76*(9), 1355–1355.

[23] J. B. Callis, D. L. Illman, B. R. Kowalski, *Analytical Chemistry* **1987**, *59*(9), 624A–637A.

[24] R. A. Nyquist, M. A. Leugers, M. L. McKelvy, R. R. Papenfuss, C. L. Putzig, L. Yurga, *Analytical Chemistry* **1990**, *62*(12), 223R–255R.

[25] K. R. Beebe, W. W. Blaser, R. A. Bredeweg, J. P. Chauvel, R. S. Harner, M. LaPack, A. Leugers, D. P. Martin, L. G. Wright, E. D. Yalvac, *Analytical Chemistry* **1993**, *65*(12), 199R–216R.

[26] N. C. Crabb, P. W. B. King, *Molecular spectroscopy*, 1 Aufl., Process Analytical Chemistry, Blackie Academic & Professional, **1995**.

[27] B. Mizaikoff, *Analytical Chemistry* **2003**, *75*(11), 258 A–267 A.

[28] E. Baughman, *Process Analytical Chemistry*, 1 Aufl., Process Analytical Technology, Blackwell Publishing, **2005**.

[29] K. Bakeev, *Process Analytical Technology*, 2 Aufl., John Wiley & Sons, Ltd., Chichester, **2010**.

[30] C. L. Putzig, M. A. Leugers, M. L. McKelvy, G. E. Mitchell, R. A. Nyquist, R. R. Papenfuss, L. Yurga, *Analytical Chemistry* **1992**, *64*(12), 270R–302R.

[31] G. M. Hamminga, G. Mul, J. A. Moulijn, *Applied Spectroscopy* **2007**, *61*, 470–478.

[32] L. R. Knöpke, N. Nemati, A. Köckritz, A. Brückner, U. Bentrup, *ChemCatChem* **2010**, *2*(3), 273–280.

[33] S. G. Kazarian, M. F. Vincent, F. V. Bright, C. L. Liotta, C. A. Eckert, *Journal of the American Chemical Society* **1996**, *118*(7), 1729–1736.

[34] M. S. Schneider, J. D. Grunwaldt, T. Bürgi, A. Baiker, *Review of Scientific Instruments* **2003**, *74*(9), 4121–4128.

[35] A. Brodhagen, M. Grünewald, M. Kleiner, S. Lier, *Chemie Ingenieur Technik* **2012**, *84*(5), 624–632.

[36] S. Winterle, M. A. Liauw, *Chemie Ingenieur Technik* **2010**, *82*(8), 1211–1214.

[37] W. Deng, M. Liu, X. Tan, Q. Zhang, Y. Wang, *Journal of Catalysis* **2010**, *271*(1), 22–32.

[38] A. Fukuoka, P. L. Dhepe, *Angewandte Chemie International Edition* **2006**, *45*(31), 5161–5163.

[39] F. Jutz, J.-M. Andanson, A. Baiker, *Journal of Catalysis* **2009**, *268*(2), 356–366.

[40] R. Palkovits, K. Tajvidi, J. Procelewska, R. Rinaldi, A. Ruppert, *Green Chemistry* **2010**, *12*(6), 972–978.

[41] Y. Zhu, Z. N. Kong, L. P. Stubbs, H. Lin, S. Shen, E. Anslyn, J. Maguire, *ChemSusChem* **2010**, *3*(1), 67–70.

[42] G. Kling, G. Maurer, *The Journal of Chemical Thermodynamics* **1991**, *23*(6), 531–541.

[43] S. Söderholm, Y. H. Roos, N. Meinander, M. Hotokka, *Journal of Raman Spectroscopy* **1999**, *30*(11), 1009–1018.

[44] B. Schröder, J. Rudolph, *Physikalische Methoden in der Chemie*, VCH Verlagsgesellschaft mbH, Weinheim, **1985**.

[45] W. A. de Groot, The Use of Spontaneous Raman Scattering for Hydrogen Leak Detection, *Techn. Ber.*, NYMA Inc., **1994**.

[46] D. G. Taylor III, H. L. Strauss, *The Journal of Chemical Physics* **1989**, *90*(2), 768–772.

[47] J. E. Hunter III, D. G. Taylor III, H. L. Strauss, *The Journal of Chemical Physics* **1992**, *97*(1), 50–59.

[48] Y. Liu, P. G. Jessop, M. Cunningham, C. A. Eckert, C. L. Liotta, *Science* **2006**, *313*(5789), 958–960.

[49] L. Phan, H. Brown, J. White, A. Hodgson, P. G. Jessop, *Green Chemistry* **2009**, *11*(1), 53–59.

[50] C. Samorì, C. Torri, G. Samori, D. Fabbri, P. Galletti, F. Guerrini, R. Pistocchi, E. Tagliavini, *Bioresource Technology* **2010**, *101*(9), 3274–3279.

[51] W. Schroth, H.-D. Schädler, J. Andersch, *Zeitschrift für Chemie* **1989**, *29*(2), 56–57.

[52] P. G. Jessop, D. J. Heldebrant, X. Li, C. A. Eckert, C. L. Liotta, *Nature* **2005**, *436*(7054), 1102–1102.

[53] L. Phan, J. R. Andreatta, L. K. Horvey, C. F. Edie, A.-L. Luco, A. Mirchandani, D. J. Darensbourg, P. G. Jessop, *The Journal of organic chemistry* **2007**, *73*(1), 127–132.

[54] T. Yamada, P. J. Lukac, T. Yu, R. G. Weiss, *Chemistry of Materials* **2007**, *19*(19), 4761–4768.

[55] V. M. Blasucci, R. Hart, P. Pollet, C. L. Liotta, C. A. Eckert, *Fluid Phase Equilibria* **2010**, *294*(1), 1–6.

[56] I. Anugwom, P. Mäki-Arvela, P. Virtanen, S. Willför, R. Sjöholm, J. P. Mikkola, *Carbohydrate Polymers* **2012**, *87*(3), 2005–2011.

[57] R. Hart, P. Pollet, D. J. Hahne, E. John, V. Llopis-Mestre, V. Blasucci, H. Huttenhower, W. Leitner, C. A. Eckert, C. L. Liotta, *Tetrahedron* **2010**, *66*(5), 1082–1090.

[58] L. Phan, D. Chiu, D. J. Heldebrant, H. Huttenhower, E. John, X. Li, P. Pollet, R. Wang, C. A. Eckert, C. L. Liotta, P. G. Jessop, *Industrial & Engineering Chemistry Research* **2008**, *47*(3), 539–545.

[59] C. Secuianu, V. Feroiu, D. Geană, *The Journal of Chemical Thermodynamics* **2010**, *42*(10), 1286–1291.

[60] J. Villermaux, R. David, *Chemical Engineering Communications* **1983**, *21*(1-3), 105–122.

[61] A. Okhotsimskii, M. Hozawa, *Chemical Engineering Science* **1998**, *53*(14), 2547–2573.

[62] T. Yamada, P. J. Lukac, M. George, R. G. Weiss, *Chemistry of Materials* **2007**, *19*(5), 967–969.

[63] A. Ahosseini, E. Ortega, B. Sensenich, A. M. Scurto, *Fluid Phase Equilibria* **2009**, *286*(1), 72–78.

[64] A. Urakawa, R. Wirz, T. Bürgi, A. Baiker, *The Journal of Physical Chemistry B* **2003**, *107*(47), 13061–13068.

[65] J.-G. Li, Y.-F. Hu, C.-W. Jin, H.-D. Chu, X.-M. Peng, Y.-G. Liang, *Journal of Solution Chemistry* **2010**, *39*(12), 1877–1887.

[66] S. S. Sekhon, D. P. Kaur, J. S. Park, K. Yamada, *Electrochimica Acta* **2012**, *60*(0), 366–374.

[67] A. Guerfi, M. Dontigny, P. Charest, M. Petitclerc, M. Lagacé, A. Vijh, K. Zaghib, *Journal of Power Sources* **2010**, *195*(3), 845–852.

[68] C. Michalik, M. Brendel, W. Marquardt, *AIChE Journal* **2009**, *55*(4), 1009–1022.

[69] G. Jander, E. Blasius, *Einführung in das anorganisch-chemische Praktikum*, 14 Aufl., S. Hirzel Verlag, Stuttgart, Leipzig, **1995**.

[70] K. Doerffel, R. Geyer, H. Müller, *Analytikum*, 9 Aufl., Deutscher Verlag für Grundstoffindustrie, Leipzig, Stuttgart, **1994**.

[71] G. Jander, E. Blasius, *Lehrbuch der analytischen und präparativen anorganischen Chemie*, 14 Aufl., S. Hirzel Verlag, Stuttgart, Leipzig, **1995**.

[72] S. Petrozzi, *Instrumentelle Analytik*, Wiley-VCH Verlag GmbH & Co. KGaA, Weinheim, **2010**.

[73] W. Ostwald, *Die wissenschaftlichen Grundlagen der analytischen Chemie / elementar dargestellt von Wilhelm Ostwald*, Engelmann, Leipzig, **1894**.

[74] D. A. Skoog, D. M. West, *Principles of Instrumental Analysis*, Holt, Rinehart and Winston, Inc., New York, Chicago, San Francisco, Atlanta, Dallas, Montreal, Toronto, London, Sydney, **1971**.

[75] F. Korte, *Analytik*, Bd. 1 von *Methodicum Chimicum*, Georg Thieme Verlag, Stuttgart, **1973**.

[76] R. W. Kessler, *Prozessanalytik*, Wiley-VCH Verlag GmbH & Co. KGaA, Weinheim, **2006**.

[77] M. Hesse, H. Meier, B. Zeeh, *Spektroskopische Methoden in der organischen Chemie*, Bd. 6, Georg Thieme Verlag, Stuttgart, New York, **2002**.

[78] D. Ende, K.-M. Mangold, *Chemie in unserer Zeit* **1993**, *27*(3), 134–140.

A. Experimental procedures

A.1. Chemicals

D-(+)-Glucose (Sigma-Aldrich, >99.0 %) and D-sorbitol (Sigma-Aldrich, >99.0 %) were used without further pretreatment.

The nanoparticular ruthenium catalyst was synthesised from a Bis(2-methylallyl)(1,5-cyclooctadien)ruthenium(II) precursor and an acidic 1-(4-butylsulfonic acid)-3-(n-butyl)-imidazolium bis(trifluoromethylsulfonyl) imide IL. The IL was dried by heating it at 90 °C under reduced pressure for 6 hours. 0.03 g of the IL and 0.41 g of the precursor were filled into a glass liner under Ar gas, a magnetic stirring bar was added and the liner was inserted into a 10 mL finger autoclave. The reactor was closed, 60 bar of hydrogen were added and the autoclave left in a 70 °C oil bath for three hours. Afterwards, the reactor was cooled down in a water/ice bath and depressurised slowly. The mixture was then dissolved in 5 mL dried THF and filled into a 100 mL round bottom flask under Ar. 1.34 g silica particles with a particle size of 60 μm were added slowly under constant stirring to give a catalyst/support ratio of 30 %. THF was removed by distillation under reduced pressure, rendering a grey powder.

For the IL synthesis, 1,8-Diazabicyclo[5.4.0]undec-7-ene was first dried under reflux over CaH_2, then distilled under reduced pressure and stored over a molar sieve under argon (Ar) atmosphere. 1-hexanol was distilled under reduced pressure, degassed and stored over a molar sieve under Ar atmosphere. The gases Ar (Westfalen AG, 99.998 vol%), hydrogen (Air

Products, UltraPure) and CO_2 (Westfalen AG, 99.995 vol%) were used without further pretreatment.

A.2. Reaction procedures

A.2.1. Hydrogenation

For reactions in the standard 10 mL finger autoclave set-up (appendix A.3.1), 0.22 g of the nanoparticular ruthenium catalyst and 1.0 g of glucose were filled into a glass liner and 2.8 g of water added. A magnetic stirring bar was added and the content mixed until the glucose was completely dissolved and the catalyst dispersed in the solution.

A background spectrum for the IR analysis was measured in air. Afterwards, the glass liner was inserted into the steel autoclave. The autoclave was then closed and lowered into a preheated oil bath at 60 °C and the stirring speed set to 600 rpm. The IR measurements were started. After 30 minutes of thermal equilibration, hydrogen was added from a second, larger storing autoclave up to a pressure of 60 bar, marking the start of the reaction.

After the chosen reaction time, the IR measurements were stopped, the autoclave removed from the oil bath and lowered into a water/ice bath for quenching. After 30 minutes, the pressure valve was opened and the remaining hydrogen slowly discharged.

For the preparation of HPLC samples, the reaction mixture was then centrifuged and the liquid filtered with 4.5 μm syringe filter. 0.1 mL of the filtrate was diluted with 1.5 mL pure water to give a final concentration of 23 mg/mL for the analysis.

For reactions in the 30 mL window autoclave (appendix A.3.2), 0.44 g

of ruthenium catalyst, 2 g of glucose and 5.6 g water were mixed. After collecting the background spectra, the mixture was filled into the autoclave using a syringe. The autoclave was closed tightly, the stirring speed set to 300 rpm and the reactor content heated to 60 °C. The Raman and IR measurements were started and afterwards, hydrogen was added up to a pressure of 30 bar. The reaction was stopped after 2.5 days by cooling down and depressurising the autoclave.

A.2.2. Switchable solvent synthesis

For the switchable solvent synthesis, the reactor (appendix A.3.3) was first dried and afterwards purged with Ar. A background spectrum was then acquired. An equimolar mixture of DBU (4.35 g) and hexanol (2.86 g) was introduced into a Schlenk tube under Ar atmosphere and stirred well. The mixture was then transferred into the autoclave purged with Ar using a syringe, noting down the exact amount added. The stirrer speed was set to 300 rpm and the autoclave well tightened. IR measurements were started and CO_2 was introduced through the control valve until the chosen pressure was reached. This time was taken as the reaction start.

For the synthesis reaction in the 150 mL autoclave with conductivity measurements (appendix A.3.4), a total amount of 30 mL equimolar mixture was used while the general approach was kept exactly the same.

A.3. Reactor set-up

A.3.1. Hydrogenation 1

For the hydrogenation of glucose, a set-up with a strong similarity to the standard reactor was chosen (fig. A.1). Reactions were carried out in a 10 mL finger autoclave made from 1.4571 stainless steel which can handle

pressures up to 100 bar and temperatures up to 120 °C. Tightening is based on a conical fitting. The reactor is equipped with a glass liner, a pressure valve (1) and a pressure gauge (2).

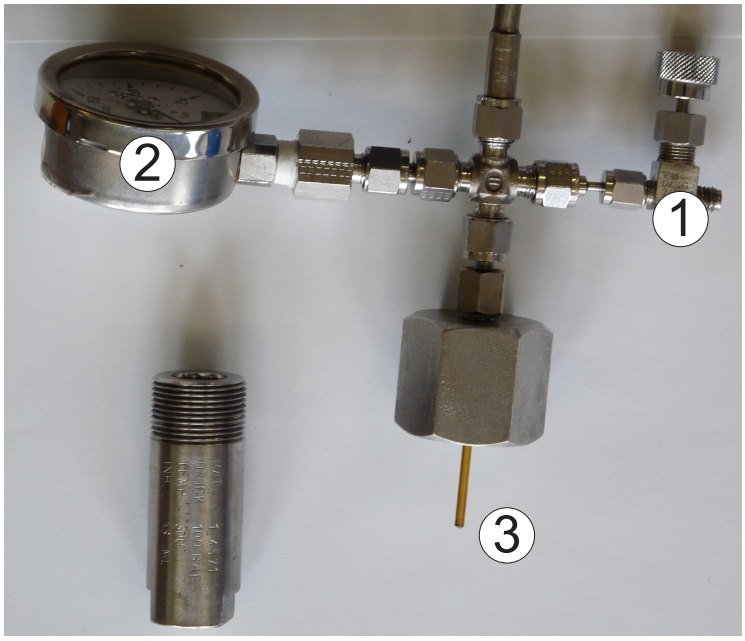

Figure A.1.: Photograph of 10 mL finger autoclave including pressure valve (1), pressure gauge (2) and mIR probe (3)

This arrangement allows the addition of gas up to a chosen pressure and the controlling of the pressure during the reaction as a safety precaution. If the pressure drops, this can likely be attributed to leaks, in which case the reaction should be stopped and the reactor depressurised in a controlled way. If the pressure increases strongly, the reactor has to be removed from the oil bath and the valve opened to release the pressure and avoid bursting. These precautions hold true for all high pressure experiments. Mixing was conducted with a magnetic stirring bar made

from Teflon. A mIR probe with a gold-coated Hastelloy shaft, a diamond ATR-prism and a diameter of 3 mm (3) enters the reactor from the top and is fitted with a cutting ring. The tip of the probe reaches far enough into the reactor to enter the liquid phase at the reactor bottom and monitor its composition. The spectroscopic measurements are carried out with a Matrix-MF multiplex spectrometer.

A.3.2. Hydrogenation 2

The design of the measuring cell allows simultaneous mIR spectroscopy and phase behaviour monitoring. The whole design is based on a 30 mL autoclave with two borosilicate glass windows opposite each other with a distance of 28.75 mm (fig. A.2). The autoclave itself is made from 1.4571 stainless steel and can handle pressures up to 250 bar and temperatures up to 100 °C. It is tightened with a teflon fitting. Through the windows (1), the phase behaviour can be checked or recorded with a camera. The windows are exchangeable and their material can be adapted to accommodate transmission or scattering spectroscopy in the near to mid IR region.

The main body is equipped with two inlets, one for gases (2a) and one for the insertion of liquids or solids (2b). Because the gas can be dosed through a different inlet, it is possible to fill the reactor under a constant inert gas stream and so introduce even air and moisture sensitive substances. An outlet at the bottom (3) enables a simple discharging and cleaning of the reactor.

Stirring is conducted via a shaft drive stirrer (4) with agitator speed control. The magnetic agitator with magnetic coupling can reach speeds of 100 to 1200 rpm and is installed in the reactor lid. The small dimensions leave room for the above mentioned gas and liquid inlets. The use of a shaft drive stirrer instead of a magnetic stirrer ensures good mixing even at higher viscosities and the agitator speed control ensures a steady

speed even if the viscosity of the reaction mixture changes during the reaction.

Measurements from a thermocouple (5) that is installed inside the reactor are used to control the temperature. This way, any heat loss to the surroundings is compensated by the control. The reactor stands on a heating plate which heats the steel body. The heat is quickly transported through the steel and then transferred to the reaction mixture inside the reactor. This reduces the temperature gradient inside the reactor to 0.2 K between the temperature at the top and at the bottom. The pressure is recorded by a pressure sensor (6) which can be connected to a computer for recording. For safety reasons, proper precautions for the operation of high pressure equipment such as that required for these experiments must be taken, including but not limited to the use of blast shields and pressure relief mechanisms, to minimize the risk of personal injury.

Two process compatible immersion probes (7) with ATR technique for mIR and Raman spectroscopy and a diameter of 6 mm are introduced horizontally with a distance of 2 mm from the bottom and enable monitoring the lower phase. This installation method reduces the minimum volume of the lower phase to only 5.5 mL. The fibre-optic mIR probe is a custom-made gold coated Hastelloy shaft with a diamond ATR-prism as IRE and resists pressures of 200 bar and temperatures of 170 °C. Its potential for inline reaction monitoring has already been shown for several applications[14, 15]. The IR probe is connected to a Matrix-MF multiplex spectrometer. The Raman probe is equipped with a sapphire window and a short focal length. It resists temperatures of 450 °C and pressures of 200 bar. Laser light with a power of 400 mW and an excitation wavelength of 785 nm was supplied by a RXN2 Raman spectrometer (Kaiser Optical Systems).

A.3.3. Switchable solvent synthesis

For the switchable solvent synthesis, the previously described set-up was altered to allow simultaneous monitoring of two phases (fig. A.3). Process compatible immersion probes are now installed at two different positions in the reactor. In addition to the probe that monitors the lower phase (1), a probe enters the reactor from the top and can monitor the upper half of the reactor content (2). The positions of the probes permit spectroscopic measurements in two phases, so that either a two phase reaction (gas-liquid or liquid-liquid) or a three phase reaction (gas-liquid-liquid) can be monitored. In the former case, only gas-liquid systems with spectroscopically active species in the gas phase, e.g. gases with an alterable dipole moment for mIR measurements, can be analysed. In the latter case the two liquid phases are for example analysed spectroscopically and the gas phase is only monitored with the pressure sensor.

A.3.4. Conductivity measurements

The combined spectroscopy and conductivity measurements were performed in a 75 mL autoclave made from 1.4571 stainless steel equipped with a pressure valve (1) and a second inlet (2) for the addition of liquids or solids (fig. A.4). Again, this combination makes the dosing of liquids under a constant inert gas stream possible. An outlet at the bottom (3) facilitates the discharging procedure.

Two ATR-IR immersion probes (4) are installed at the reactor bottom, facing each other and each monitoring the lower liquid phase. They both have a diameter of 6 mm and are fitted with a Teflon fitting and a Teflon insulating bushing (5) to avoid conductive contact between the probes and the reactor walls. By taking these measures and attaching an electrical contact to each probe shaft, conductivity measurements can be carried out where the electricity can be conducted from one probe tip

surface to the other via the liquid.

For the conductivity measurements, a power supply with a maximum of 30 V and 10 A was used. To lower the noise of the voltage signal, a voltage divider with a 10 and a 100 Ω resistance was introduced and the measuring voltage of the autoclave taken over the 10 Ω resistance (fig. A.5). The voltage and current were measured using different channels of a NI 9201 analog input module with a measuring frequency of 500 kHz and analysed with a LabVIEW program. For the impedance spectroscopic measurements, a frequency generator with a range of 0.2 to 250 kHz and a maximum voltage of 12 V was integrated into the set-up. The oscillation was analysed by fitting 10000 measuring points to a sine function and analysing its frequency, amplitude and phase shift.

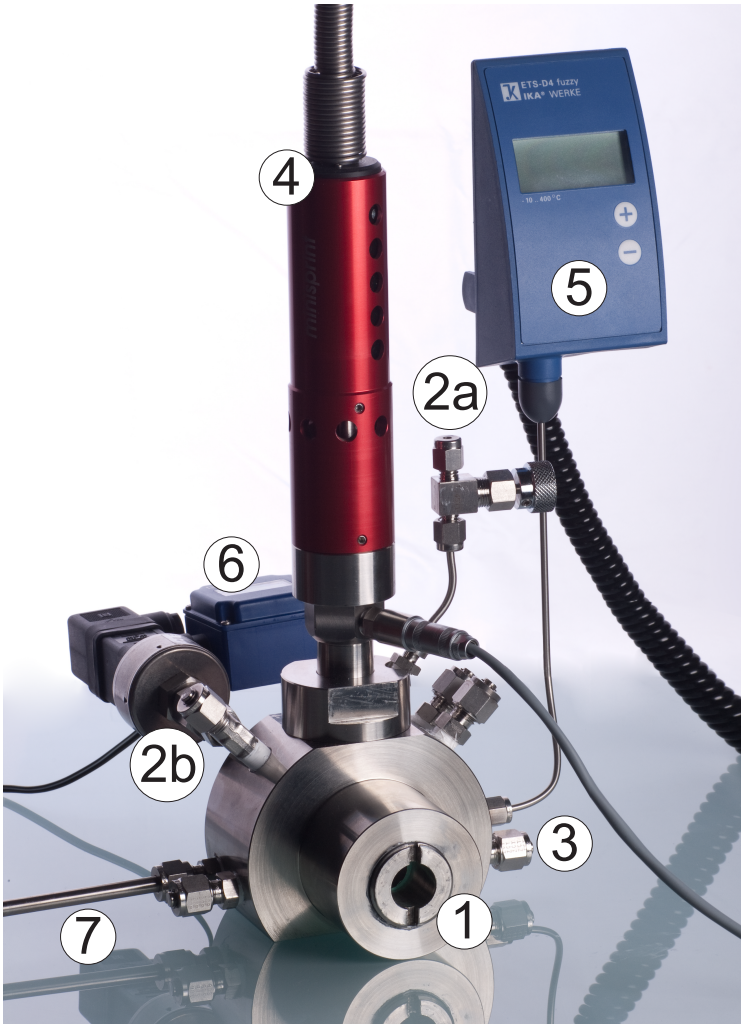

Figure A.2.: Photograph of 30 mL window autoclave including windows (1), gas inlet (2a), liquid/solid inlet (2b), outlet (3), shaft drive stirrer (4), thermocouple (5), pressure sensor (6), mIR and Raman probes (7)

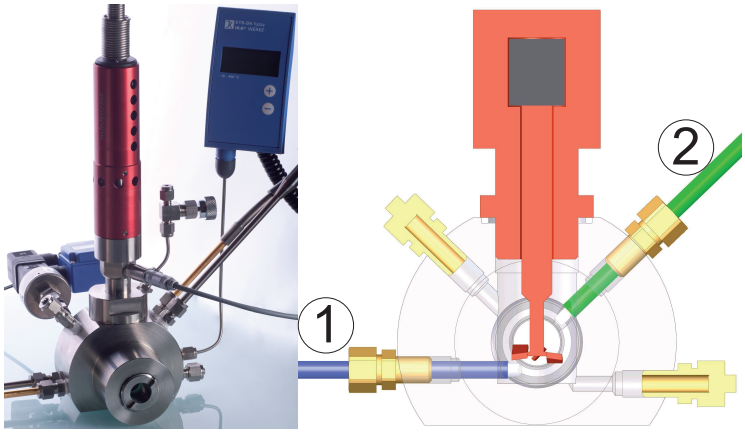

Figure A.3.: Photograph of 30 mL window autoclave including mIR probes at the top (1) and at the bottom (2) of the autoclave

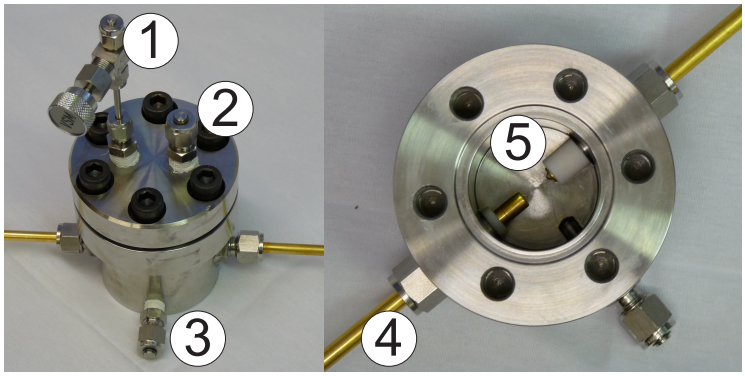

Figure A.4.: Photograph of 75 mL autoclave including pressure valve (1), liquid/solid inlet (2), outlet (3), mIR probes (4) and insulating bushing (5)

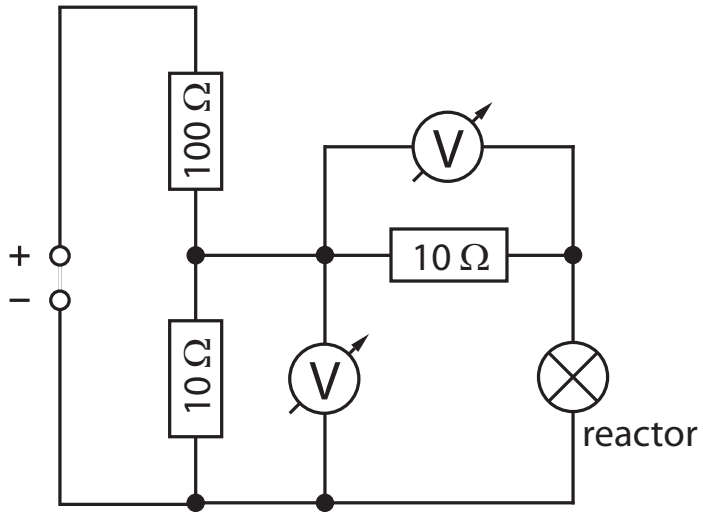

Figure A.5.: Schematic of conductivity measurement circuit

B. Calibrational data

Table B.1.: Results of glucose IR quantification

true concentration [mol/g]	**predicted concentration [mol/g]**	**difference [mol/g]**
0.00184	0.00184	0.00000
0.00176	0.00177	−0.00001
0.00160	0.00162	−0.00002
0.00153	0.00153	0.00000
0.00129	0.00132	−0.00002
0.00117	0.00120	−0.00003
0.00096	0.00099	−0.00003
0.00089	0.00091	−0.00002
0.00049	0.00047	0.00002
0.00041	0.00036	0.00005
0.00144	0.00143	0.00001
0.00133	0.00132	0.00001
0.00127	0.00127	0.00000
0.00143	0.00142	0.00001
0.00137	0.00136	0.00001
0.00107	0.00108	−0.00001
0.00100	0.00099	0.00001
0.00091	0.00092	−0.00001
0.00083	0.00083	0.00000
0.00076	0.00076	−0.00001
0.00070	0.00069	0.00000

Table B.1.: Results of glucose IR quantification (continued)

true concentration	**predicted concentration**	**difference**
0.00037	0.00037	0.00000
0.00033	0.00033	0.00000
0.00030	0.00030	−0.00001
0.00120	0.00120	0.00000
0.00112	0.00112	0.00000
0.00103	0.00103	0.00000
0.00114	0.00115	−0.00001
0.00105	0.00105	0.00001
0.00078	0.00077	0.00001
0.00081	0.00083	−0.00002
0.00058	0.00058	0.00000
0.00055	0.00056	−0.00001
0.00066	0.00065	0.00001
0.00062	0.00062	0.00000
0.00046	0.00045	0.00001
0.00024	0.00023	0.00001
0.00019	0.00019	0.00000
0.00015	0.00015	−0.00001
0.00009	0.00007	0.00002
0.00139	0.00139	0.00000
0.00000	0.00000	0.00000
0.00000	−0.00001	0.00001
0.00000	−0.00001	0.00001
0.00006	0.00006	0.00001
0.00120	0.00121	−0.00001
0.00000	−0.00002	0.00002
0.00000	−0.00002	0.00002
0.00000	−0.00002	0.00002
0.00000	−0.00002	0.00002
0.00000	−0.00005	0.00005

Table B.1.: Results of glucose IR quantification (continued)

true concentration	**predicted concentration**	**difference**
0.00000	0.00000	0.00000
0.00000	0.00000	0.00000
0.00000	0.00000	0.00000
0.00000	0.00000	0.00000
0.00000	0.00000	0.00000
0.00000	0.00001	−0.00001
0.00000	0.00004	−0.00004
0.00000	0.00000	0.00000
0.00000	−0.00001	0.00001
0.00000	0.00002	−0.00002
0.00000	0.00001	−0.00001
0.00000	0.00002	−0.00002
0.00000	0.00003	−0.00003
0.00248	0.00242	0.00006
0.00195	0.00194	0.00001
0.00180	0.00180	0.00000
0.00168	0.00168	0.00000
0.00223	0.00220	0.00004
0.00208	0.00206	0.00002
0.00190	0.00187	0.00003
0.00164	0.00165	−0.00001
0.00155	0.00156	−0.00001
0.00000	0.00000	0.00000
0.00000	−0.00001	0.00001
0.00000	−0.00002	0.00002
0.00000	0.00002	−0.00002
0.00000	0.00007	−0.00007
0.00000	0.00001	−0.00001
0.00000	−0.00001	0.00001
0.00000	0.00004	−0.00004

Table B.1.: Results of glucose IR quantification (continued)

true concentration	**predicted concentration**	**difference**
0.00000	0.00000	0.00000
0.00000	0.00000	0.00000
0.00000	0.00000	0.00000
0.00000	−0.00001	0.00001
0.00000	0.00001	−0.00001
0.00000	0.00002	−0.00002
0.00000	0.00001	−0.00001
0.00000	0.00000	0.00000
0.00000	−0.00003	0.00003
0.00000	0.00000	0.00000
0.00000	0.00003	−0.00003
0.00000	0.00000	0.00000
0.00000	0.00003	−0.00003
0.00000	−0.00001	0.00001
0.00000	0.00000	0.00000
0.00000	0.00000	0.00000
0.00000	0.00000	0.00000
0.00000	0.00002	−0.00002
0.00000	0.00001	−0.00001
0.00000	−0.00002	0.00002
0.00000	0.00000	0.00000
0.00000	0.00000	0.00000
0.00000	0.00001	−0.00001
0.00000	−0.00002	0.00002
0.00000	−0.00001	0.00001
0.00000	0.00000	0.00000
0.00168	0.00172	−0.00004
0.00133	0.00134	0.00000
0.00096	0.00094	0.00001
0.00041	0.00044	−0.00003

Table B.1.: Results of glucose IR quantification (continued)

true concentration	**predicted concentration**	**difference**
0.00031	0.00029	0.00001
0.00023	0.00021	0.00003
0.00000	0.00001	−0.00001
0.00000	0.00005	−0.00005
0.00000	−0.00002	0.00002
0.00069	0.00066	0.00002
0.00016	0.00014	0.00001
0.00000	0.00000	0.00000
0.00067	0.00065	0.00002
0.00052	0.00050	0.00002
0.00040	0.00039	0.00001
0.00028	0.00026	0.00002
0.00136	0.00131	0.00005
0.00134	0.00133	0.00002
0.00136	0.00141	−0.00005
0.00137	0.00135	0.00002
0.00136	0.00132	0.00004
0.00134	0.00126	0.00009
0.00135	0.00136	−0.00001
0.00133	0.00135	−0.00002
0.00136	0.00142	−0.00006
0.00137	0.00133	0.00004
0.00136	0.00137	−0.00001
0.00122	0.00121	0.00001
0.00133	0.00133	0.00000
0.00137	0.00151	−0.00015
0.00123	0.00118	0.00006
0.00135	0.00137	−0.00001
0.00134	0.00129	0.00005

Table B.2.: Results of glucose Raman quantification

true fraction [-]	**predicted fraction** [-]	**difference** [-]
0.00000	0.11770	0.11770
0.10038	0.16209	0.06171
0.29808	0.38829	0.09021
0.49689	0.43705	−0.05985
0.00000	0.18137	0.18137
1.00000	0.81425	−0.18575

Table B.3.: Results of DBU/hexanol IR quantification

true fraction [-]	**predicted fraction** [-]	**difference** [-]
0.26040	0.23170	−0.02870
0.30508	0.22609	−0.07899
0.36302	0.22147	−0.14155
0.40315	0.21916	−0.18400
0.42800	0.21679	−0.21121
0.46259	0.22032	−0.24227
0.48762	0.23858	−0.24904
0.51532	0.25533	−0.25998
0.53330	0.27513	−0.25817
0.56074	0.28986	−0.27088
0.58398	0.31076	−0.27322
0.60815	0.33210	−0.27606
0.63258	0.35468	−0.27790
0.65393	0.38982	−0.26411
0.67122	0.44045	−0.23077
0.70110	0.53794	−0.16316

Table B.3.: Results of DBU/hexanol IR quantification (continued)

true fraction	predicted fraction	difference
0.70829	0.63762	−0.07067
0.72056	0.65668	−0.06388
0.73435	0.75476	0.02041
0.74683	0.81210	0.06527
0.75327	0.79040	0.03713
0.76124	0.82761	0.06637
0.76910	0.81506	0.04595
0.77506	0.82361	0.04854
0.78033	0.86088	0.08055
0.79555	0.85713	0.06158
0.80580	0.87704	0.07124
0.80949	0.88697	0.07747
0.81572	0.86803	0.05231
0.82621	0.90377	0.07756
0.91861	0.97351	0.05490
0.87751	0.90107	0.02355
0.80125	0.85576	0.05451
0.73868	0.88028	0.14160
0.69330	0.90742	0.21412
0.60864	0.87850	0.26986
0.57523	0.86443	0.28920
0.54947	0.61039	0.06092
0.51295	0.70839	0.19544
0.49694	0.76992	0.27298
0.47959	0.77774	0.29815
0.46324	0.57644	0.11321
0.44083	0.59463	0.15380
0.41816	0.48905	0.07089
0.97931	0.96228	−0.01703
0.97707	0.95775	−0.01932

Table B.3.: Results of DBU/hexanol IR quantification (continued)

true fraction	predicted fraction	difference
0.95553	0.93460	−0.02093
0.94397	0.92024	−0.02374
0.93438	0.91941	−0.01497
0.88223	0.86865	−0.01358
0.85860	0.83901	−0.01959
0.83737	0.82054	−0.01683
0.80743	0.81141	0.00398
0.79175	0.77503	−0.01672
0.79013	0.78574	−0.00439
0.76613	0.75991	−0.00622
0.74360	0.74790	0.00430
0.72967	0.72167	−0.00800
0.71238	0.70768	−0.00470
0.69912	0.71211	0.01299
0.69703	0.69909	0.00207
0.45345	0.32613	−0.12732
0.51359	0.47610	−0.03749
0.55647	0.53043	−0.02605
0.60407	0.57268	−0.03140
0.63556	0.66219	0.02663
0.65909	0.70474	0.04564
0.71334	0.72277	0.00943
0.72915	0.85796	0.12881
0.76426	0.82182	0.05756
0.78129	0.82063	0.03934
0.18746	0.22522	0.03776
0.24353	0.36106	0.11753
0.29750	0.39043	0.09293
0.32023	0.47111	0.15088
0.34244	0.46033	0.11789

Table B.3.: Results of DBU/hexanol IR quantification (continued)

true fraction	**predicted fraction**	**difference**
0.36689	0.60026	0.23336
0.38135	0.51956	0.13821
0.40903	0.54718	0.13815
0.42630	0.52167	0.09537
0.44221	0.55302	0.11081
0.45676	0.53388	0.07712
0.47577	0.53757	0.06180
0.49057	0.59597	0.10540
0.51352	0.65339	0.13987
0.52865	0.61321	0.08457
0.53855	0.62539	0.08684
0.55081	0.65297	0.10216
0.56377	0.64765	0.08388
0.58062	0.69640	0.11578
0.59323	0.68660	0.09337
0.61427	0.69669	0.08242
0.62772	0.70252	0.07480
0.64207	0.72170	0.07962
0.64931	0.72643	0.07712
0.65827	0.73715	0.07888
0.66902	0.72798	0.05896
0.67836	0.75826	0.07990
0.69195	0.75141	0.05946
0.69853	0.77261	0.07408
0.70639	0.79202	0.08563
0.71456	0.78280	0.06824
0.72187	0.82328	0.10142
0.73160	0.79206	0.06047

Table B.4.: Results of IL IR quantification

true fraction [-]	**predicted fraction** [-]	**difference** [-]
0.73960	0.76831	0.02870
0.69492	0.77391	0.07899
0.63698	0.77853	0.14155
0.59685	0.78084	0.18400
0.57200	0.78321	0.21121
0.53741	0.77969	0.24227
0.51238	0.76142	0.24904
0.48468	0.74467	0.25998
0.46671	0.72487	0.25817
0.43926	0.71014	0.27088
0.41602	0.68924	0.27322
0.39185	0.66791	0.27606
0.36742	0.64532	0.27790
0.34607	0.61018	0.26411
0.32878	0.55955	0.23077
0.29890	0.46206	0.16316
0.29171	0.36238	0.07067
0.27944	0.34332	0.06388
0.26565	0.24524	−0.02041
0.25317	0.18790	−0.06527
0.24673	0.20960	−0.03713
0.23876	0.17239	−0.06637
0.23090	0.18495	−0.04595
0.22494	0.17639	−0.04854
0.21967	0.13912	−0.08055
0.20445	0.14287	−0.06158
0.19420	0.12296	−0.07124
0.19051	0.11303	−0.07747

Table B.4.: Results of IL IR quantification (continued)

true fraction	predicted fraction	difference
0.18428	0.13197	−0.05231
0.17380	0.09623	−0.07756
0.08139	0.02649	−0.05490
0.12249	0.09893	−0.02355
0.19875	0.14424	−0.05451
0.26132	0.11972	−0.14160
0.30670	0.09258	−0.21412
0.39136	0.12150	−0.26986
0.42477	0.13557	−0.28920
0.45053	0.38961	−0.06092
0.48705	0.29161	−0.19544
0.50306	0.23008	−0.27298
0.52041	0.22226	−0.29815
0.53677	0.42356	−0.11321
0.55917	0.40537	−0.15380
0.58184	0.51095	−0.07089
0.02069	0.03772	0.01703
0.02293	0.04225	0.01932
0.04447	0.06540	0.02093
0.05603	0.07976	0.02374
0.06562	0.08059	0.01497
0.11777	0.13135	0.01358
0.14140	0.16099	0.01959
0.16263	0.17946	0.01683
0.19257	0.18859	−0.00398
0.20825	0.22497	0.01672
0.20987	0.21426	0.00439
0.23388	0.24009	0.00622
0.25640	0.25210	−0.00430
0.27033	0.27833	0.00800

Table B.4.: Results of IL IR quantification (continued)

true fraction	predicted fraction	difference
0.28762	0.29232	0.00470
0.30088	0.28789	−0.01299
0.30298	0.30091	−0.00207
0.54655	0.67387	0.12732
0.48641	0.52390	0.03749
0.44353	0.46957	0.02605
0.39593	0.42732	0.03140
0.36445	0.33781	−0.02663
0.34091	0.29526	−0.04564
0.28666	0.27723	−0.00943
0.27085	0.14204	−0.12881
0.23574	0.17818	−0.05756
0.21871	0.17937	−0.03934
0.81254	0.77478	−0.03776
0.75647	0.63894	−0.11753
0.70250	0.60957	−0.09293
0.67977	0.52889	−0.15088
0.65756	0.53967	−0.11789
0.63311	0.39975	−0.23336
0.61865	0.48044	−0.13821
0.59097	0.45283	−0.13815
0.57370	0.47833	−0.09537
0.55779	0.44699	−0.11081
0.54324	0.46612	−0.07712
0.52423	0.46243	−0.06180
0.50943	0.40403	−0.10540
0.48648	0.34661	−0.13987
0.47136	0.38679	−0.08457
0.46145	0.37461	−0.08684
0.44919	0.34703	−0.10216

Table B.4.: Results of IL IR quantification (continued)

true fraction	**predicted fraction**	**difference**
0.43623	0.35235	−0.08388
0.41938	0.30361	−0.11578
0.40677	0.31340	−0.09337
0.38573	0.30331	−0.08242
0.37229	0.29748	−0.07480
0.35793	0.27830	−0.07962
0.35069	0.27358	−0.07712
0.34173	0.26285	−0.07888
0.33098	0.27202	−0.05896
0.32164	0.24174	−0.07990
0.30805	0.24859	−0.05946
0.30147	0.22739	−0.07408
0.29361	0.20798	−0.08563
0.28544	0.21720	−0.06824
0.27813	0.17672	−0.10142
0.26841	0.20794	−0.06047

Table B.5.: Results of CO_2 IR quantification

true concentration [mol/L]	**predicted concentration [mol/L]**	**difference [mol/L]**
0.08441	0.07960	0.00481
0.39186	0.37320	0.01871
0.87690	0.88450	−0.00756
1.92586	1.92100	0.00446
3.57057	3.60600	−0.03510
5.13347	5.13200	0.00196
7.11362	7.06500	0.04858
8.71854	8.82100	−0.10220

Table B.5.: Results of CO_2 IR quantification (continued)

true concentration	**predicted concentration**	**difference**
8.84772	8.74000	0.10810
9.84096	9.96500	−0.12360
10.79480	10.92000	−0.12190
11.91780	11.88000	0.03995
12.80940	12.67000	0.14070
14.30270	14.18000	0.12730
15.09860	15.03000	0.06724
15.41820	15.44000	−0.01899
15.97130	15.90000	0.06896
16.13130	16.17000	−0.03695
16.50060	16.55000	−0.04489
16.62520	16.68000	−0.05039
17.29930	17.37000	−0.07214
18.07290	18.10000	−0.02927
18.56630	18.60000	−0.03570
19.46360	19.51000	−0.04656
20.08790	20.14000	−0.05098
20.55910	20.41000	0.14550

C. Additional figures

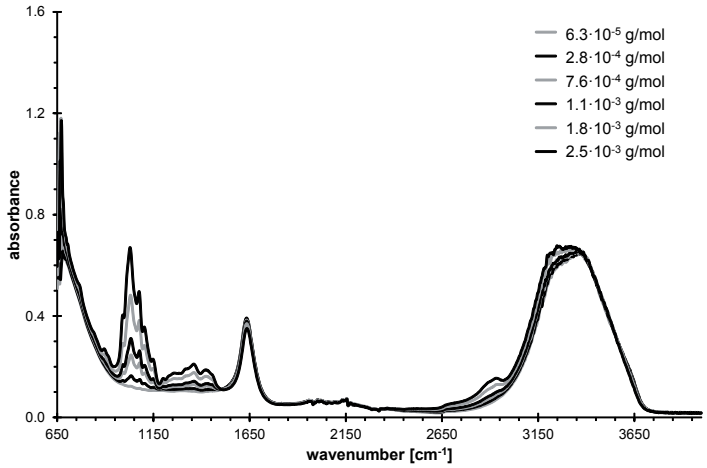

Figure C.1.: IR spectra of glucose in water at different concentrations

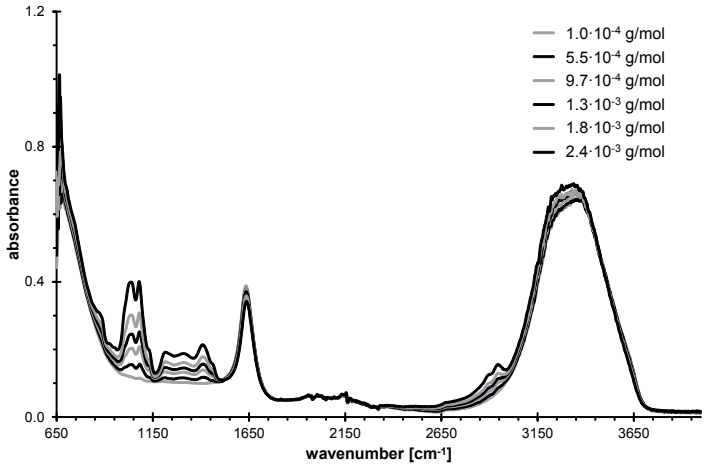

Figure C.2.: IR spectra of sorbitol in water at different concentrations

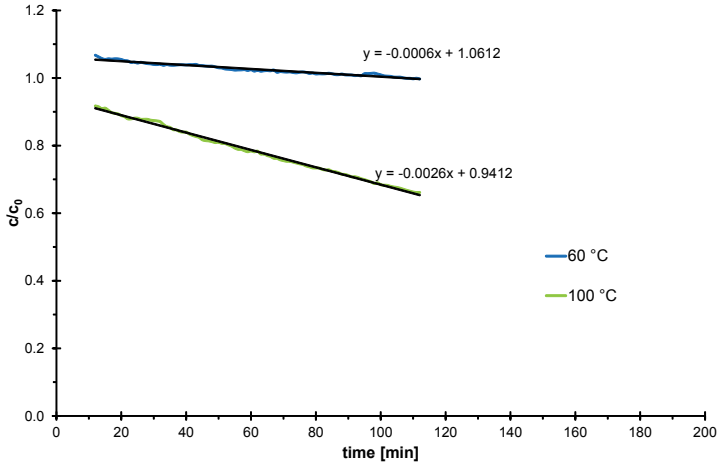

Figure C.3.: Initial slopes of temperature variation

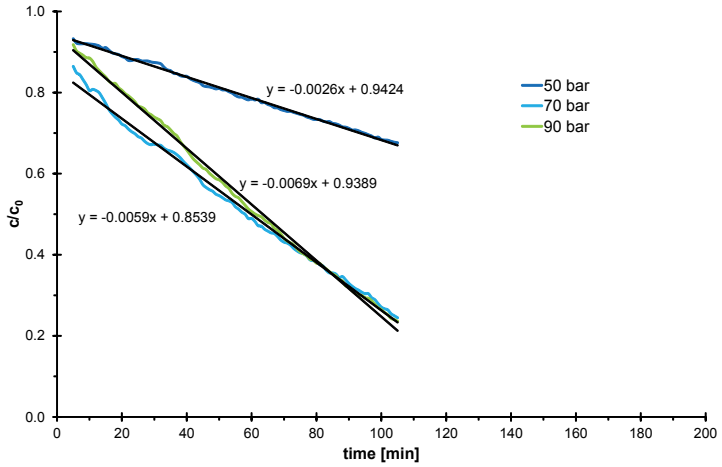

Figure C.4.: Initial slopes of pressure variation

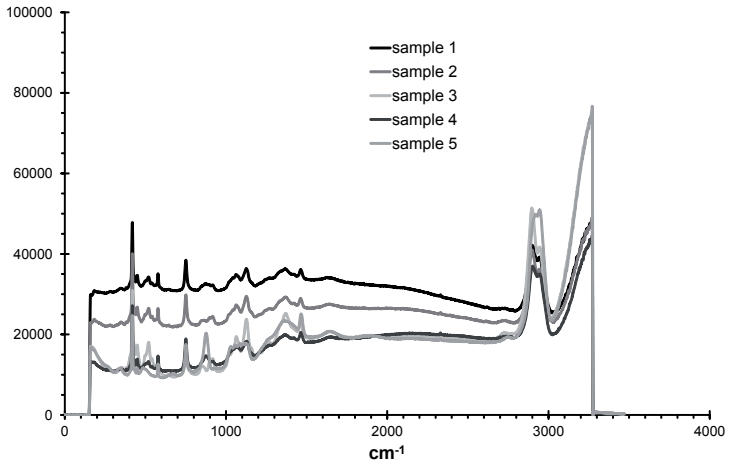

Figure C.5.: Raman spectra of different glucose/sorbitol mixtures (table C.1)

Table C.1.: Sample compositions of Raman calibration

	water [g]	**glucose** [g]	**sorbitol** [g]
sample 1	2.8019	0.6997	0.3005
sample 2	2.8048	0.8995	0.1015
sample 3	2.8067	0.9902	0.0000
sample 4	2.8201	0.5119	0.5113
sample 5	2.8023	0.0000	1.0118

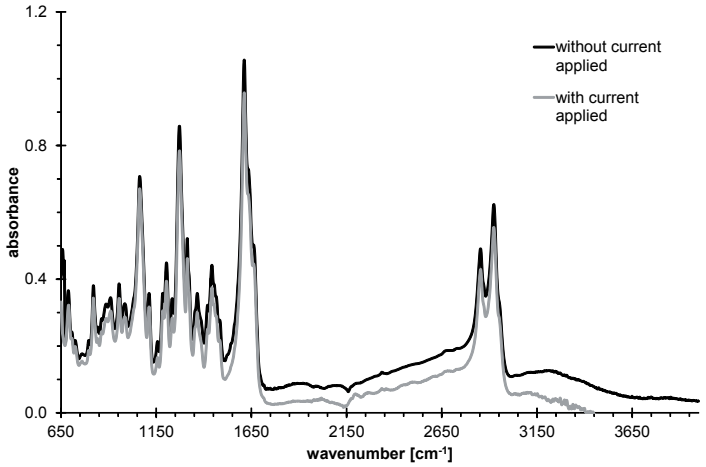

Figure C.6.: IR spectra of IL synthesis reaction with and without current applied to the system